Volume 3, Issue S1 2023 ISSN 2772-6541

17th International Workshop on Osteoarthritis Imaging

Lausanne, Switzerland

June 28-30, 2023

Bienvenu!

Dear IWOAI attendees,

Welcome and Bienvenu to the 17th International Workshop in Osteoarthritis Imaging! We are very excited to host you in Lausanne, one of the most vibrant cities in Europe.

This workshop takes place in Lausanne, in the midst of a booming region on the shores of Lake Geneva, Switzerland. Lausanne is the Olympic Capital, home of the International Olympic committee since 1915 and of 55 international sports federations. During four days of plenary sessions mixed with ample opportunities for informal interactions, attendees will be updated about latest scientific results and have the chance to engage in discussions on current challenges and priorities for future research. Since there will be participation of fundamental and clinical researchers, clinicians and industry representatives working with different imaging modalities, this workshop will cover a wide variety of topics spanning the range from technical development, validation, clinical application, image analysis, as well as industry and patient perspectives.

Thank you for being part of IWOAI 2023 and enjoy the meeting!

Patrick Omoumi, MD, PhD
Julien Favre, PhD
IWOAI 2023 co-Chairs

17th International Workshop in Osteoarthritis Imaging

The many roles of imaging for a multifaceted disease

Chairs

Patrick Omoumi, MD, PhD (Head of Musculoskeletal Imaging, Lausanne University Hospital)
Julien Favre, PhD (Head of Swiss Biomotion Lab, Lausanne University Hospital)

Local Organizers

Patrick Omoumi, MD, PhD, Head of Musculoskeletal Imaging, Lausanne University Hospital
Julien Favre, PhD, Head of Swiss Biomotion Lab, Lausanne University Hospital
Paul Margain, Lausanne University Hospital
Charbel Mourad, MD, PhD, Lausanne University Hospital
Marinella Celli, Lausanne University Hospital

Scientific Committee

Jamie Collins, PhD (Boston, MS/USA)
Vicky Duong, PhD (Sydney, Australia)
Mylene Jansen, PhD (Utrecht, The Netherlands)
Mohamed Jarraya, MD (Boston, MA/USA)
Wolfgang Wirth, PhD (Salzburg, Austria)

Conference timetable

Wednesday June 28, 2023

10.00 – 12.00 **Pre-Congress workshop: Biomechanical assessment – How do we do it?**
Visit of the Swiss Biomotion Lab (SBML)
Julien Favre, Patrick Omoumi, members of the SBML

12.00 – 14.00 Lunch

14.15 – 14.30 **Opening:** Patrick Omoumi and Julien Favre (Chairs of the meeting)

14.30 – 16.00 **Session 1: "Seeing through biomechanics thanks to imaging"**
Moderator: Julien Favre
14.30 – 14.45 Keynote speaker: Studying joint mechanics by imaging – David Wilson
14.45 – 15.00 Keynote speaker: A multiscale approach to osteoarthritis – Jos Runhaar

15.00 – 16.00 Scientific Session
1-Paul Margain – Cartilage thickness, subchondral bone mineral density, and ambulatory loading are correlated in non-osteoarthritic femoral condyles
2-Mylene Jansen – Can gait patterns in knee osteoarthritis patients be explained by radiography and MRI-based joint structure?
3-Tom Turmezei – Weight-bearing 3-D joint space width distribution at the knee varies according to location and extent of the meniscal extrusion: A MOST investigation
4-Ananya Goyal – Evaluation of metabolic response in bone marrow lesions after exercise in relation to changes in adjacent cartilage T2 values

16.00 – 16.30 Break

16.30 – 18.00 **Session 2: "Bone"**
Moderator: Jeroen Geurts
16.30 – 16.45 Keynote speaker: Subchondral Bone: How Relevant is it to Osteoarthritis? – Ali Mobasheri
16.45 – 17.00 Keynote speaker: Bone Imaging: what have we learnt? – Klaus Engelke

17.00 – 18.00 Scientific Session
1-Patrick Omoumi – The spatial correlation between cartilage thickness and subchondral bone mineral density inverses with increasing OA severity
2-Andy Wong – Subchondral bone mineral density: What to do when you don't have access to QCT
3-Signe Brinch – Predicting trochlear dysplasia from 3-D cortical bone and shape parameters
4-Anthony Gatti – Neural shape models encode bone shape features not captured by statistical shape models

18.00 – 18.10 **Acknowledgements of Young Investigator Award winners**
Three best abstracts

18.10 – 18.30 **IWOAI/ISOAI businesses**
Ali Guermazi, President
Frank Roemer, Editor-in-Chief, Osteoarthritis Imaging

Thursday June 29, 2023

09.00 – 10.30	**Session 3: "Compositional MRI"** Moderator: Patrick Omoumi
09.00 – 09.30	Keynote speaker: Compositional MRI – where are we in 2023? The QIBA experience – Thomas Link
09.30 – 10.30	Scientific Session 1-Camilla Nielsen – Impact of weight loss on knee joint cartilage measured by MRI T2 mapping in patients with osteoarthritis – An imaging sub-study of the Lose-It trial 2-Simon Herger – Between-knee differences in deep zone T2 are greater after unilateral ACL injury than in healthy controls 3-Marco Barbieri – Improving accuracy and repeatability of T2 mapping in OAI data through extend phase graph remodeling 4-Suzanne Maschek – Agreement and precision of femorotibial cartilage transverse relaxation time (T2) obtained at four different magnetic field strengths
10.30 – 11.00	Break
11.00 – 12.30	**Session 4: "Imaging: what is new?"** Moderator: Thomas Link
11.00 – 11.15	Keynote speaker: Novel imaging methods: what is in the pipeline? – John Carrino
11.15 – 11.30	Keynote speaker: Imaging of OA: beyond the joints – Shadpour Demehri
11.30 – 12.30	Scientific Session 1-Ananya Goyal – Comparison of new MR approaches for accelerated knee imaging 2-Vidyani Suryadevara – A multimodality-based imaging approach using a novel radiotracer, [18F]-PyGal to detect senescence in small and large animal models 3-Jessica Kupper – The relationship between contrast-enhanced computed tomography (CECT) attenuation and axial strain in total knee arthroplasty tissue 4-Mohamed Jarraya – Dual energy CT cannot effectively differentiate between calcium pyrophosphate and basic calcium phosphate
12.30 – 12.45	Poster pitches
12.45 – 13.45	Lunch
13.45 – 14.30	Poster session
14.30 – 16.00	**Session 5: "AI in OA: research perspective"** Moderator: Olga Kubassova
14.30 – 14.45	Keynote speaker: The hype of AI in OA: where are we in 2023? – Richard Kijowski
14.45 – 15.00	Keynote speaker: Building disease models using AI – Jonas Richiardi
15.00 – 16.00	Scientific Session 1-Jeffrey Duryea – Deep learning approach to measure cartilage volume: Data from the Osteoarthritis Initiative 2-Veronica Ravano – Synthetic CT generation from T1-weighted knee MRIs using UNET 3-Jukka Hirvasniemi – Early detection of knee osteoarthritis using deep learning on knee MRI 4-Anders Lenskjold – Establishing a consecutive clinical knee osteoarthritis imaging cohort using artificial intelligence tools to analyze knee radiographs: A proof of principle
16.00 – 16.30	Break

16.30 – 17.45	**Session 6: "Big data and data sharing in practice"**
	Moderator: Jonas Richiardi
16.30 – 16.45	Keynote speaker: Big data in a university hospital: our experience – Raphael Gottardo
16.45 – 17.00	Keynote speaker: Data sharing and federated learning – Henning Mueller
17.00 – 17.45	Scientific Session 1-Wofgang Wirth – Imaging-based characterization of 3 different OA endotypes derived from biomechanical markers – Data from two observational cohorts 2-Mathias Brejnebøl – External validation of an artificial intelligence tool for radiographic knee osteoarthritis classification: A multi-center, retrospective diagnostic cohort study 3-Tom Turmezei – Computed tomography osteoarthritis knee score (COAKS) construction, reproducibility and potential structural phenotyping

Friday June 30, 2023

09.00 – 10.30	**Session 7: "Hip OA"**
	Moderator: David Hunter
09.00 – 09.15	Keynote speaker: Hip OA update: concepts on etiology and clinical perspective – Moritz Tannast
09.15 – 09.30	Keynote speaker: Challenges in MRI assessment – Bruno Vande Berg
09.30 – 10.30	Scientific Session 1-Felix Eckstein – Agreement of automated laminar femorotibial cartilage transverse relaxation time (T2) analysis with manual expert segmentation 2-Jessica Berberi – Bone marrow edema-like in femoral head osteonecrosis: A surrogate of early collapse? 3-Hoglin Zhang – Early hip cartilage degeneration in young patients meeting a consensus definition of femoroacetabular impingement syndrome 4-Luke Johnson – Severe residual Legg-Calve-Perthes disease deformity is associated with reduced hip clearance and cartilage health in adolescents and young adults
10.30 – 11.00	Break
11.00 – 12.00	**Session 8: "Hand OA"**
	Moderator: Jeremie Sellam
11.00 – 11.15	Keynote speaker: Update on epidemiology and treatment – Philip Conaghan
11.15 – 11.30	Keynote speaker: Update on imaging – Ida Haugen
11.30 – 12.00	Scientific Session 1-Rafael Heiss – T2 and T2* relaxometry of cartilage at the wrist joint: A comparative study of 3T and 7T MRI 2-Taylor Trentadue – Four-dimensional computed tomography-derived radiolunate arthrokinematics with a case study in four-corner arthrodesis
12.00 – 12.15	Poster pitches
12.15 – 13.30	Lunch
13.30 – 14.30	Poster session

14.30 – 16.00	**Session 9: "Pain in OA"**
	Moderator: Thomas Hügle
14.30 – 14.45	Keynote speaker: Why does it hurt? – Jérémie Sellam
14.45 – 15.00	Keynote speaker: Clinical/Imaging Correlation – Edwin Oei
15.00 – 15.15	Keynote Speaker: Pain at eligibility: who to include in clinical trials? – Kent Kwoh
15.15 – 16.00	Scientific Session 1-Charbel Mourad – Prevalence of structural lesions and osteoarthritis in femorotibial joints of asymptomatic participants from the Lausanne Knee study 2-Kent Kwoh – Extent of subregional involvement of subchondral BML in incident knee OA is associated with weight-bearing knee pain 3-Mohamed Jarraya – Patients with neuropathic-like pain phenotype exhibit markedly less MRI-detected structural joint tissue damage compared to without a neuropathic-like pain phenotype: Data from the IMI-APPROACH study
16.00 – 16.30	Break
16.30 – 18.00	**Session 10: "Wet biomarkers and imaging: Update on large studies and relevance for DMOAD development: OAI, FNIH, APPROACH"**
16.30 – 17.30	Kent Kwoh, David Hunter, Anne Christine Bay-Jensen, Niti Goel (Trialspark), Moon Jong Noh (Kolon TissueGene) Moderator: Philip Conaghan
17.30 – 18.00	Panel discussion
18.00 – 18.30	**Adjourn and invitation to IWOAI 2024: Ali Guermazi (Marrakech, Morocco)**
19.30 – 2.00	Gala dinner at Olympic Museum, Lausanne

Saturday July 1, 2023

9:00 – 19:00	Lake Geneva, Swiss Riviera and Lavaux Vineyard Terraces, UNESCO World Heritage Site

Posters:

Poster #1: Tom Turmezei – The relationship between knee joint alignment, 3-D joint space width and subchondral bone parameters in individuals with radiographic osteoarthritis: A MOST investigation

Poster #2: Jemina Schadow – Systematic review of computed tomography parameters used for the assessment of subchondral bone in osteoarthritis

Poster #3: Andy Wong – Calf muscle fat and frailty as serial culprits in worsening knee symptoms after 5 in women: The 7-year Ambers Cohort Study

Poster #4: Anna Wisser – Comparison of fully automated vs. manual image segmentation for the assessment of articular cartilage T2 relaxation times in KLG 0 knees with and without cartilage damage – On behalf of the OA-BIO Consortium

Poster #5: Felix Eckstein – Cartilage transverse relaxation time (T2) after ACL injury in copers, non-copers and ACL-reconstructed patients and healthy controls

Poster #6: Christoph Salzlechner – Predicting mechanical leg alignment from knee X-ray images by utilizing deep-learning neural networks

Poster #7: Tom Turmezei – A deep learning approach to predicting pain progression in osteoarthritis from 3-D knee joint parameters: A MOST investigation

Poster #8: Jukka Hirvasniemi – MRI-based radiomics for assessment of the infrapatellar fat pad's influence on patellofemoral pain

Poster #9: Marijn Mostert – Dynamic contrast-enhanced MRI of the synovium in knee osteoarthritis: semi-automatic segmentation of synovial subregions and test-retest reliability

Poster #10: Salim Zenkhri – Meniscal extrusion in asymptomatic knees: The 3 mm cutoff must be revisited

Poster #11: Kathryn Stok – A longitudinal imaging protocol for 3D quantitative morphometric analysis of the mouse knee

Poster #12: Hector Lise de Moura – Age-dependence of single- and multi-exponential T2 parameters in knee ligaments and tendons

Poster #13: Signe Brinch – 3-D statistical shape modelling of the distal femur in trochlear dysplasia

Poster #14: Frank Roemer – Low-field MRI of non-traumatic temporomandibular disorders: A comparative study of 0.55T and 1.5T MRI

Poster #15: Neil Segal – Presence and severity of cartilage lesions on weight-bearing CT in comparison with MRI

Poster #16: Luke Johnson - A three-dimensional statistical shape model to describe clinical shape variation of the proximal femur in patients with Legg-Calvé-Perthes Disease deformity

Poster #17: Kathryn Stok – A model-invariant approach for 3D assessment of structural changes in preclinical animal models of OA

Poster #18: Killian Cosendey – Bone cuts and implant placements accuracy in total knee arthroplasty performed with an active robotic system

Poster #19: Tom Turmezei – Where are we with weight-bearing computed tomography in OA research? A poll of attendees at the OARSI 2023 breakfast workshop

Poster #20: Tom Turmezei – The role of MRI in osteoarthritis clinical trial imaging: A poll of attendees at the OARSI 2023 imaging discussion group session

THIS MEETING IS SUPPORTED BY

GOLD SUPPORT

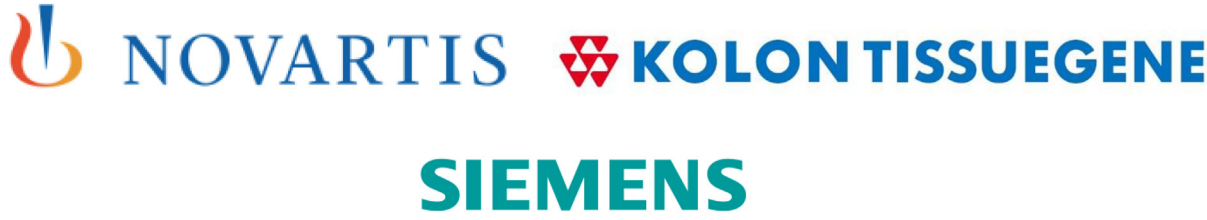

SILVER SUPPORT

BRONZE SUPPORT

Osteoarthritis Imaging 3 (2023) 100093

Contents lists available at ScienceDirect

Osteoarthritis Imaging

journal homepage: www.elsevier.com/locate/ostima

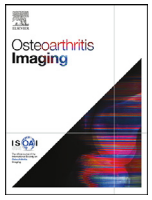

17th International Workshop on Osteoarthritis Imaging: Oral Presentations

CARTILAGE THICKNESS, SUBCHONDRAL BONE MINERAL DENSITY, AND AMBULATORY LOADING ARE CORRELATED IN NON-OSTEOARTHRITIC FEMORAL CONDYLES

P. Margain [1], C. Mourad [1,2], M. Donalisso [1], B.M. Jolles [1], P. Omoumi [1], J. Favre [1]

[1] *Lausanne University Hospital and University of Lausanne (CHUV-UNIL), Lausanne, Switzerland*

[2] *Department of Radiology, Lebanese Hospital Geitaoui, Beirut, Lebanon*

INTRODUCTION: A few studies have reported correlations between structural and functional parameters in healthy knees, and sometimes alterations of these correlations with OA. These observations suggested a new concept where knee OA could be related to a maladaptation between joint features. However, studies analyzing multiple features from different domains simultaneously are missing, which makes it difficult to fully understand the importance of relationships in maintaining joint homeostasis and their role in the development of OA.

OBJECTIVE: To assess the correlations among cartilage thickness (CTh), subchondral bone mineral density (sBMD), and ambulatory loading in non-OA femoral condyles. As commonly done, ambulatory loading was quantified using the peak knee adduction moment during walking (pKAM), which is a proxy for the distribution of load between medial and lateral compartments. To analyze comparable data, CTh and sBMD were expressed as medial-to-lateral (M/L) ratios. Therefore, this study tested the hypothesis that CTh M/L ratios, sBMD M/L ratios, and pKAM are positively correlated in non-OA femoral condyles.

METHODS: This study analyzed a subgroup of 48 young (25.7 ± 4.8 years; 22 males) asymptomatic volunteers with healthy knees enrolled in the HIPPA-compliant IRB-approved Lausanne Knee Study. This study aims at characterizing the structure and function of the knee, with a particular emphasis on the relationships among knee features The study protocol included clinical evaluation, radiographic imaging (weight-bearing Schuss and lateral radiographs of both knees), CT imaging (calibrated by a solid calcium hydroxyapatite-based bone mineral reference phantom) and 3T MRI of one randomly selected knee. 3D gait recordings were performed using a 16-camera motion capture system and force plates.

CTh was obtained by manually segmenting the cartilage and bone on the DESS images, building 3D mesh models of bone and cartilage, and calculating the distance between the models. sBMD was obtained by registering the bone models from the DESS segmentation to the CT images and calculating the average CT intensity in the 3 mm of bone adjacent to cartilage. Mean CTh and sBMD were then calculated for six common regions of interest (ROIs) in the medial and lateral condyles and expressed as M/L ratios. pKAM was obtained following a standard inverse dynamics procedure applied to the marker-based motion capture and force plate recordings. Data processing was done using in-house software and algorithms previously validated. The relationship among CTh M/L ratios, sBMD M/L ratios and pKAM were assessed using Pearson correlation, with an α-level set a priori at 5%.

RESULTS: All statistically significant correlations were positive, indicating larger CTh M/L ratios in knees with larger sBMD M/L ratios and larger pKAM, and vice versa. Specifically, CTh and sBMD M/L ratios were correlated in 5 of the 6 ROIs ($0.31 \leq r \leq 0.53$; $0.001 \leq p \leq 0.035$), CTh M/L ratios in 4 ROIs were correlated with pKAM ($0.29 \leq r \leq 0.33$; $0.021 \leq p \leq 0.047$), and sBMD M/L ratio in one ROI was correlated with pKAM ($r = 0.31$; $p = 0.032$).

CONCLUSION: The hypothesis was supported, confirming the idea that structural and mechanical features of the knee are positively correlated, or adapted, in non-OA knees. This first study to show correlations among bone, cartilage, and mechanical loading provided insight into the functioning of the joint and underlined the potential of evaluating knee health based on relationships among features rather than on individual features in isolation. The analyses in this study will be extended to OA knees in future studies in order to determine the alterations of the relationships between knee features with OA.

SPONSOR: Swiss National Science Foundation, SNSF Grant No 177155.
DISCLOSURE STATEMENT: none to declare.
CORRESPONDENCE ADDRESS: Paul.Margain@chuv.ch.

doi: 10.1016/j.ostima.2023.100094

CAN GAIT PATTERNS IN KNEE OSTEOARTHRITIS PATIENTS BE EXPLAINED BY RADIOGRAPHY- AND MRI-BASED JOINT STRUCTURE?

M.P. Jansen [1], D. Hodgins [2], S.C. Mastbergen [1], M. Kloppenburg [3], F.J. Blanco [4], I.K. Haugen [5], F. Berenbaum [6], F.P.J.G. Lafeber [1], F. Eckstein [7], F.W. Roemer [8], W. Wirth [7]

[1] *UMC Utrecht, Utrecht, Netherlands*
[2] *Dynamic Metrics Limited, Codicote, UK*
[3] *Leiden UMC, Leiden, Netherlands*
[4] *INIBIC-Univ.e de A Coruña, A Coruña, Spain*
[5] *Diakonhjemmet Hosp., Oslo, Norway*
[6] *Sorbonne Univ. & AP-HP Saint-Antoine Hosp, Paris, France*
[7] *Paracelsus Med. Univ, Salzburg, AT & Chondrometrics GmbH, Freilassing, Germany*
[8] *University of Erlangen, Erlangen, Germany & Boston University, Boston, MA, USA*

INTRODUCTION: Patients with knee OA are known to display some alterations in function, particularly gait. While gait alterations are often considered to be the result of knee pain, we here explore whether they are potentially due to structural joint characteristics as well, as measured from radiographs or MRI.

OBJECTIVE: To analyze whether 1) baseline gait patterns can be explained by baseline joint structure and 2) longitudinal gait alterations can be predicted by baseline joint structure in patients with knee OA.

METHODS: IMI-APPROACH recruited 297 patients with clinical knee OA at 5 sites in Europe. At baseline and two year follow-up, full gait kinematic data was collected from all participants using the GaitSmart® system (Dynamic Metrics Limited, Codicote, UK). The measures included were range of motion (ROM) of the hip, thigh, knee in swing phase, knee in stance phase, and calves, of the index leg in the sagittal plane. Stride duration and speed were included as well. The GaitSmart parameters were compared between baseline and two years with paired t-tests.
Radiographs and MRI scans of the index knee were acquired for evaluating joint structure, including KLG at baseline. Based on these, knees were divided in those with (KLG≥2) and without radiographic OA (ROA; KLG≤1). From the radiographs, the minimum JSW, FT angle, mean whole-joint subchondral bone density (SBD), and total whole-joint osteophyte area were determined. From the MRI scans, mean whole-joint FT cartilage thickness (FTC) was determined as well as MOAKS scores for synovitis, effusion, meniscal extrusion and meniscal tear. For the meniscal parameters, the maximum score across all regions was used.
For the comparisons of gait with joint structure, principal component analyses (PCA) was performed on the gait parameters first, to discover underlying domains. To analyze how joint structures explain gait or gait changes over two years, univariate linear regression models were applied, with each of the discovered GaitSmart domains as a dependent variable All structural parameters, and in addition age, sex and BMI, were included as independent variables in a stepwise backwards regression model; models were corrected for presence of contralateral ROA. Sensitivity analyses were performed in addition, including WOMAC pain in the models. Analyses were not corrected for multiple testing.

RESULTS: Of 271 participants with baseline GaitSmart and imaging data, 149 (55%) had ROA. 205 participants (109 ROA) had two-year data. Patients with ROA had significantly lower baseline ROM of the thigh, calf, and knee in the swing and stance phase (all $p<0.014$). Over a two-year observation period, only knee ROM in swing phase decreased significantly for both groups (both $p<0.033$). PCA identified two gait domains: upper leg (speed, duration, thigh ROM and hip ROM), and lower leg (knee ROM in stance and swing, calf ROM).
At baseline, higher BMI was associated with worse upper leg function in patients with ROA, while there were no significant associations with upper leg measures for those without ROA (Table 1). For lower leg gait, female sex and higher SBD were associated with worse gait (i.e. smaller ROM) in participants without ROA, while in those with ROA, these included female sex, higher BMI and increased osteophyte size, both models with an R^2 of 0.14, indicating 14% of gait variability could be explained by the included parameters.
Longitudinally, higher BMI was associated with increased lower leg gait deterioration in participants with ROA, although with a small R^2 of 0.04, whereas no statistically significant associations were observed for change in lower leg gait in participants without ROA, or for change in upper leg gait for either group.
None of the other structural parameters (JSW, FT angle, SBD, MOAKS scores, FTC) significantly contributed to any of the regression models. Adding WOMAC pain to the models did not change results, except for baseline lower leg gait in participants without ROA, where age additionally negatively contributed and the R^2 increased from 0.14 to 0.24.

CONCLUSION: Radiographic joint structure partially explained lower leg gait in patients with clinical knee OA, but could not predict two-year changes in gait. Parameters indicating more severe OA (higher SBD, larger osteophytes) were generally associated with more impaired gait, providing some (statistically significant) association between OA symptoms (gait) and joint structure, independent from pain.

SPONSOR: EU/EFPIA (APPROACH grant n° 115770).
DISCLOSURE STATEMENT: FE, WW: Chondrometrics GmbH; FWR: BICL
CORRESPONDENCE ADDRESS: m.p.jansen-36@umcutrecht.nl.

Table 1: Linear regression models with baseline characteristics and joint structure parameters associated with gait.

	Without ROA		With ROA	
Gait domain	Variables	R^2	Variables	R^2
Baseline				
Upper leg	-	-	BMI (β=-0.293; p<0.001)	0.09
Lower leg	Sex (β=0.35; p<0.001) SBD (β=-0.28; p=0.003)	0.14	Sex (β=0.24; p=0.003) BMI (β=-0.20; p=0.010) Osteophytes (β=-0.27; p=0.001)	0.14
Two-year changes				
Upper leg	-	-	-	-
Lower leg	-	-	BMI (β=-0.25; p=0.012)	0.04

ROA: radiographic OA, SBD: subchondral bone density.

doi: 10.1016/j.ostima.2023.100095

WEIGHT BEARING 3-D JOINT SPACE WIDTH DISTRIBUTION AT THE KNEE VARIES ACCORDING TO LOCATION AND EXTENT OF MENISCAL EXTRUSION: A MOST INVESTIGATION

S.E. Ghobrial [1], C.J. Tonkin [2], G.M. Treece [3], A.H. Gee [3], K.E.S. Poole [4], M.C. Nevitt [5], J.A. Lynch [5], N.A. Segal [6], T.D. Turmezei [7]

[1] *Royal College of Surgeons of Ireland, Ireland*
[2] *Annapolis Community Health Centre, Annapolis Royal, NS, Canada*
[3] *University of Cambridge, Cambridge, UK*
[4] *NIHR Biomedical Research Centre at Cambridge University Hospitals NHS Foundation Trust*
[5] *University of California San Francisco, San Francisco, CA, USA*
[6] *University of Kansas Medical Center, Kansas City, KS, USA*
[7] *Norfolk and Norwich University Hospital, Norwich, UK*

INTRODUCTION: Quantitative 3-D measurement of joint space width (JSW) from weight bearing computed tomography (WBCT) allows analysis of knee tibiofemoral compartments in a loaded stance without subregional constraints on analysis. The relationship between 3-D JSW distribution and meniscal extrusion is yet to be established.

OBJECTIVE: To demonstrate topographic variations in 3-D JSW distribution at the knee derived from WBCT imaging data according to meniscal extrusion location and extent.

METHODS: WBCT knee imaging was acquired at the 144-month visit of the Multicenter Osteoarthritis Study (MOST). A subset of individuals had medial and lateral meniscal extrusion grading according to the MRI Osteoarthritis Knee Score to identify medial extrusion of the medial meniscus (MMmed), anterior extrusion of the medial meniscus (MMant), anterior extrusion of the lateral meniscus (LMant), and lateral extrusion of the lateral meniscus (LMlat). The extent of extrusion was graded as 0: <2 mm; 1: 2 to 2.9 mm, 2: 3 to 4.9 mm; and 3: >5 mm. After semi-automatic segmentation of 663 baseline knees, joint space mapping was performed to create 3-D JSW maps for each knee registered to a template surface. Statistical parametric mapping (SPM) was performed using a general linear model to test the dependence of 3-D JSW distribution on each of meniscal extrusion type in turn. SPM results were plotted on the canonical joint surface, with unmasked regions demonstrating the topographic difference in JSW for each increment in extrusion score.

RESULTS: 568 knees from 330 participants had meniscal extrusion grading available. Participants (178 female) had mean ± SD age 62.0 ± 9.3 years, body mass 82.2 ± 17.4 kg, height 170 ± 9.5 cm, and BMI 28.3 ± 4.8 kg/m^2. Analysed knees were bilateral for 238 participants and unilateral for 92 participants. For MMmed (cohort score range 0-3), the central-to-posterior medial compartment had significantly lower JSW by up to 0.4 mm for each increment in meniscal extrusion grade. Both MMmed and MMant (score range 0-3) were associated with a small region of similarly significantly lower JSW along the medial margin of the lateral compartment, but also with significantly greater JSW at the anterior medial compartment of up to 0.6 mm per grade. The posterior medial joint space was significantly narrower (up to 3 mm) comparing knees with LMant scores of 0 vs 1. This same magnitude of narrowed JSW was detected along the periphery of the lateral joint space comparing grades in the lateral tibiofemoral compartment, but this was not statistically significant. LMlat (score range 0-2) was associated with a trend for greater reduction in JSW in the central lateral compartment of up to 0.5 mm per grade, but this was not statistically significant. Direction of meniscal extrusion is represented by the black arrowhead in the figure.

CONCLUSION: Both medial and anterior extrusion of the medial meniscus are associated with significant reduction in JSW at the medial margin of the lateral joint space and widening of the anterior margin, likely from a posteromedial shift of the femoral condyles with respect to the tibia. Medial extrusion of the medial meniscus is also associated with narrowed JSW in the central to posterior medial joint space, likely as a direct effect of the loss of meniscal hoop tension. Anterior (but not lateral) extrusion of the lateral meniscus is associated with significantly lower JSW in the posterior medial joint space. These findings confirm that the extent and location of meniscal extrusion are key factors in weight bearing 3-D JSW distribution.

SPONSOR: National Institutes of Health, University of Kansas (R01AR071648), University of Iowa (U01AG18832) and University of California-San Francisco (U01AG19069).
DISCLOSURE STATEMENT: NS is a consultant for Integra BioLife, Trice Medical and Pacira Biosciences. TT has been a consultant for Curvebeam AI.
ACKNOWLEDGEMENT: The authors would like to thank participants and staff of the MOST study.
CORRESPONDENCE ADDRESS: tom@turmezei.com.

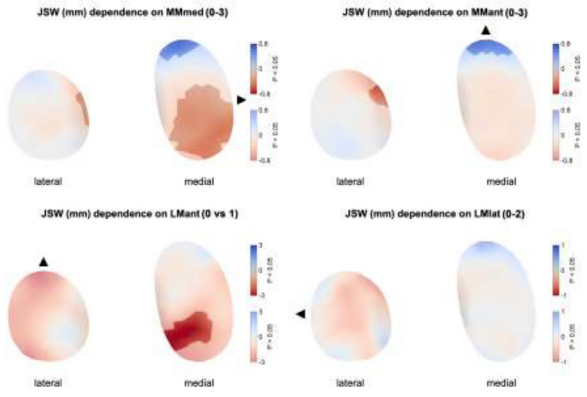

doi: 10.1016/j.ostima.2023.100096

EVALUATION OF METABOLIC RESPONSE IN BONE MARROW LESIONS AFTER EXERCISE IN RELATION TO CHANGES IN ADJACENT CARTILAGE T2 VALUES

A. Goyal [1], Y. Vainberg [1], J. Asay [1], M. Yoon [1], F. Kogan [1]

[1] *Department of Radiology, Stanford University, Palo Alto, CA, USA*

INTRODUCTION: Patellofemoral pain syndrome (PFPS) is one of the most common causes of anterior knee pain in active populations. Due to its multifactorial nature, patellofemoral pain is hard to diagnose and treat. Increased stress in the subchondral bone is associated with PFPS and is correlated to elevated bone remodelling. [^{18}F]NaF PET-MR imaging can localize regions of elevated bone remodelling and provide information about the metabolic processes involved (1, 2). Further, [^{18}F]NaF uptake changes after exercise, thus showing that it is sensitive to changes in bone physiology resulting from acute bone loading (3, 4). For cartilage, T2 relaxation times have been used to study cartilage hydration and microstructure changes after exercise. While some studies have observed a decrease in T2 times after exercise, changes are usually transient and have largely been evaluated in the context of healthy subjects (5). An early sign of persistent abnormal mechanical stress is Bone Marrow Lesions (BMLs), which are strongly associated with pain and structural disease progression. We aimed to reproduce prior work which has shown that acute loading results in a large physiological response in bone regions with BMLs. Further, we wanted to explore if there is breakdown of the cartilage microstructure, either at baseline or in response to loading in cartilage regions adjacent to BMLs. The purpose of this study is to detect changes in the functional response of the knee joint to loading using [^{18}F]NaF PET-MR imaging after a stair-climbing exercise in subjects with unilateral patellofemoral pain.

OBJECTIVE: The aims of this feasibility study are 1) to detect acute loading-induced changes in [^{18}F]NaF uptake in bone regions with BMLs and 2) compare consequent T2 values in the cartilage adjacent to BMLs at baseline and in response to loading.

METHODS: 4 subjects (3 F, aged 39.5±15.0 years, BMI 26.1±5.9 kg/m^2) with unilateral knee pain and BMLs (3 in patella, 1 in femur) underwent two consecutive 30-min [^{18}F]NaF PET/MRI scans of both knees, at baseline and then repeated after a stair-climbing exercise [112 stairs, up and down]. Bone metabolic activity was quantified by calculating maximum standardized uptake values (SUV_{max}) in areas of BMLs in the painful leg and the corresponding region in the contralateral leg. T2 maps were calculated from quantitative DESS images [TE(1,2)=6.04, 30.44 ms] in the cartilage regions adjacent to the BMLs and in the same regions in the contralateral leg. Segmentations of cartilage were done manually in MATLAB, while SUV_{max} in BMLs was calculated using ROIs drawn in Horos. Pre- and post-exercise changes in SUV_{max} and T2 values were compared to account for loading-induced response in both metabolic and structural parameters in painful vs healthy knees.

RESULTS: Increased [^{18}F]NaF uptake was observed post-exercise in areas with BMLs (as compared to contralateral leg regions), confirming that PET findings correspond to structural changes observed in MRI (Fig-1). The average SUV_{max} values increased from 6.35±3.98 to 10.49±5.42 in the painful leg and from 1.71±1.96 to 4.04±3.21 in the contralateral leg after exercise. The average T2 relaxation times increased from 30.61±1.87 ms to 31.61±1.55 ms in the painful leg and from 27.17±2.73 ms to 27.65±2.29 ms in the contralateral leg (Fig-2). The mean change in SUV_{max} due to exercise was 4.15±2.42 in the BML vs 2.34±2.06 in the contralateral leg. In adjacent cartilage, a mean change in T2 values of 1.01±1.45 ms in the BML region of the painful leg and 0.47±0.48 ms in the contralateral leg was observed.

CONCLUSION: In this feasibility study, [^{18}F]NaF PET-MR showed acute loading-induced changes in BMLs, with a 2-fold increase in SUV_{max} in the painful leg vs the contralateral leg. While there seemed to be a higher cartilage T2 in regions adjacent to BMLs compared to the contralateral leg, the change induced by exercise was small.

REFERENCES

1. Czernin J, Satyamurthy N, Schiepers C. Molecular mechanisms of bone 18F-NaF deposition. J Nucl Med. 2010;51(12):1826-9.
2. Kogan F, Fan AP, McWalter EJ, Oei EHG, Quon A, Gold GE. PET/MRI of metabolic activity in osteoarthritis: A feasibility study. J Magn Reson Imaging. 2017;45(6):1736-45.
3. Watkins LE, Haddock B, MacKay JW, Baker J, Uhlrich SD, Mazzoli V, et al. [(18)F]Sodium Fluoride PET-MRI Detects Increased Metabolic Bone Response to Whole-Joint Loading Stress in Osteoarthritic Knees. Osteoarthritis Cartilage. 2022.
4. Haddock B, Fan AP, Uhlrich SD, Jorgensen NR, Suetta C, Gold GE, et al. Assessment of acute bone loading in humans using [(18)F]NaF PET/MRI. Eur J Nucl Med Mol Imaging. 2019;46(12):2452-63.
5. Crowder HA, Mazzoli V, Black MS, Watkins LE, Kogan F, Hargreaves BA, et al. Characterizing the transient response of knee cartilage to running: Decreases in cartilage T2 of female recreational runners. J Orthop Res. 2021;39(11):2340-52.

SPONSOR: General Electric Healthcare, Wu Tsai Human Performance Alliance Fellowship, NIH (R01 AR077604, AR079431, AR074492 & R21EB030180)
DICLOSURE STATEMENT: Research Support from GE Healthcare
ACKNOWLEDGMENT: Dawn Holley and Kim Halbert for their support with PET/MRI.
CORRESPONDENCE ADDRESS: agoyal5@stanford.edu.

Figures can be found on next page.

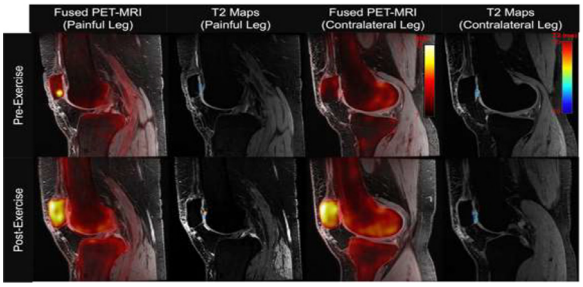

Figure 1. Representative images from a 53-year-old subject with unilateral knee pain are shown above. Fusion PET-MR images are shown for the painful leg (column 1) and the contralateral leg (column 3) along with combined qDESS and T2 maps for the painful leg (column 2) and the contralateral leg (column 4). The top panel showcases the pre-exercise images while the bottom panel shows the post-exercise images.

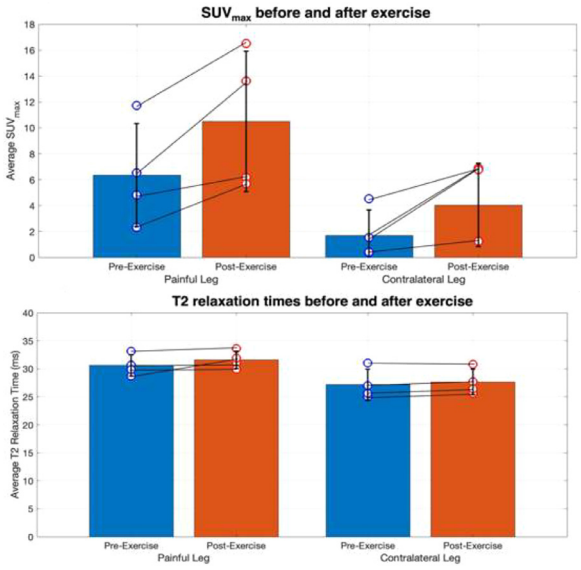

Figure 2. Average values of SUV_{max} (top) and T2 relaxation times (bottom) are reported for 4 subjects with unilateral knee pain and BMLs, for both the painful and contralateral legs, before and after a stair-climbing exercise.

doi: 10.1016/j.ostima.2023.100097

THE SPATIAL CORRELATION BETWEEN CARTILAGE THICKNESS AND SUBCHONDRAL BONE MINERAL DENSITY INVERSES WITH INCREASING OA SEVERITY

P. Omoumi [1], P. Margain [1], H. Babel [1], T.P. Andriacchi [2], B.M. Jolles [1], J. Favre [1]

[1] *Lausanne University Hospital and University of Lausanne (CHUV-UNIL), Lausanne, Switzerland*
[2] *Stanford University, Stanford, CA, USA*

INTRODUCTION: While several properties of bone and cartilage have been extensively studied with respect to knee osteoarthritis (OA), little is known about the relationship between these tissues.

OBJECTIVE: To assess the spatial correlation between cartilage thickness (CTh) and subchondral bone mineral density (sBMD) in OA femoral condyles of varying disease severities.

METHODS: CT arthrograms of 60 knees (from 27 men, 33 females, 64.3 ± 9.1 years old) with various severities of medial compartment OA were analyzed in this IRB-approved study (26 K/L2, 25 K/L3, and 9 K/L4). CT images were manually segmented to reconstruct 3D mesh models of the femoral bone and cartilage. 3D CTh maps were calculated based on the distance between bone and cartilage models, and 3D sBMD maps were obtained by averaging the CT intensity in the 3mm of subchondral bone adjacent to cartilage. The spatial correlation between CTh and sBMD maps was quantified for the medial and lateral condyles of each knee using a statistical index ranging between –1.0 (CTh is thinner where sBMD is denser) and 1.0 (CTh is thicker where sBMD is denser). For comparison with standard methods described in the literature, the average CTh and sBMD were calculated for the load-bearing region of the medial and lateral condyles. Wilcoxon rank-sum tests were used to compare the spatial correlations and the average CTh and sBMD between the three OA severity groups. The level of significance was set at 5%, with Bonferroni correction for multiple comparisons.

RESULTS: In the medial compartment, the spatial relationship between CTh and sBMD progressively shifted from being positively correlated in K/L2 knees to negatively correlated in K/L4 knees, with statistically significant differences among the three groups (Table 1). The average CTh and sBMD showed irregular patterns, with differences among groups rarely reaching statistical significance. No statistically significant difference was observed in the lateral compartment.

CONCLUSION: The spatial correlation supported the concept of bone and cartilage working as a functional unit and the alteration of this functional unit with OA. The positive correlation in early disease suggests a link with mechanical loading, where cartilage is thicker and bone denser in areas of larger mechanical stimulation. Interestingly, evaluating the CTh-sBMD relationship instead of CTh or sBMD individually showed more consistent patterns across the stages of the disease.

SPONSOR: Swiss National Science Foundation, SNSF Grant No 177155.
DISCLOSURE STATEMENT: None to declare.
CORRESPONDENCE ADDRESS: patrick.omoumi@chuv.ch.

Table 1: Spatial correlation between CTh and sBMD, as well as mean CTh and sBMD in the load-bearing regions. Data are presented as median [1st quartile, 3rd quartile]. The superscripts indicate K/L groups (K/L2, 3 or 4) with statistically significant differences ($p<0.017$).

	Spatial correlation		CTh (mm)		sBMD (HU)	
	Medial	Lateral	Medial	Lateral	Medial	Lateral
K/L 2 (n=26)	0.57 [0.31, 0.71]^{3,4}	0.58 [0.40, 0.68]	1.31 [1.13, 1.72]^{3,4}	1.27 [1.07, 1.52]	1670.7 [1591.3, 1705.3]^{4}	1514.5 [1468.4, 1581.1]
K/L 3 (n=25)	0.05 [-0.36, 0.42]^{2,4}	0.56 [0.35, 0.60]	0.86 [0.66, 1.29]^{2}	1.28 [0.93, 1.50]	1657.1 [1609.5, 1741.1]^{2}	1481.7 [1427.4, 1525.3]
K/L 4 (n=9)	-0.52 [-0.68, -0.18]^{2,3}	0.56 [0.18, 0.58]	0.75 [0.60, 0.83]^{2}	1.64 [1.19, 1.71]	1730.6 [1684.0, 1872.2]^{2}	1477.9 [1398.5, 1540.9]

doi: 10.1016/j.ostima.2023.100098

SUBCHONDRAL BONE MINERAL DENSITY: WHAT TO DO WHEN YOU DON'T HAVE ACCESS TO QCT

E. Ha [1,2], J. Brooks [1], P.M. Smith [1], A.K. Wong [1,2]

[1] *Dalla Lana School of Public Health, University of Toronto, Toronto, ON, Canada*
[2] *Joint Department of Medical Imaging, University Health Network, Toronto, ON, Canada*

INTRODUCTION: Bone marrow lesions and osteophytes are established characteristics of knee OA and are correlates of knee pain. However, the link between subchondral bone mineral density (BMD) and knee OA and pain is less clear. This may, in part, be due to the challenge quantifying subchondral BMD due to limited access to affordable and low-dose computed tomography (CT). Moreover, while structural properties could be estimated from magnetic resonance (MR) images, they are unable to yield BMD measures. Although in many cases CT and MR imaging is not feasible, potential correlates of subchondral BMD often collected as part of the standard of care could be used to represent its conceptual unity. Leveraging previous work that has already developed a latent subchondral BMD construct using established correlates (i.e., total hip BMD, previous fractures, previous falls, and anthropometrics) in a smaller cross-sectional study (N=50), the objective of this study was to re-develop and externally validate a latent subchondral BMD construct, and determine its cross-sectional and longitudinal association with knee pain.

OBJECTIVES: 1) Re-model a subchondral BMD latent construct in a larger cohort, 2) externally validate the subchondral BMD latent construct against directly measured subchondral BMD, and 3) determine the association between subchondral BMD and knee pain at baseline and 5-years later.

METHODS: Data from the Bone Ancillary Study of the OAI (N=1,068) was used to re-develop and validate the subchondral BMD latent construct. Data from the United Kingdom (UK) Biobank (N=12,790) was used to externally validate the latent construct against directly-measured subchondral BMD from DXA, and to determine its association with knee pain at baseline and 5-years later.
Latent subchondral BMD (g/cm^2) was re-developed in the OAI using confirmatory factor analysis and model fit was assessed using absolute (Standardized Root Mean Square Residual<0.08), parsimonious (Root Mean Square Error of Approximation<0.08), and incremental (Comparative Fit Index, Tucker Lewis Index≥0.95) fit indices. We repeated the same procedure using UK Biobank data and externally validated it against medial and lateral BMD obtained by knee DXA (Lunar Prodigy Advance, GE Lunar Corp., Madison WI, USA) with investigational knee (enCORE 2007 Version 11.20.068) or spine analysis software. Knee pain was determined based on dichotomized responses to the Knee injury and Osteoarthritis Outcome Score (KOOS) pain subscale (≥80) and self-reported experience of knee pain (yes/no) for OAI and UK Biobank, respectively. Structural equation modeling with a full information maximum likelihood estimation was used to determine the relationship between latent subchondral BMD with knee pain using a log-link function, controlling for age, ethnicity, smoking status, alcohol use, physical activity, comorbidities, and medications (e.g., bisphosphonates, glucocorticoids). Risk ratios were reported with 95% confidence intervals.

RESULTS: The subchondral BMD latent construct had good model fit (benchmarks), as assessed by absolute (0.04), parsimonious (0.08) and incremental (0.96) fit indices in both OAI and UK Biobank cohorts. The directionality and effect size of coefficients for both models were similar, indicating that the latent construct modeled in both cohorts was theoretically consistent. In addition, the subchondral BMD latent construct was significantly correlated with directly measured subchondral areal BMD in the medial (B=0.940, SE=0.024, p<0.001) and lateral (B=0.885, SE=0.027, p<0.001) compartments by DXA. Using the latent construct in the UK Biobank, each standard deviation higher subchondral BMD was significantly associated with 2.28 (1.87,3.58) times higher risk of having knee pain at baseline and 1.91 (1.34,2.72) times higher risk of having knee pain 5-years later, adjusting for confounders.

CONCLUSIONS: In the absence of quantitative CT imaging, subchondral BMD can be represented as a reflective latent construct comprised of indicator variables commonly collected as part of standard of care for older adults. In addition, higher BMD was associated with acute and long-term knee pain. Overall, this study offers a unique and accessible method to estimate subchondral BMD for those with suspected knee OA, and demonstrates its clinical sensitivity to knee pain.

SPONSOR: EH is supported by an Arthritis Society PhD Salary Award 21-0000000100. AKOW is supported by a Ken Smith Arthritis Society Stars Career Award 21-035. This project was supported by CIHR Project Grants PJT-166012 and 156274.
DICLOSURE STATEMENT: The authors have no conflicts of interest to declare.
ACKNOWLEDGMENT: The Osteoarthritis Initiative (OAI) is a public-private partnership comprised of five contracts (N01-AR-2-2258; N01-AR-2-2259; N01-AR-2-2260; N01-AR-2-2261; N01-AR-2 2262) funded by the National Institutes of Health, a branch of the Department of Health and Human Services, and conducted by the OAI Study Investigators. This research has been conducted using the UK Biobank Resource under Application Number 76691.
CORRESPONDENCE ADDRESS: andy.wong@uhn.ca.

doi: 10.1016/j.ostima.2023.100099

PREDICTING TROCHLEAR DYSPLASIA FROM 3-D CORTICAL BONE AND SHAPE PARAMETERS

S. Brinch [1], P. Hansen [1], F.H. Linden [1], M. Krogsgaard [1], P. Lavard [1], M. Boesen [1], K.E.S. Poole [2], T.D. Turmezei [3]

[1] *Bispebjerg and Frederiksberg Hospital Copenhagen, Denmark*
[2] *NIHR Biomedical Research Centre at Cambridge University Hospitals NHS Foundation Trust, Cambridge, UK*
[3] *Norfolk and Norwich University Hospital, Norwich, UK*

INTRODUCTION: Abnormal shape of the distal femur is the defining characteristic of trochlear dysplasia (TD), leading to abnormal contact forces and early degeneration at the patellofemoral joint, as well as an increased risk of lateral patellar dislocation. In severe clinical cases treatment with various surgical techniques aims to normalise trochlea morphology and medialise patellofemoral knee forces.

OBJECTIVE: 1) To evaluate differences in 3-D bone distribution at the distal femur between normal individuals and TD; and 2) to demonstrate how these parameters discriminate between these two groups.

METHODS: 20 healthy volunteers without radiological signs of TD and 20 individuals with Dejour type B or D dysplasia and patellar instability were recruited, both groups aged 18-45 years with no history of arthritis, connective tissue disease, or traumatic knee conditions requiring physical or operative treatment. The TD group were awaiting surgical trochleoplasty after failing conservative treatment. With a 50:50 proportion of left and right knees in the TD group, a random matched 50:50 split of left and right knees were chosen for comparison in the healthy volunteers. Weight bearing computed tomography (WBCT) of the target knee in 20°of flexion using a Carestream Onsight© scanner, with full imaging details. The distal femur was semi-automatically segmented using inhouse software Stradview. A canonical distal femur was registered to each individual to build a 3-D statistical shape model from the registrations using inhouse software wxRegSurf. Cortical bone mapping was also performed on all femurs to measure 3-D distribution of cortical thickness (CTh) and trabecular attenuation (TA), which were then transferred to the canonical femur. Statistical parametric mapping (SPM) tested the dependence of the 3-D distribution of the bony parameters on the presence of TD. Mean values were taken from within the largest SPM significant region of interest (ROI) for CTh and TA, and used along with sex, age and shape mode coefficients in receiver operating characteristic analysis to deliver area under the curve (AUC) in a leave-one-out cross-validation classifier predictive model for TD.

RESULTS: Mean (± SD) age of all participants was 30.5 ± 5.2 years, with an even split of sexes in both groups. SPM showed significantly thicker CTh in the TD group along the outer lateral margin of the lateral trochlea by up to 0.6 mm (left figure, unmasked blue patch). TA was significantly lower by up to 100 units in the TD group at the medial trochlea region (right figure, unmasked red patch). Shape mode 3 had already been demonstrated in another study as the only mode to be significantly related to TD (not shown). AUC (95% CI) in prediction of TD with age + sex was 0.75 (0.59-0.88), for shape mode 3 was 0.84 (0.69-0.94), for the TA ROI mean was 0.84 (0.68-0.95), and the CTh ROI mean was 0.97 (0.87-1).

CONCLUSION: Trochlear dysplasia cases selected for surgical treatment have a 3-D distribution of cortical bone thickness and density around the distal femur significantly different to normal individuals in patterns that suggest abnormal shift of contact forces laterally. Cortical bone thickness was an excellent classifier, followed by shape mode 3. These 3-D derived parameters should be further evaluated in separate populations. Since morphological normalisation of the trochlea groove and medialisation of patellofemoral joint forces is the goal of surgical correction to protect the joint for early degeneration, monitoring of these bone and shape parameters seems promising and may be useful to monitor in long term post-surgical follow-up.

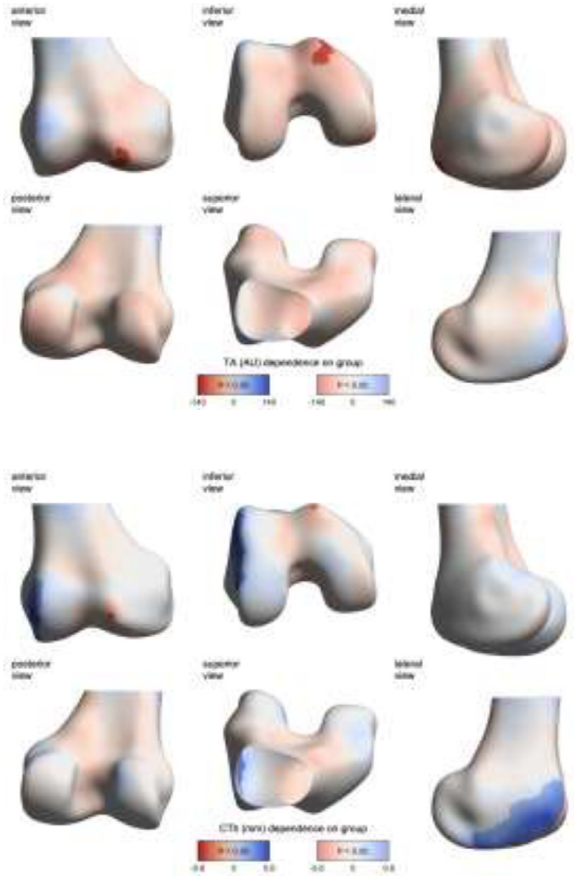

SPONSOR: Department of Radiology and Section for Sports Surgery, Bispebjerg and Frederiksberg Hospital, Denmark.
DISCLOSURE STATEMENT: TT has been a consultant for Curvebeam AI.
ACKNOWLEDGEMENT: None.
CORRESPONDENCE ADDRESS: signe.brinch@regionh.dk.

doi: 10.1016/j.ostima.2023.100100

NEURAL SHAPE MODELS ENCODE BONE SHAPE FEATURES NOT CAPTURED BY STATISTICAL SHAPE MODELS

A.A. Gatti [1,2], F. Kogan [1], G.E. Gold [1], S.L. Delp [1], A.S. Chaudhari [1]

[1] *Stanford University, Stanford, CA, USA*
[2] *NeuralSeg Ltd., Hamilton, ON, Canada*

INTRODUCTION: The recently proposed B-Score uses statistical shape models (SSM) to represent femur shape as a scalar value similar to the osteoporosis T-score. The B-Score quantifies OA bone shape and is defined as the distance from the mean healthy bone shape (B-Score=0) to the mean OA bone shape, where 1-unit is equal to the standard deviation of the healthy B-Scores [Bowes et al. 2021]. However, SSMs require finding matching points between subjects' femurs, and learn linear features, potentially limiting their ability to capture physiologic shape. Neural Shape Models (NSM) have been shown to represent object surfaces without requiring matching points between subjects using non-linear neural networks. Here, we use NSMs to reconstruct bone shapes and use these features to encode information about OA.

OBJECTIVE: To compare B-Scores learned from a NSM and a SSM.

METHODS: Data from the 24 and 48-month visit of the right knee of 562 participants enrolled in the OAI were included (335 females, mean age 63.5(8.9) years, BMI 30.8(4.8) kg/m^2, and KLG counts of 0=35, 1=79, 2=269, 3=167, 4=12). **Fig 1** depicts the data analysis pipeline; sagittal DESS MRIs were segmented using a CNN and femur surfaces were extracted using marching cubes. The NSM and SSM models were fit to the 24-month data of half the subjects. The NSM and SSM learned feature spaces were 256 and 90 dimensions, respectively. Fitted models were used to obtain shape features from the 48-month data of all subjects. Finally, NSM and SSM B-scores were computed to assess how the NSM and SSM feature spaces affect the learned B-scores. To determine whether each model has the capacity to represent the other's B-Score, the amount of variance in the B-Score explained by the feature space of the other model was calculated using linear regression. Since the B-Score produces a range of scores within each KL grade, the distribution of B-Scores per KLG were plotted. The odds ratios (OR) for knee pain and TKA were computed between B-Score quartiles (1 vs 2, 3, 4) in OA knees (KLG >=2). Pain was defined using previous criteria [Morales et al. 2021].

RESULTS: The NSM explained 82% of the variance in SSM B-score, yet the SSM only explained 55% of the variance in NSM B-score (**Fig 2**). **Fig 3** shows the distribution of B-Scores per KLG demonstrating that within a KLG there is a range of B-Scores providing more specific shape information. **Table 1** includes ORs for pain and TKA between quartile 1 and all other quartiles for both B-scores.

CONCLUSION: The NSM learned non-linear shape features that encode clinically relevant information about OA without a need to find matching points between subjects. The NSM and SSM performed similarly for predicting clinical outcomes. The NSM had a broader range of B-scores between KLGs primarily driven by a large difference between KLG 0 and 1, potentially indicating greater expressivity for the NSM. The SSM did a poor job predicting the NSM B-score, which was particularly evident in KLG 0 knees where the SSM was unable to reproduce NSM B-Scores in the healthy range (**Fig 2**). Small samples of KLG 0 and 4 knees likely limit both SSM and NSM B-Scores. More data from the OAI will likely enable the more flexible NSM to learn more expressive representations particularly in under-represented sub-samples, like KLG 4 knees. Results from this study indicate that the NSM captures novel bone shape information that cannot be learned by the SSM.

SPONSOR: NIH (R01 AR077604, EB002524, AR079431, P41 EB027060, and K24 AR062068), Wu Tsai Human Performance Alliance, CIHR Postdoctoral Fellowship.
DICLOSURE STATEMENT: A.S. Chaudhari has provided consulting services to Subtle Medical; and is a shareholder in Subtle Medical, LVIS Corp, and Brain Key
CORRESPONDENCE ADDRESS: aagatti@stanford.edu.

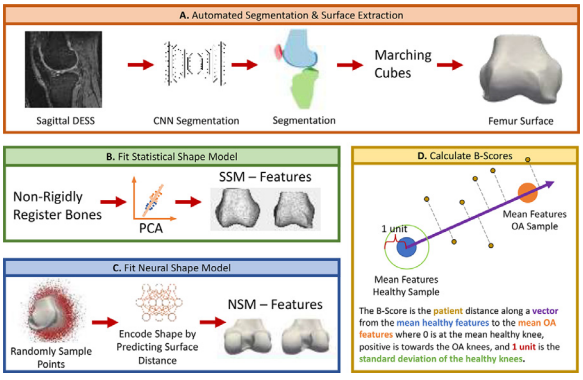

Figure 1. Overview of the methods. The SSM (B) and NSM (C) were fit to 281 subjects from the 24-month visit of the OAI. These models were then used to extract features from all 562 subjects at the 48-month visit; the extracted features were used to calculate the B-Scores (D).

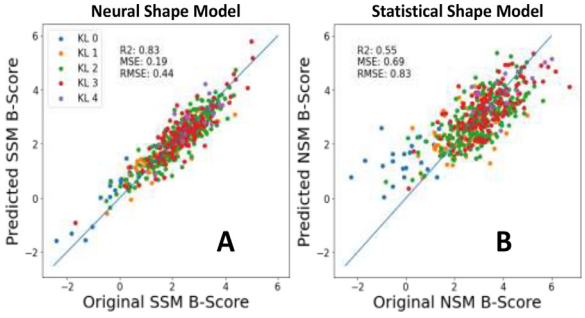

Figure 2. Plots of the SSM B-Score predicted by the NSM vs. the original SSM B-Score (A) and the NSM B-Score predicted by the SSM vs. the original NSM B-Score (B). (A) shows that the NSM is able to predict the whole range of SSM B-Scores while (B) shows that the SSM does not contain information necessary to accurately predict low NSM B-Scores in the healthy range (-2 to 2).

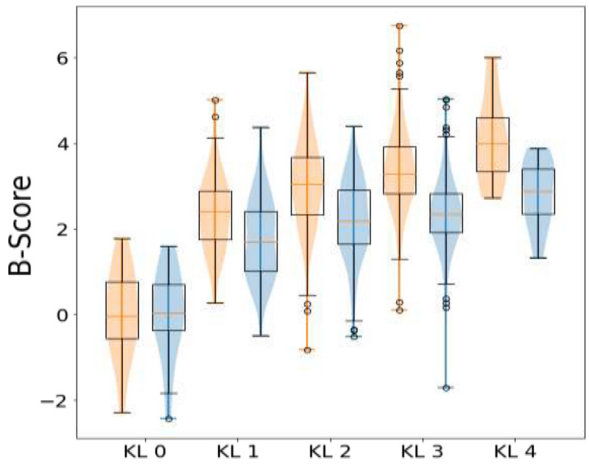

Figure 3. B-Scores per KLG. The distribution of B-Scores per KLG highlights a single KLG has a range of shapes. Orange = NSM, Blue = SSM.

Table 1. ORs and 95% CIs for predicting pain and TKA.

	Quartile 2	Quartile 3	Quartile 4
Pain - NSM	**2.4 (1.0-5.7)**	**4.2 (1.7-10.5)**	**3.4 (1.4-8.3)**
Pain – SSM	2.0 (0.86-4.7)	**3.7 (1.5-9.1)**	**4.9 (1.9-12.4)**
TKA - NSM	1.0 (0.3-3.6)	1.0 (0.3-3.6)	1.7 (0.5-5.2)
TKA – SSM	4.3 (0.9-20.9)	1.5 (0.3-9.4)	**5.5 (1.2-25.6)**

Bold = p<0.05

doi: 10.1016/j.ostima.2023.100101

IMPACT OF WEIGHT LOSS ON KNEE JOINT CARTILAGE MEASURED BY MRI T2 MAPPING IN PATIENTS WITH OSTEOARTHRITIS – AN IMAGING SUB-STUDY OF THE LOSE-IT TRIAL

C.T. Nielsen [1], P. Hansen [1], C.L. Daugaard [2], M. Henriksen [2], H.R. Gudbergsen [3], M.P. Boesen [1], J.U. Nybing [1]

[1] *Department of Radiology, Bispebjerg-Frederiksberg Hospital, Copenhagen, Denmark*
[2] *The Parker Institute, Bispebjerg-Frederiksberg Hospital, Copenhagen, Denmark*
[3] *Department of Public Health, Centre for General Practice, University of Copenhagen, Denmark*

INTRODUCTION: Weight loss can have beneficial effects not only on symptomatic knee OA but perhaps also on structural changes such as cartilage degeneration. T2 mapping is an interesting candidate as an OA imaging biomarker, as it has the potential to detect changes in cartilage composition that precedes macroscopic cartilage damage. Few studies have looked at the association between weight loss and T2 values and have predominately used data from the OAI. They have collectively shown that weight loss is associated with a smaller increase in T2 cartilage values. It is still, to the best of our knowledge, widely unknown how a treatment intervention, such as weight loss, affects T2 values in patients with different radiographic knee OA disease severities.

OBJECTIVE: The purpose of this study was to investigate if change in body mass index (BMI) was associated with change in cartilage T2 values in patients with concomitant overweight or obesity and pre-, mild or moderate knee OA.

METHODS: We included patients with BMI ≥ 27 and KLG 1-3 allocated to the placebo arm of a larger RCT, the LOSE-IT trial. Patients underwent a low-calorie diet for 8 weeks followed by a 52-week weight maintenance period. 3T MRI of the target knee was performed at baseline and week 60. T2 mapping sequence: 3 mm slice thickness, 0.4 × 0.4 in-plane resolution, 160 mm field of view, with a five-echo approach ranging from 13.8 ms to 69.0 ms. The 2nd echo (27.6 ms) was chosen for segmentation due to the best visual cartilage delineation. The cartilage of the medial tibia plateau was manually segmented on sagittal images by a junior doctor with three years of experience in radiology and rheumatology using a commercially available software, Philips IntelliSpace Portal v.11.1 (Philips Medical Systems, The Netherlands). Each segmentation took approximately 10 minutes.

RESULTS: We included 51 patients (KLG 1: n=11, KLG 2: n=21, KLG 3: n=19). The mean weight loss was 11.29 kg (11.5%) (SD ± 7.87, 95% CI: 9.08; 13.50, $p < 0.001$), mean change in BMI was 3.95 kg/m2 (SD ± 2.67, 95% CI: 3.20; 4.70, $p < 0.001$) and mean change in T2 value was 0.60 ms (SD ± 2.16 ms, 95% CI: -1.21; 0.01, $p = 0.052$). Using Spearman's rho no significant correlation was found for change in T2 value and change in BMI, $\rho = 0.133$ (95% CI: -0.156; 0.401, $p = 0.353$). When stratifying by KLG there was a significant correlation between change in T2 value and change in BMI in patients with KLG 3, even after adjusting for multiple analyses by Bonferroni correction, $\rho = 0.628$ (adjusted 95 % CI: 0.123; 0.875, $p = 0.012$,). No significant correlation was found for change in T2 value and change in BMI in KLG 1 and KLG 2. For patients with KLG 3 multiple regression analysis found a significant association between change in T2 value and change in BMI, controlled for gender and age ($R^2 = 0.424$, p=0.036) with a slope, $\beta = 0.573$ (95% CI: 0.193; 0.953, $p = 0.006$), but when adjusting for multiple testing by Bonferroni the p-value became non-significant ($p = 0.108$).

CONCLUSION: We found very little change in cartilage T2 value over 60 weeks with no effect of weight loss on T2 values in the medial tibial cartilage in patients with concomitant overweight or obesity and pre- to moderate knee OA. Even though there was a trend towards an association in patients with moderate knee OA, the observed change in T2 values was below a clinically relevant minimal detectable change. Additionally, the applicability of T2 mapping in patients with more advanced OA disease is still debated.

SPONSOR: The Parker Institute is supported by a core grant from The Oak Foundation (OCAY-18-774-OFIL). The LOSE-IT trial was initiated by the Parker Institute and supported by Cambridge Weight Plan UK and Novo Nordisk A/S. None of the funders influenced the study design, collection, analysis and interpretation of data or writing of manuscripts for publication.
DISCLOSURE: none
CORRESPONDENCE ADDRESS: camilla.toft.nielsen@regionh.dk.

doi: 10.1016/j.ostima.2023.100102

BETWEEN-KNEE DIFFERENCES IN DEEP ZONE T2 ARE GREATER AFTER UNILATERAL ACL INJURY THAN IN HEALTHY CONTROLS

S. Herger [1,2], C. Nüesch [1,2], F. Eckstein [3,4], W. Wirth [3,4], C. Egloff [1,2], A. Mündermann [1,2]

[1] *Department of Orthopaedics and Traumatology, University Hospital Basel, Basel, Switzerland*
[2] *Department of Biomedical Engineering, University of Basel, Basel, Switzerland*
[3] *Institute of Anatomy & Cell Biology, Paracelsus Medical University, Salzburg, Austria*
[4] *Chondrometrics GmbH, Freilassing, Germany*

INTRODUCTION: Cartilage transverse relaxation time (T2) has been reported to be sensitive to OA-related changes in cartilage composition, but no study previously reported reference values for femorotibial (FTJ) cartilage T2 side-to-side differences for persons with or without previous ACL injury. Since articular cartilage extracellular matrix has a layered organization, this study focused on laminar (deep and superficial) T2 cartilage times.

OBJECTIVE: To assess 1) whether laminar cartilage T2 obtained in two different age groups differs between ACL-injured and contralateral knees and 2) whether between-knee differences differ between ACL injured and healthy controls of the two age groups. In addition, we report laminar T2 thresholds for between-knee differences of healthy controls.

METHODS: 85 participants in four groups (20–30 years healthy, $HEA_{20–30}$, n=24; 20–30 years ACL injured, $ACL_{20–30}$, n=23; 40–60 years healthy, $HEA_{40–60}$, n=24; 40–60 years ACL injured, $ACL_{40–60}$, n=14) completed data collection. ACL injured participants had a unilateral ACL injury 2–10 years before inclusion. MRIs of HEA left (HEA_l) and right (HEA_r) or ACL injured (ACL_in) and uninjured (ACL_unin) side were acquired using a quantitative 3D DESS sequence (in plane resolution 0.3125*0.3125mm, slice thickness 1.5mm, resolution 512*512, TR 17 ms, TE1 4.85ms, TE2 9.75 ms, FA 15°). Weight-bearing FTJ cartilage plates were manually segmented by Chondrometrics into deep 50% (.D) and superficial 50% (.S) zones and total (.T) cartilage. Between-knee differences in T2 for the FTJ (dif_FTJ) were computed from T2 means (HEA_l–HEA_r or ACL_in–ACL_unin). Nonparametric Dunn and Conover-Iman tests were used for between-group and between-knee comparisons, respectively. Holm correction was used to adjust for multiple comparisons ($P<0.05$). 80% thresholds for detecting differences between knees were computed from healthy participants as mean(dif_FTJ $HEA_{20–30}$) ± 1.28*SD(dif_FTJ $HEA_{20–30}$), and the numbers of participants showing differences in each group exceeding these thresholds were obtained.

RESULTS: Deep zone T2 was longer in ACL_in than in ACL_unin and HEA knees (Fig. A). Between-knee differences were only bigger in $ACL_{20–30}$ and $ACL_{40–60}$ than in $HEA_{20–30}$ or $HEA_{40–60}$ for deep zone dif_FTJ (Fig. B) and not for superficial dif_FTJ (Fig. C) or total dif_FTJ (Fig. D). For deep zone dif_FTJ, the number of participants outside the 80% threshold limits of -1.57 to 1.60 ms was 3/24 (12.5 %) for $HEA_{20–30}$, 15/23 for (65.2 %) for $ACL_{20–30}$, 5/24 (20.8 %) for $HEA_{40–60}$ and 11/14 (78.6 %) for $ACL_{40–60}$.

CONCLUSION: Elevated FTJ deep zone T2 2 to 10 years after ACL injury (with or without surgical ACL reconstruction) suggests a reduction in cartilage quality (i.e. alterations in cartilage composition and mechanics) after trauma. Comparable deep zone dif_FTJ after ACL injury for both age groups suggests that trauma affects cartilage quality in both groups equally. We conclude that the effects of ACL injury were most pronounced in deep zone T2 and most ACL injured participants showed between-knee differences outside the threshold limits for healthy articular cartilage.

SPONSOR: Funded in part by the Swiss National Science Foundation (#320030_184912) and the Department of Orthopaedics and Traumatology (University Hospital Basel, Switzerland).
DICLOSURE STATEMENT. Felix Eckstein is co-owner and CEO of Chondrometrics GmbH and has consulted for Merck, Bioclinica, Servier, Samumed, Roche, Kolon Tissuegene, Galapagos and Novartis
ACKNOWLEDGMENT: Prof. Oliver Bieri and Tanja Haas for assisting with the qDESS MRIs
CORRESPONDENCE ADDRESS: simon.herger@unibas.ch.

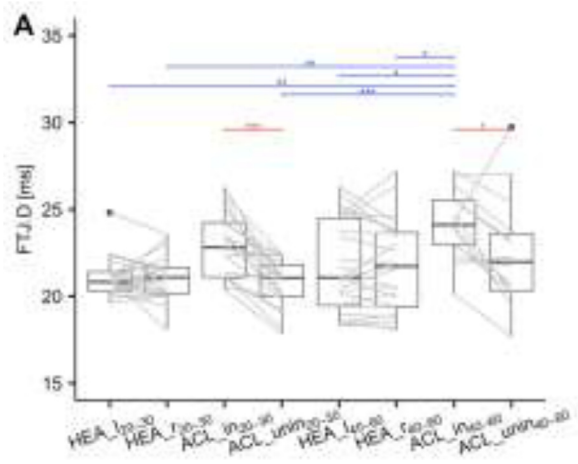

Boxplots of the femorotibial joint deep zone T2 (FTJ.D); grey lines connect data fromone participant; significant between-group (blue) and between-knee differences (red); * p<0.05, ** p<0.01; *** p<0.001 Boxplots.

Figures continued on next page.

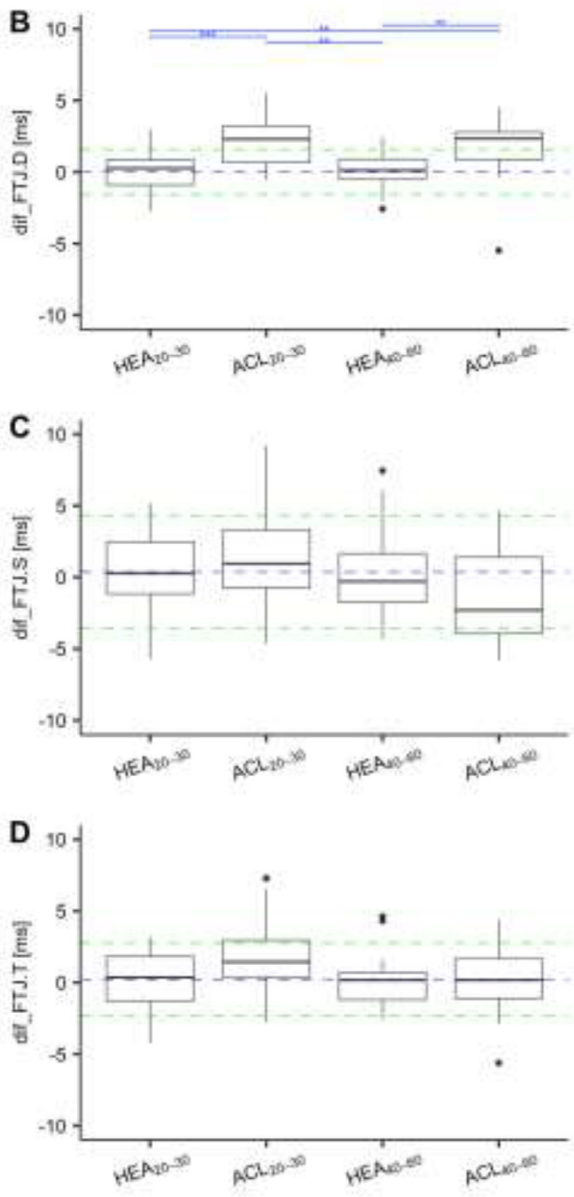

Boxplots of between-knee differences for deep (.D), superficial (.S) and total (.T) T2 of the femorotibial joint (FTJ),significant between-group differences (blue); * $p<0.05$, ** $p<0.01$; *** $p<0.001$; 80% thresholds (green dashed line); threshold bias (blue dashed line).

doi: 10.1016/j.ostima.2023.100103

IMPROVING ACCURACY AND REPEATABILITY OF T_2 MAPPING IN THE OAI DATA THROUGH EXTEND PHASE GRAPH MODELING

M. Barbieri [1], A.A. Gatti [1], F. Kogan [1]

[1] *Department of Radiology, Stanford University, Stanford, CA, USA*

INTRODUCTION: The Osteoarthritis Initiative was a longitudinal study of osteoarthritis that prospectively collected a trove of imaging data including Multi-Echo Spin-Echo (MESE) data for cartilage T2 relaxation time assessment in one knee. While this data remains underutilized, several analyses have been performed over the past years to assess T2 sensitivity to OA exploiting the OAI dataset. However, fitting procedures to compute T2 maps from the MESE data in the OAI largely rely on mono-exponential modelling, which is inherently sub-optimal as it does not account for stimulated echoes produced by RF slice-profile and B1 inhomogeneities and it often fails to account for low SNR in longer TEs. To mitigate errors, a common practice is to drop the first echo and fit the remaining 6 echoes at the expense of discarding information and degrading SNR efficiency. T2 fitting of MESE data using Extended phase graph (EPG) modelling, whether based on nonlinear least square (NLSQ) dictionary matching (DM) or deep learning (DL), can account for stimulated echoes, and can potentially provide more accurate and robust fitting for T_2 mapping in the OAI.

OBJECTIVE: This work proposes to 1) set up three EPG fitting approaches for T2 mapping in the OAI dataset (NLSQ-based, DM-based and DL-based), 2) assess methods for their performance in accuracy and robustness to noise using both simulations and in-vivo data, and 3) compare them against standard fitting methods based on mono-exponential methods.

METHODS: MESE simulations were performed in Matlab (R2022b) using the EPG formalism considering the sequence parameters of OAI data. Hanning-windowed Sinc pulses were used for slice-profile simulations. Three EPG-based fitting methods and three exponential (EXP)-based methods used in prior OAI literature were considered and are summarized in Figure 1.

To investigate fitting accuracy and repeatability robustness to noise experiments with simulations as well as using in-vivo data from OAI database were performed. 2000 MESE signals were simulated with T_2 ranging from 20 to 80 ms and B_1 ranging from 0.9 to 1.1. Each method was used to fit T2 values after adding increasing levels of Gaussian noise. For each SNR, the procedure was repeated 10 times with re-sampling of noise. Accuracy was assessed using the mean percentage error (MPE) and mean absolute percentage error (MAPE), while repeatability was assessed with coefficient of variation (CV). MESE data from 5 subjects in the OAI database (1 in each KLG) were corrupted by injecting Gaussian noise to the MESE images twice with increasing variance. Method repeatability was assessed through Bland-Altman (BA) analysis.

To assess agreement among fitting methods and how this affected inference of the presence of OA, 50 subjects were randomly selected from the OAI dataset: 10 subjects (5F & 5M) per KLG (0,1,2,3,4). Patellar (P) and Tibiofemoral (TF) cartilage T_2 maps were computed pixel-wise with all the described fitting methods. Mean T2 was computed in 7 ROIs (P, MT, LT, central and posterior regions for the MF and LF) extracted using automatic segmentation of DESS images registered to MESE images. BA analysis was used to asses pair-wise agreement in mean T2 values using Limits of Agreement (LOA) and mean bias. The Lin's concordance coefficient (ρ_c) and CV were also used as metrics of agreement. A logistic regression model was then performed using OA presence (KLG≥2) as a dependent variable, T_2 as independent variable and body mass index as covariate in the MT and the central MF regions.

RESULTS: MPE, and CV for different fitting methods from the simulation experiment are reported in Fig. 2 (top panel) as a function of SNR. The EPG methods outperformed the exponential-based methods in terms of accuracy at all SNR levels. The EPG-DL approach had the best overall performance in terms of accuracy and repeatability. In-vivo analysis of LOA and CV as function of SNR (Fig. 2, bottom panel) showed that the EPG-based methods had higher repeatability than EXP-based procedures. The EPG-DL approach also had the best overall performance in *in vivo* data. T_2 pair-wise method comparison in-vivo (Fig. 3) showed that overall, the EPG-based methods had higher inter-method agreement (-0.1 ms < Bias < 0.05 ms, 0.2 < LOA < 1.13 ms, $\rho_c \sim 0.99$) compared to exponential-based methods (-0.7 ms < Bias < 2 ms, 3.2 ms < LOA < 5.3 ms, 0.86 < ρ_c < 0.94). Poor agreement was found between EPG-based and exponential-based methods (0.34 < ρ_c < 0.44, Bias ~ 10 ms and LOA ~ 4 ms). With reference to Tab. 1, using the EPG-based methods resulted in higher T_2-associated OA odd ratios than EXP-based methods in the MT region (EPG OR ~ 1.19, 1.13 < EXP OR < 1.18).

CONCLUSION: EPG-based T2 relaxation time fitting methods resulted in more accurate and repeatable T_2 estimation than EXP-based approaches in simulations. Preliminary in-vivo experiments also suggest higher robustness to noise of EPG methods compared to EXP-based methods. Furthermore, the EPG-methods showed high inter-method agreement. The lower T_2 inter-method agreement of EXP-based approaches greatly affected inference of OA severity. Despite the limited sample size, these results suggest that EPG-based methods to compute T_2 maps in the OAI may result in low method-dependent variability. Among the EPG-based methods, the DL approach showed the highest repeatability. The high repeatability of EPG-DL paired with its computational efficiency may allow better exploitation of T_2 information in the OAI dataset, especially when longitudinal analysis is involved. We plan to use the EPG-DL approach to compute T_2 maps of the entire OAI dataset and make it publicly available for researchers to use it.

SPONSOR: NIH (R01AR079431, R21EB030180, R01AR077604, R01EB002524), Wu Tsai Human Performance Alliance, CIHR Postdoctoral Fellowship

DICLOSURE STATEMENT: FK receives research support from GE Healthcare. AAG is a shareholder of NeuralSeg Ltd.

CORRESPONDENCE ADDRESS: mb7@stanford.edu.

Figures can be found on next page.

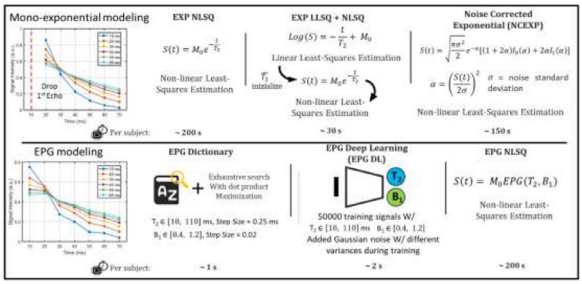

Figure 1: Summary of fitting methods used in this work. (Top panel) mono-exponential based methods used in OAI literature. (Bottom panel) Proposed EPG-based fitting methods that have yet to be applied in the OAI literature.

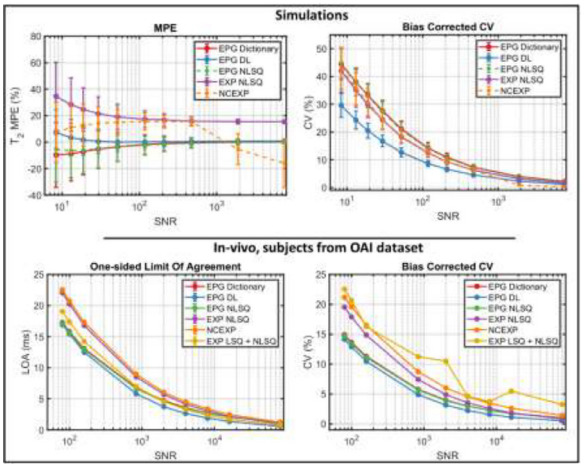

Figure 2: (Top panel) Accuracy and robustness to noise of different fitting methods form simulation experiment. (Bottom panel) Robustness to noise of different fitting methods from in-vivo data. SNR is defined as the ratio between the power of the signal and the power of the simulated Gaussian noise.

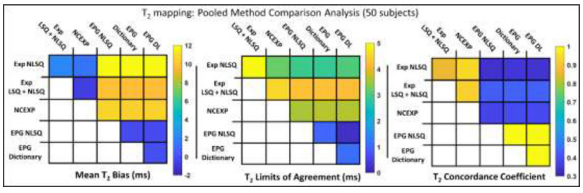

Figure 3: Summary of T_2 pair-wise method comparison using T_2 mean bias (left), T2 limits of agreement (center) and Lin's concordance coefficient (right).

Table1: Odd Ratio of presence of OA associated to T2 from the logistic regression analysis on 50 subjects of the OAI dataset.

Method	EPG DL	EPG Dictionary	EPG NLSQ	EXP NLSQ	EXP LSQ + NLSQ	NCEXP
Medial Tibia						
$T_{2\text{-associated. Odd Ratio (2.5\%, 95\%)}}$	1.192 (1.02, 1.39)	1.194 (1.02, 1.39)	1.196 (1.02, 1.40)	1.159 (1.01, 1.33)	1.18 (1.01, 1.40)	1.13 (0.99, 1.30)
Medial Central Femur						
$T_{2\text{-associated. Odd Ratio (2.5\%, 95\%)}}$	1.133 (1.01, 1.26)	1.136 (1.01, 1.28)	1.130 (1.01, 1.28)	1.139 (1.01, 1.29)	1.123 (0.99, 1.28)	1.118 (0.99, 1.26)

doi: 10.1016/j.ostima.2023.100104

AGREEMENT AND PRECISION OF FEMOROTIBIAL CARTILAGE TRANSVERSE RELAXATION TIME (T2) OBTAINED AT FOUR DIFFERENT MAGNETIC FIELD STRENGTHS

S. Maschek [1,2], A. Wisser [1,2], W. Wirth [1,2], F. Eckstein [1,2], R. Heiss [3], S. Lévy [3,4], A.M. Nagel [3,5], M. Bachl [3], M. Uder [3], F.W. Roemer [3,6]

[1] *Institute of Anatomy & Cell Biology and Ludwig Boltzmann Institute for Arthritis and Rehabilitation (LBIAR), Paracelsus Medical University (PMU), Salzburg, Austria*
[2] *Chondrometrics GmbH, Freilassing, Germany*
[3] *Universitätsklinikum Erlangen & Friedrich Alexander Universität Erlangen-Nürnberg (FAU), Erlangen, Germany*
[4] *Siemens Healthineers, Melbourne, Australia*
[5] *Medical Physics in Radiology, German Cancer Research Center (DKFZ), Heidelberg, Germany*
[6] *Boston University School of Medicine, Boston, MA, USA*

INTRODUCTION: Spin-spin (transverse) relaxation time (T2) is considered to reflect cartilage composition, such as hydration, collagen content and orientation. It can be computed from multi-echo spin-echo (MESE) MRI and is associated with age, sex, and structural joint pathology. Cartilage T2 is dependent on the magnetic field strength. Lower field strength is characterized by lower signal to noise ratios (SNR) compared to standard 1.5Tesla (T) and 3T systems, resulting in longer acquisition times, while access to ultra-high field 7T MRI is still limited. A direct comparative evaluation of cartilage T2 across different field strengths has not been performed to date.

OBJECTIVE: To analyze the agreement and the intra-reader test-retest precision of laminar femorotibial cartilage T2, acquired from four different scanner models with 0.55T,1.5T, 3T, and 7T.

METHODS: Six healthy volunteers (5 female, age 21.5±3.5 y) without knee pain had two MESE MRIs acquired each, with repositioning of the knee between test and retest scans, using a 1) MAGNETOM Free.Max 0.55T (acquisition matrix (AM) 304×248, slice thickness [ST] 3mm, TR 3020ms, 6 echoes from 16.1 to 96.6ms, acquisition time (AT) 14 min 56 sec) 2) MAGNETOM Sola 1.5T (AM 384×384, ST 3mm, TR 2700ms, 7 echoes from 11.7 to 81.9ms, AT 10 min 31 sec) 3) MAGNETOM Vida 3T (AM 384×384, ST 3mm, TR 3210ms, 9 echoes from 11.5 to 103.5ms, AT 8 min 17 sec) 4) MAGNETOM Terra 7T (AM 384×384, ST 3mm, TR 4490ms, 9 echoes from 8.1 to 72.9ms, AT 8 min 22 sec) (Fig. 1). The field of view was 12×12cm for all MESE MRIs. Segmentation of the medial and lateral femorotibial compartment cartilage (MFTC/LFTC) was performed manually by an expert reader; the T2 values were computed for each voxel using custom software. The cartilage layers were divided into the top 50% (superficial [sf]) and bottom 50% (deep) layer, based on the local distance between the cartilage surface and bone interface. The test-retest precision across the entire femorotibial joint (FTJ), the MFTC, and the LFTC was measured using the root mean square coefficient of variation (RMS CV in %). The absolute values of laminar T2 were compared between field strengths using ANOVA, with Bonferroni-Dunn post-hoc correction.

RESULTS: The RMS CV across the FTJ was lowest at 3T (0.9%/1.4% sf/deep) and greatest at 0.55T (3.2%/4.0%). The RMS CV was 1.3%/3.4% at 1.5T and 2.3%/1.4% at 7T. Sf RMS CV at 0.55/1.5/3/7T was 3.9/1.7/1.0/3.5% for the MFTC, and 3.0/1.7/1.2/2.7% for the LFTC. The deep layer RMS CV was 5.4/3.4/3.1/2.6% for the MFTC and 5.0/4.1/1.1/2.9% for the LFTC.
Sf and deep layer T2 differed significantly between field strengths for the FTJ, the MFTC, and the LFTC (all $p<0.001$). Both sf and deep layer T2 across the FTJ, the MFTC and also the LFTC were shortest at 7T and longest at 0.55T (Fig. 2). Interestingly, T2 was shorter at 1.5T than at 3T, but this difference reached statistical significance only for the deep layer in the FTJ and in the MFTC (Fig. 2).

CONCLUSION: Based on the protocols implemented in this study, laminar cartilage T2 systematically varied with magnetic field strength. The shortest values were observed at 7T, and the longest at 0.55T. These findings suggest that cartilage T2 measurements in multicenter studies are not directly comparable when different field strengths (potentially also different manufacturer and scanner models) are included. The test-retest precision error was lowest at 3T and highest at 0.55T, suggesting that, in clinical studies, measurements should be performed at 3T. However, test-retest precision is highly dependent on the protocol and might be improved for lower field strengths, applying different acquisition parameters (e.g. longer acquisition times and higher resolution). Implementation on the 7T magnet may require further improvement to leverage the full potential benefit of the higher field strength.

SPONSOR: OA-BIO Eurostars (E! 114932). The German project partners received funding from the Bundesministerium für Bildung und Forschung (BMBF).
DISCLOSURE STATEMENT: FE, WW, SM and AW are part time employees of Chondrometrics GmbH; FE, WW, and SM are co-owners of Chondrometrics GmbH; FE has provided consulting services to Merck KGaA, Kolon-TissueGene, and Novartis; FWR is shareholder of BICL
ACKNOWLEDGMENT: Imaging Science Institute Erlangen.
CORRESPONDENCE ADDRESS: maschek@chondrometrics.de.

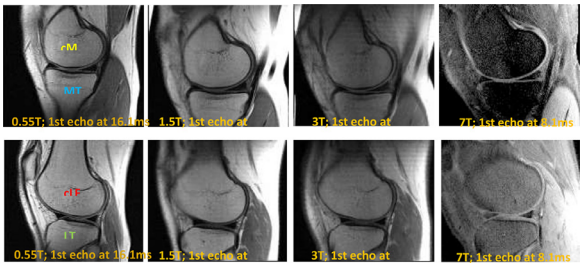

Figure 1: First echo of MESE MRIs acquired at 0.55, 1.5, 3 and 7 Tesla.
Top row: medial compartment; bottom row: lateral compartment.
MT = medial tibia; LT = lateral tibia; cMF = central medial femur; cLF = central lateral femur; T = Tesla.

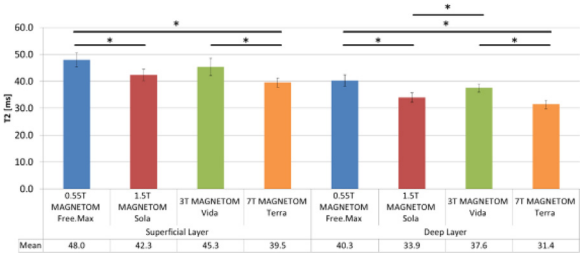

Figure 2: Superficial and deep layer cartilage T2 across the entire femorotibial joint measured from MESE MRI acquired using 4 scanner models with different field strengths. Horizontal bars indicate significant differences between scanner models with different field strengths.

doi: 10.1016/j.ostima.2023.100105

COMPARISON OF NEW MR APPROACHES FOR ACCELERATED KNEE IMAGING

A. Goyal [1], M. Petterson [1], R. Van der Heijden [2], K. Stevens [1], M. Yoon [1], J. MacKay [3], M. Fung [4], F. Kogan [1]

[1] *Department of Radiology, Stanford University, Palo Alto, CA, USA*
[2] *Erasmus MC, Rotterdam, The Netherlands*
[3] *University of Cambridge, Cambridge, UK*
[4] *GE Healthcare, New York, NY, USA*

INTRODUCTION: Conventional knee MRI protocols use numerous 2D FSE sequences with multiple contrasts, often repeated in multiple scan planes. This approach requires long scan times and does not fully utilize modern reconstruction, 3D, acceleration, and improved coil SNR technologies. Numerous approaches have been proposed to improve the value of knee imaging by reducing protocol times to less than 6 minutes and perhaps adding utility through quantitative data or oblique reformats. In this abstract, we present preliminary data and outline four such approaches: (1) an accelerated conventional 2D protocol; (2) a SNR-efficient 3D qDESS protocol, (3) a CUBE protocol, and (4) a thin-slice protocol with high resolution and compare them to a standard knee protocol.

OBJECTIVE: To determine diagnostic accuracy and confidence of 4 new knee MRI protocols compared to a reference knee protocol with respect to pathology, diagnostic confidence, and utility of novel image data.

METHODS: 32 participants with knee pain and/or diagnosed OA were recruited for this study. Each participant was scanned on a whole-body 3T MRI system (GE Healthcare) using a 16-channel receive-only phased-array coil. All subjects underwent 5 protocols in a single scan session, described below (Table-1). Five radiologists independently evaluated the retrospectively constructed knee MRI protocols for diagnostic confidence with respect to fluid sensitivity, tissue pathology, and image artifacts. Beyond diagnostic confidence, we evaluated the utility of image reformats in 3D and Thin-Slice datasets as well as the utility of new data such as synovitis hybrid images and cartilage T2 relaxation time maps in the qDESS protocol. Each radiologist was blinded to patients and scan protocol and received 5 compilations of 32 datasets (one protocol per patient - randomized) with a two-week washout period in-between.
Protocol Information: The reference standard was a conventional 2D FSE accelerated knee protocol, which included six scans: axial T2 fat-saturated (FS), coronal proton density (PD) FS, sagittal T2 FS, sagittal PD, coronal PD, and coronal T1 FSE scans. The first new approach was a DL 2D FSE protocol, which includes the above sequences, further accelerated by a factor of 2, reconstructed using the GE AIR deep learning (DL) algorithm (images in Fig-1). The second fast approach was based around a multi-contrast 3D quantitative DESS (qDESS) sequence, which has shown near diagnostic equivalence to the conventional protocol. This protocol also included a 2D Cor PD-FS-FSE sequence for evaluation of BM lesions and collateral ligaments. The high SNR efficiency allows higher through-plane resolution to support oblique reformats and provides synovitis hybrid images (joint-fluid-suppressed images created from qDESS images) and cartilage T2 maps (Thoenen et al., 2021). The third approach was a 3D PD-FSE sequence with variable flip-angle refocusing (CUBE) and a 2D Cor PD-FS-FSE sequence for visualization of BM lesions (images in Fig-2). The fourth approach included a thin-slice 2D Sag PD-FS-FSE sequence, with a 4x improvement (0.8 mm) in slice resolution and a 2D Cor T1-FSE sequence (images in Fig-3).

RESULTS: At present, two readers have completed scoring of all 5 compilations of data and diagnostic quality scores for anatomical features including bone marrow, ligament, meniscus, and cartilage pathology were compared. Both readers graded the DL 2D FSE protocol as having the highest diagnostic quality compared to the other protocols, for all features compared. Among the other three approaches, the thin-slice protocol scored better than the CUBE and qDESS protocols for evaluation of bone marrow pathology. This pattern was reversed in cartilage, where qDESS had the higher quality scores. The CUBE protocol had the best quality for evaluating ligaments and the meniscus, comparable to the DL protocol. The utility of 3D reformats for the qDESS, CUBE and thin-slice protocols was similar for one reader, while thin-slice had higher utility for the second reader. Specifically, for the qDESS protocol, readers found the cartilage T2 relaxation maps useful 61.87% of the time to either confirm a particular pathology (58.31%) or even change the reader's assessment (3.56%). Similarly, readers found the synovitis hybrid images useful 55% of the time to distinguish between synovitis and effusion confidently (35%) or moderately (20%).

CONCLUSION: Preliminary results indicate that accelerated knee scans with similar contrasts resulted in higher diagnostic quality scores. We look to assess the sensitivity and specificity of each method to pathology as well as the inter-reader agreement for each approach once all readers finish scoring the study.

SPONSOR: General Electric Healthcare, Wu Tsai Human Performance Alliance
DISCLOSURE STATEMENT: Research Support from GE Healthcare
ACKNOWLEDGMENT: None
CORRESPONDENCE ADDRESS: agoyal5@stanford.edu.

Table 1. Overview of the reference and four novel protocols.

Reference Protocol	DL 2D FSE Protocol	3D qDESS Protocol	3D CUBE Protocol	2D Thin-Slice Protocol
Ax T2 FS (1:58 min)	Ax T2 FS (0:51 min)	qDESS (4:32 min, res $0.4\times0.4\times1$ mm^3, TE: 6, 29 ms)	Sag PD CUBE (5:04 min, res $0.5\times0.5\times0.6$ mm^3)	Sag PD FS FSE (3:54 min, res $0.4\times0.6\times0.8$ mm^3)
Cor PD FS (2:22 min)	Cor PD FS (1:15 min)	Cor PD FS FSE (0:45 min)	Cor PD FS FSE (0:45 min)	Cor T1 FSE (1:09 min)
Sag T2 FS (2:09 min)	Sag T2 FS (1:11 min)	Cartilage T2 maps		
Sag PD (1:50 min)	Sag PD (1:15 min)	Synovitis Hybrid images		
Cor PD (1:25 min)	Cor PD (0:45 min)			
Cor T1 FSE (1:38 min)	Cor T1 FSE (1:09 min)			

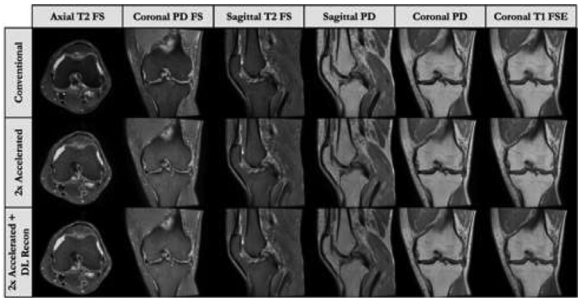

Figure 1. Example multiplanar images from the 2D Conventional (accelerated) protocol are shown in the top row. The 2x Accelerated protocol is in the middle row, while the 2x Accelerated protocol with DL reconstruction is shown in the bottom row.

Figures continued on next page.

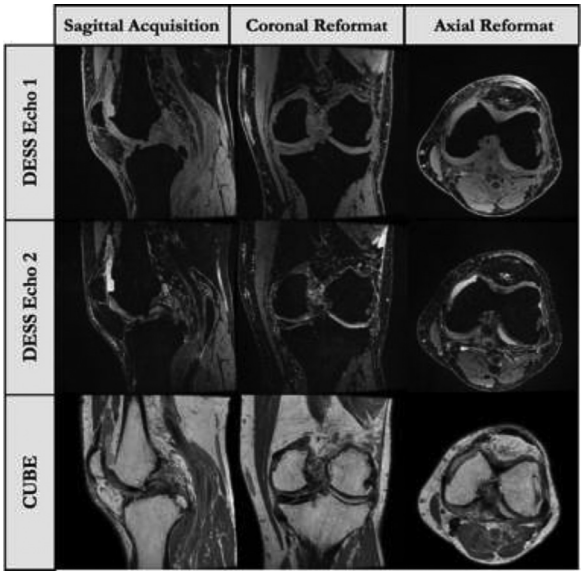

Figure 2. Example multiplanar images from the quantitative DESS protocol are shown for both Echo 1 and Echo 2 [top and middle rows]. Images from the CUBE protocol- a 3D proton density-weighted sequence, are shown in the bottom row. The data was acquired in the sagittal plane and has been reformatted in both coronal and axial planes for both protocols.

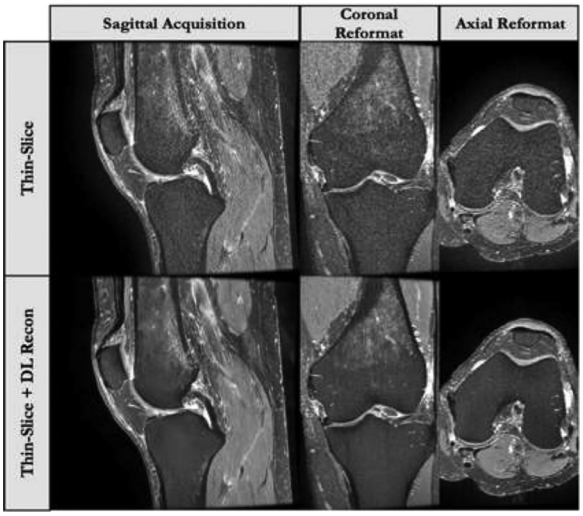

Figure 3. Example multiplanar images from the 3D Thin Slice protocol, which is a 2D sagittal proton density-weighted fast spin-echo (FSE) fat-suppressed sequence [top row]. Images with DL reconstruction are shown in the bottom row. The data was acquired in the sagittal plane, and has been reformatted in both coronal and axial planes.

doi: 10.1016/j.ostima.2023.100106

A MULTIMODALITY BASED IMAGING APPROACH USING A NOVEL RADIOTRACER, [18F] -PYGAL TO DETECT SENESCENCE IN SMALL AND LARGE ANIMAL MODELS

V. Suryadevara [1], M.J. Hajipour [1], F.G. Habte [1], W. Morakote [1], N. Malik [1], E. Chang [1], D. Mangarova [1], L. Baratto [1], L.C. Adams [1], L.J. Pisani [1], K. Nernekli [1], B. Pichler [2], N. Bézière [2], H.E. Daldrup-Link [1]

[1] *Department of Radiology, Molecular Imaging Program at Stanford (MIPS), Stanford University School of Medicine, Palo Alto, CA, USA*
[2] *Werner Siemens Imaging Center, University of Tübingen, Tübingen, Germany*

INTRODUCTION: Cellular senescence has been implicated in age-related pathophysiologies, including osteoarthritis (OA). The targeted removal of senescent cells can ameliorate the development of OA. To advance our understanding of the role of senescent cells in OA and monitor novel senolytic therapies, there is a pressing need for imaging biomarkers that can detect senescence in arthritic joints.

OBJECTIVE: Senescent cells overexpress β-galactosidase. Our objective was to detect senescent cells in knee joints of small (mice) and large (pigs) animal models using a novel β-galactosidase-based radiotracer, [18F]-PyGal, using PET imaging. We hypothesized that senescent cells will demonstrate increased [18F]-PyGal radiotracer uptake compared to viable cells, in vitro and in vivo.

METHODS: Triplicate samples of murine primary chondrocytes incubated with 400 nM doxorubicin (doxo) to induce senescence, followed by incubation with 20 μM [18F]-PyGal radiotracer for one hour and PET-CT imaging. Non-doxo-exposed cells served as controls. Next, senescence was induced in the left knee joint of 30 C57BL/6 mice (5, 12, and 23-month-old mice, both sexes) by intra-articular doxorubicin injection. The contralateral knee served as control. All knees underwent PET/CT and PET/MRI imaging at 1 hour after intravenous injection of 250uCi [18F]-PyGal. The radiotracer signal of senescent and viable joints was measured using operator defined regions of interest (ROI; %ID/g) and compared with a student's t-test. Next, senescent mesenchymal stromal cells (MSC) or viable controls were implanted into twelve cartilage defects of six knees of three Yucatan pigs. 24 hours later, 250uCi [18F]-PyGal was injected into the knee joint, followed by integrated PET-MRI. The standardized uptake value (SUV) of senescent and viable cell implants was compared with a t-test. IL-6, CXCL5 and β-galactosidase immunostains served as reference standards for all experiments.

RESULTS: Compared to untreated controls, doxorubicin-exposed chondrocytes demonstrated significantly increased expression of IL6 (Control: 18.39±5.10 pg/mL; senescence 58.85±1.43pg/mL, p<0.005), CXCL5 (Control 153.8162±38.14pg/mL, senescence:1163.24±169.09pg/mL p<0.005) and beta-gal (Control 9.16±0.7%, Senescence 90±2%, p<0.0005). Senescent cells exhibited a 2.28-fold higher uptake of [18F]-PyGal compared to controls (Control 1754±247.22, Senescence 3704.23±570.76, p=0.005). In 12-month-old mice, senescent knees demonstrated significantly higher retention of [18F]-PyGal (0.47±0.18 %ID/g, 0.47±0.12 %ID/g), compared to control knees (0.22±0.03%ID/g, 0.29±0.08, p=0.02, p=0.03 female and male respectively). Accordingly senescent knees demonstrated significantly increased p-16 staining, p-21 staining, and β-gal staining compared to normal controls. In the large animal model, cartilage defects implanted with senescent cells showed significantly higher [18F]-PyGal uptake (39.835±7.3 SUVmax) compared to control knees (19.69±0.69 SUVmax, p<0.05). Histopathologic correlations of large animal studies are ongoing.

CONCLUSION: [18F]-PyGal can detect senescent cells in knee joints of small (mice) and large (pigs) animal models using a novel β-galactosidase-based radiotracer, [18F]-PyGal and PET imaging. Senescent cells demonstrated significantly increased [18F]-PyGal radiotracer uptake compared to viable cells, in vitro and in vivo, in small and large animal models of OA.

SPONSOR: Project is funded by NIH Cellular Senescence Network Funded Research (SENET) Technology Development and Application Grant: 1UG3CA268112-01.
DICLOSURE STATEMENT: No disclosures; ACKNOWLEDGMENT: None
CORRESPONDENCE ADDRESS: vidyani@stanford.edu.

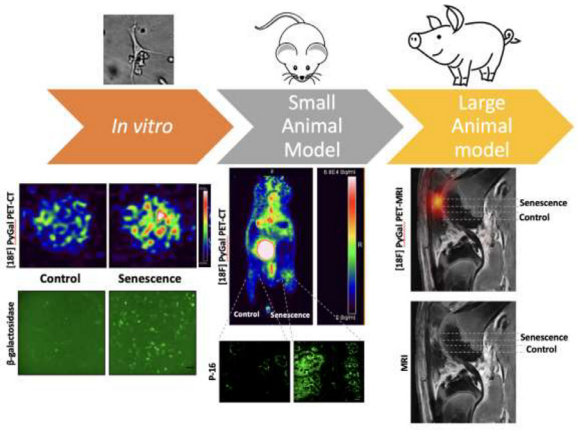

Figure: [18F]PyGal, a novel ß-galactosidase based marker to assess senescence in primary chondrocytes, doxorubicin-induced senescence in mice and in cartilage-defects in pigs loaded with senescent cells. The findings from the multimodality approach encompassing PET-CT and PET-MRI have been validated with traditional approaches.

doi: 10.1016/j.ostima.2023.100107

THE RELATIONSHIP BETWEEN CONTRAST ENHANCED COMPUTED TOMOGRAPHY (CECT) ATTENUATION AND AXIAL STRAIN IN TOTAL KNEE ARTHROPLASTY TISSUE

J.C. Küpper [1], E.S. Sullivan [2], A. Joenathan [3], B.A. Masri [1], M.W. Grinstaff [3], D.R. Wilson [1]

[1] *Department of Orthopaedics*
[2] *School of Biomedical Engineering, Centre for Aging SMART, University of British Columbia (UBC), Vancouver, BC, Canada*
[3] *Departments of Chemistry and Biomedical Engineering, Boston University; the Centre for Advanced Orthopaedic Studies, Beth Israel Deaconess Medical Center, Harvard Medical School, Boston, MA, USA*

INTRODUCTION: Mechanical factors such as cartilage strain are thought to drive the onset and progression of OA (Wilson et al., 2009). Contrast enhanced computed tomography (CECT) using CA4+, a cationic contrast agent that is highly attracted to GAG, yields high resolution (≥41 μm) cartilage images that map GAG (R^2=0.83; Lusic and Grinstaff, 2013). CECT attenuation may change with axial strain because of changes in GAG concentration as fluid flows from loaded cartilage, but it is not clear how strong this association is.

RESEARCH QUESTION: What is the strength of association between CECT attenuation and axial strain?

METHODS: We answered our question by measuring strain and CECT attenuation [in Hounsfield units (HU)] in loaded human specimens. Intact human tibial (T) and femoral (F) compartment pairs from independent total knee arthroplasty surgeries (n=3 samples) were used in this UBC ethics board approved study [ages: 81, 69, 60 years; 1 female and 2 male; ICRS grades 3F 4T, 2F 3T, 2F 3T). Tissue was stored at -20°C and fully thawed before testing. Compartments were cut (~1.5 × 2 × 0.5 cm), soaked in 30 mL of CA4+ solution (12 mg I/mL) for 68-72 hours, and then glued to plastic plates using cyanoacrylate adhesive. The two plates (T, F) were mounted in a custom actuator (CCA; Küpper et al., 2023) that allows for cartilage-on-cartilage samples to be compressed axially under load control. The CCA was mounted in an Xtreme CT scanner (Scanco Medical, Switzerland). Samples were imaged unloaded, and after 30 minutes at three load levels (37-40, 43-46, and 52-54 kPa). Images were obtained with 41 μm isotropic voxels, 300 μA current and 120 kVp voltage and then downsampled to 164 × 164 × 41 μm with the highest resolution perpendicular to the cartilage surface. A custom algorithm (Desrochers et al., 2020) was used to calculate mean axial strain and HU in the tissue across one sagittal slice through the center of contact for each sample at each load. We determined strength of association between CECT attenuation and axial strain in both the tibia and femur using a repeated measures correlation analysis (Bakdash and Marusich, 2017) (α=0.05).

RESULTS: CECT attenuation increased with decreasing axial strain (compression), except in some regions where we observed cartilage bulging (positive strain). For the tibia (strain range -0.3 to 0), the correlation was strong and significant ($r_{rm}(8)$=-0.96, $p<0.001$). We did not find a significant correlation in the femur (strain range -0.07 to 0.1; $r_{rm}(8)$=-0.59, p=0.07).

CONCLUSION: Though preliminary, the tibial cartilage results suggest that CECT attenuation has promise as a surrogate measure of strain. The lower correlation in femoral cartilage is likely due to stiffer, thinner cartilage and cartilage bulging effects (Sullivan, 2023). CECT may be used as a tool to estimate cartilage strain, in particular through the cartilage layers and in healthy and OA tissue.

SPONSOR: The Arthritis Society, MSFHR; NSERC
DICLOSURE STATEMENT: N/A
ACKNOWLEDGMENT: A. Burden, W. Hornaday, C. Harasym, and E. Hoptioncann for technical assistance.
CORRESPONDENCE ADDRESS: jessica.kupper@ubc.ca.

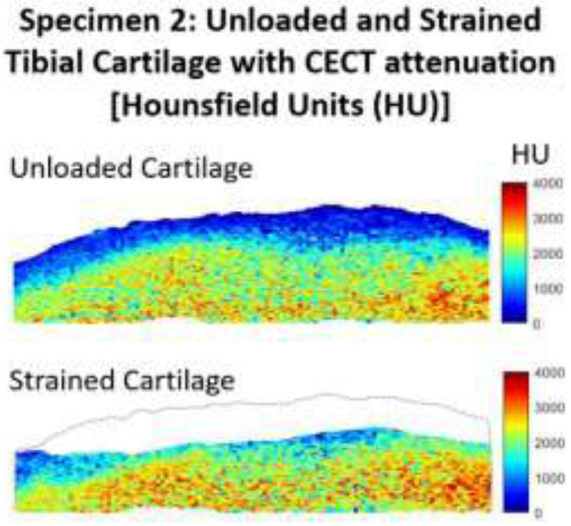

doi: 10.1016/j.ostima.2023.100108

DUAL ENERGY CT CANNOT EFFECTIVELY DIFFERENTIATE BETWEEN CALCIUM PYROPHSOPHATE AND BASIC CALCIUM PHOSPHATE

M. Jarraya [1], O. Bitoun [1], R. Balza [1], A. Guermazi [2], R. Gupta [1], G.P. Nielsen [3], A.Z. Blackburn [4], E. Guermazi [5], E. Omoumi [6], C.M. Melnic [4], S. Yee [1]

[1] *Department of Radiology, Massachusetts General Hospital, Harvard Medical School, Boston, MA, USA*
[2] *VA Boston Healthcare, Boston University School of Medicine, Boston, MA, USA*
[3] *Department of Pathology, Massachusetts General Hospital, Harvard Medical School, Boston, MA, USA*
[4] *Department of Orthopedics, Massachusetts General Hospital, Harvard Medical School, Boston, MA, USA*
[5] *Boston University, Boston, MA, USA*
[6] *Centre Hospitalier Universitaire Vaudoix (CHUV), Lausanne, Switzerland*

INTRODUCTION: Over the past few years, the potential of dual-energy CT (DECT) and multi-energy CT in distinguishing between basic calcium phosphate (BCP) and calcium pyrophosphate (CPP) crystal deposition in and around the joint has been an important topic of interest, not only for the characterization of calcium crystal arthropathies, but also in osteoarthritis (OA) research.

OBJECTIVE: Our aim was to test the hypothesis if DECT can effectively discriminate between BCP and CPP crystals in a clinical setting using a knee arthroplasty specimen.

METHODS: This study was IRB-compliant. One male participant aged 71 with radiographically detected chondrocalcinosis (**figure 1**), scheduled for a total knee replacement was consented for this study. Surgical specimens of the medial meniscus, lateral meniscus, medial femoral condyle, and lateral tibial plateau were separately labeled, and examined under light microscopy, confirming the presence of CPP (and no BCP) in all 4 samples. Prior to pathology examination, specimens were also scanned using a Siemens Somatom Force with standard clinical parameters (80/150 kV, FOV: 250, exposure: 165 mAs, slice thickness: 0.6 mm, resolution: 0.488×0.488 mm2). Two readers (MJ and RB) obtained 4 DECT parameters: CT numbers at 80 and 150 kV; Dual-energy index (DEI); Electron density (Rho); and effective atomic number (Z_{eff}). These parameters were obtained by placing multiple ROIs in several regions (3 ROIs per region), categorized as subchondral bone BCP (S-BCP), cortical bone BCP (C-BCP), and CPP (from ROIs placed within foci of microscopy-proven CPP in menisci and articular cartilage), as shown in **figure 1**. The mean and standard deviations of all parameters were calculated for both readers. P-values were also calculated using t-test.

RESULTS: DECT parameters of both readers within different areas of mineralization are shown in **table 1**. Statistically significant differences in CT attenuation at 80 and 150 KV, and Rho were noted between C-BCP, S-BCP and CPP for both readers, with corresponding CPP parameters lying between those C-BCP and S-BCP **(figure 2)**. Differences in DEI between S-BCP, C-BCP an CPP were all statistically significant for reader 2, with corresponding CPP parameters also lying between those C-BCP and S-BCP. For reader 1, the difference in DEI was statistically significant between CPP and C-BCP, and between S-BCP and C-BCP, but not between CPP and S-BCP. For both readers, Z_{eff} was statistically different between CPP and C-BCP, but not statistically different between CPP and S-BCP.

CONCLUSION: The DECT parameters of CPP lied between S-BCP (lower calcium concentration) and C-BCP (higher calcium concentration). Differences in DECT parameters between BCP and CPP are driven by calcium concentration (density) rather than the elemental composition of these substrates.

SPONSOR: None.
DISCLOSURE STATEMENT: AG has received consultancies fees from Pfizer, Novartis, AstraZeneca, Coval, Medipost, ICM and TissueGene and is shareholder of Boston Imaging Core Lab (BICL), LLC a company providing image assessment services. CMM has received consultancy fees from Smith and Nephew.
CORRESPONDENCE ADDRESS: mjarraya@mgh.harvard.edu.

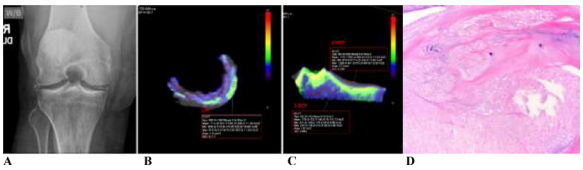

Figure 1: (A) Preoperative anteroposterior knee radiograph of the study's participant showing meniscal calcinosis with more subtle mineralization of the hyaline cartilage. **(B)** *Ex vivo* DECT axial reformat of the lateral meniscus with an ROI placed in a focus of CPP, as proven by microscopy. **(C)** *Ex vivo* DECT coronal reformat of the lateral tibial plateau, ROI placement in the cortical bone (C-BCP) and within the subchondral bone (S-BCP). (D) Histologic examination of the lateral meniscus. Hematoxylin and eosin (H&E) staining shows presence of CPP crystals.

Table 1: Mean CT attenuation values, Dual energy index (DEI), electron density (Rho) and effective atomic numbers (Zeff) in cortical bone (C-BCP), subchondral bone (S-BCP) and foci of calcium pyrophosphate (CPP) for both readers. In each region, 3 ROIs were placed.

READER 1	CT (80Kv)	CT (150Kv)	DEI	Rho	Z_{eff}
S-BCP	459	205.6	0.09	115.5	10.5
C-BCP	893.6	464.7	0.13	323.5	11.4
CPP	532	252.9	0.1	194.9	10.4
p-value (S-BCP v. C-BCP)	0.277	0.168	0.001	<0.001	0.002
p-value (CPP v. C-BCP)	<0.001	<0.001	0.006	<0.001	<0.001
p-value (CPP v. S-BCP)	<0.001	<0.001	0.59	0.001	0.54
READER 2	CT (80Kv)	CT (150Kv)	DEI	Rho	Z_{eff}
S-BCP	425	179	0.09	91.6	10.5
C-BCP	1133	572	0.15	396.6	11.9
CPP	622	293	0.11	227.3	10.7
p-value (S-BCP v. C-BCP)	<0.001	<0.001	<0.001	<0.001	0.002
p-value (CPP v. C-BCP)	<0.001	<0.001	<0.001	<0.001	<0.001
p-value (CPP v. S-BCP)	<0.001	<0.001	0.01	<0.001	0.38

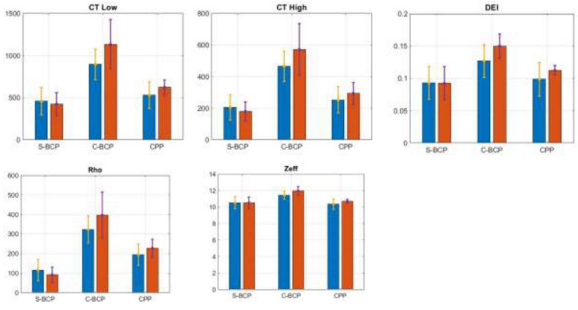

Figure 2: Bar graphs for CT attenuation values at 80 (CT Low) and 150Kv (CT High), Dual energy index (DEI), electron density (Rho) and effective atomic numbers (Zeff) in cortical bone (C-BCP), subchondral bone (S-BCP) and foci of calcium pyrophosphate (CPP) for both readers.

doi: 10.1016/j.ostima.2023.100109

DEEP LEARNING APPROACH TO MEASURE CARTILAGE VOLUME: DATA FROM THE OSTEOARTHRITIS INITIATIVE

J. Duryea [1], F. Preiswerk [1], H. Ragati Haghi [1], R. Amesbury [1], T. Laffaye [1], R. Stein [1], A. Mathiessen [2], C.K. Kwoh [3]

[1] *Brigham and Women's Hospital, Boston, MA, USA*
[2] *Diakonhjemmet Hospital, Oslo, Norway*
[3] *University of Arizona Arthritis Center, the University of Arizona College of Medicine, Tucson, AZ, USA*

INTRODUCTION: Change in cartilage volume on Magnetic Resonance Imaging (MRI) has been suggested as a potential surrogate endpoint for knee osteoarthritis (KOA) in clinical trials. We have developed the semi-automated Local-Area Cartilage Segmentation (LACS-SA) software, to measure cartilage volume in central weight-bearing areas of the MF, LF, MT, and LT. Though currently fast (requiring approximately 40 minutes per scan) improvements to the efficiency will be necessary to handle the workload for very large studies. Software segmentation methods are generally validated using metrics that directly compare the regions of interest such as the Dice similarity coefficient (DSC). However for cartilage, this approach may not capture the subtle changes that account for KOA-related loss where even a single voxel change in thickness can be substantial.

OBJECTIVES: The goal of our current work was to use a highly powered study to evaluate a deep learning (DL) version (LACS-DL) that can be used as a valid and more automated replacement by demonstrating a high correlation and equivalent responsiveness to change,

METHODS: 700 participants from the OAI) with KL scores of 1, 2, or 3 at baseline (BL) had MRI scans acquired at the BL, 24 mo., 48 mo., 72 mo., and 96 mo. time points (i.e., a total of 3,095 MRI scans). Cartilage volumes in the MF, LF, MT, and LT were measured using LACS-SA on the sagittal 3D double-echo steady-state (DESS) sequence. To develop LACS-DL, the 3,095 scans were segmented using the LACS_SA and used to train a U-Net convolutional neural network (CNN). The data were divided into two sets (Set 1 and Set 2) with a 50% split by subject ID. Set 1 was used to train the CNN for testing on Set 2, and Set 2 was used to train for testing on Set 1. We measured the coefficient of variation (CoV), and correlation (Pearson's R^2) between BL cartilage volumes calculated with LACS-SA and LACS-DL. To evaluate the performance of LACS-DL for use in clinical trials, we calculated the responsiveness to change between BL and the other time points using standardized response mean (SRM) values.

RESULTS: The BL KL grade distribution was KL1 23%, KL2 48%, and KL3 29%, and the participants were 59% female, had a mean (SD) age of 61.3 (8.9) years, and mean (SD) BMI of 29.0 (4.6) kg/m^2. The R^2 and CoV values ranged from 0.89 to 0.95 and 5.0% to 7.3% respectively. The reader time for LACS-DL is approximately 2 minutes/scan, or about 5% of the time needed for LACS-SA. Table 1 provides the SRM values for LACS-SA and LACS-DL. The data suggest that the DL approach has similar responsiveness. The average DSC was 0.90.

CONCLUSIONS: The results offer compelling evidence that LACS-DL is a valid substitute for LACS-SA both through concurrent validity and responsiveness to change. The 20-fold improvement in reader time and equivalent performance to LACS-SA suggest that LACS-DL could be utilized in large longitudinal studies and clinical trials of KOA.

SPONSOR: NIH/NIAMS R01AR071409
DICLOSURE STATEMENT: CKK is a consultant to Tissue Gene, Novartis, Trial Spark, Moebius Therapeutics, Xalud Therapeutics and Express Scripts.
ACKNOWLEDGMENT: We acknowledge the assistance of Quinley Miao.
CORRESPONDENCE ADDRESS: jduryea@bwh.harvard.edu.

Table 1. SRM values (LACS-SA, *LACS-DL*) for each cartilage plate and follow-up time point.

Time points	N	MF	LF	MT	LT
BL-24mo	700	-0.40, *-0.38*	-0.08, *-0.08*	-0.35, *-0.32*	-0.30, *-0.31*
BL-48mo	682	-0.43, *-0.46*	-0.04, *-0.15*	-0.48, *-0.47*	-0.38, *-0.36*
BL-72mo	533	-0.59, *-0.67*	-0.22, *-0.26*	-0.75, *-0.86*	-0.66, *-0.64*
BL-96mo	480	-0.66, *-0.66*	-0.25, *-0.19*	-0.71, *-0.76*	-0.61, *-0.50*

doi: 10.1016/j.ostima.2023.100110

SYNTHETIC CT GENERATION FROM T1-WEIGHTED KNEE MRIs USING A UNET

V. Ravano [1,2,3], A. Elwakil [1,3], T. Hilbert [1,2,3], J. Richiardi [2], J.P. Thiran [3], C. Mourad [2], P. Magrain [4], J. Favre [4], T. Kober [1,2,3], S. Sommer [1,5,#], P. Omoumi [2,#]

[1] *Advanced Clinical Imaging Technology, Siemens Healthineers International AG, Lausanne and Zurich, Switzerland*
[2] *Department of Radiology, Lausanne University Hospital and University of Lausanne, Lausanne, Switzerland*
[3] *LTS5, École Polytechnique Fédérale de Lausanne (EPFL), Lausanne, Switzerland*
[4] *Swiss biomotion lab, Lausanne University Hospital and University of Lausanne, Lausanne, Switzerland*
[5] *Swiss Center for Musculoskeletal Imaging (SCMI) Balgrist Campus, Zurich, Switzerland*

[#] shared last authorship

INTRODUCTION: Despite recent evolution in magnetic resonance imaging (MRI) techniques for musculoskeletal applications, computed tomography (CT) remains the reference modality for the assessment of bone structure. The use of generative deep learning models, such as U-Nets, was shown to enable the synthesis of CT-like contrasts from MRI images. However, the development and validation of such tools have been hindered by the need for large datasets with paired CT and MRI acquisitions.

OBJECTIVE: In this preliminary work, we propose to train a U-Net, a supervised deep learning technique, to generate synthetic CT (sCT) knee images from three-dimensional T1-weighted MRI scans by leveraging a large knee dataset with paired acquisitions. The synthetic CT images were then assessed quantitatively and qualitatively.

METHODS: A cohort consisting of 249 patients (39.7±16.0 years old, 133 females) received both a knee MR examination (3T MAGNETOM Prisma^{fit}, Siemens Healthcare, Erlangen, Germany) and a CT scan (Revolution, General Electronics Healthcare). T1-weighted MR images (TR 700ms, TE 11ms, 0.5mm isotropic) were spatially registered to the down-sampled CT data (originally 0.3mm isotropic). To ensure a good voxel-to-voxel correspondence, the 99 best registered image pairs were selected and split between training (80%), testing (10%) and validation sets (10%). During training, 100 central slices were extracted for each orientation (axial, coronal and sagittal) and fed to a 2.5D network as stacks of three consecutive MRI slices. At inference, sCT slices were generated for each orientation, and the voxel-wise median across orientations was computed.

RESULTS: Qualitatively, our method successfully generated images with a CT-like contrast exhibiting satisfactory levels of anatomical details, including bone contours, and the femoral and tibial physes. However, the sCT images looked generally oversmoothed compared to the original CT data, hindering the visualization of some of the bone trabeculae, especially in the epiphyses. Some anatomical details such as vascular canals were not depicted accurately. In terms of quantitative evaluation, our model achieved a mean average error of 167±23.1 and 49.5±6.76 Hounsfield Units (HU) in bone and soft tissue, respectively.

CONCLUSION: In this preliminary work, we showed the feasibility of generating sCT images from T1-weighted MR data with a good level of anatomical details and quantitative HU estimation. Future work will focus on reducing the impact of registration errors to further improve the model accuracy.

SPONSOR: this work was performed with the support of the Swiss National Science Foundation, Switzerland (Sinergia grant CRSII5_177155)
DISCLOSURE STATEMENT: T. Kober and S. Sommer are employees and hold stocks of Siemens Healthineers International AG, Switzerland; Charbel Mourad has received the Swiss Government Excellence Scholarship for post-doctoral research (2022-2023).
CORRESPONDENCE ADDRESS: veronica.ravano@epfl.ch.

doi: 10.1016/j.ostima.2023.100111

EARLY DETECTION OF KNEE OSTEOARTHRITIS USING DEEP LEARNING ON KNEE MRI

A. Alexopoulos [1,2], J. Hirvasniemi [2], S. Klein [2], C Donkervoort [1,2], E.H.G. Oei [2], N. Tümer [1]

[1] *Department of Biomechanical Engineering, Delft University of Technology (TU Delft), Delft, The Netherlands*
[2] *Department of Radiology and Nuclear Medicine, Erasmus MC University Medical Center, Rotterdam, The Netherlands*

INTRODUCTION: Majority of the previous studies using deep learning approaches to predict knee OA incidence have used a radiography-based outcome variable. However, an MRI-based outcome variable could provide a more comprehensive view of OA.

OBJECTIVE: The aim of this study was to investigate the ability of three different deep learning algorithms to predict MRI-based knee OA incidence within 24 months from MR images.

METHODS: The intermediate-weighted turbo spin echo (IW-TSE) sequence of 593 OAI participants was used to predict knee OA incidence. Knee OA was defined using the MRI OA knee score (MOAKS) features except for osteophytes which were evaluated on radiographs. The IW-TSE MRIs were cropped to a region with a size of 250×320 voxels containing the knee joint. The position of the cropping box was defined as follows. First, a 2D U-Net model was used to segment tibial and femoral bone on a DESS sequence. The U-Net model was trained using the manual segmentations of femoral and tibial bone of 507 knees from the OAI-ZIB dataset. The performance of the segmentation algorithm was evaluated using the Dice similarity coefficient. Subsequently, IW-TSE and DESS sequences were registered using the Elastix software and the DESS segmentations were transformed to the corresponding IW-TSE scans. Finally, the coordinates of the tibial and femoral bones were used to define the position of the cropping box. Three different deep learning architectures using 3D MRI data as input were used to extract features from the cropped IW-TSE scans: a residual network (ResNet-50), a densely connected convolutional network (DenseNet-121), and a convolutional variational autoencoder (CVAE). Several combinations of batch size, learning rate, regularization, and data augmentation were tested. Furthermore, different combinations of discriminative penalties and latent space dimensions were tested for CVAE. 70% of the knees were included in the training set, 15% in the validation set, and 15% in the holdout test set. For comparison, a logistic regression model was trained using only age, gender, and BMI of the participants. Furthermore, a logistic regression model that combined the aforementioned basic variables and the image features was trained. Performance of the basic model (age, gender, BMI), image features model, and basic+image features model to predict knee OA incidence was assessed using the area under the receiver operating characteristic curve (ROC AUC) and the precision-recall curve (PR AUC) metrics using Python.

RESULTS: The Dice similarity coefficients for the automatic segmentation of tibial and femoral bones were 0.985 and 0.987, respectively. The basic model had an ROC AUC of 0.639 and an PR AUC of 0.364 to predict knee OA incidence in the test set. Of the models based on the images only, CVAE was the best performing model according to the ROC AUC values (ROC AUC: 0.669, PR AUC: 0.346). Of the models combining basic variables and images, the basic + CVAE model was the best performing model according to the ROC AUC values (ROC AUC: 0.670, PR AUC: 0.359). When combined with the basic model, the best performing ResNet-50 model had an ROC AUC of 0.651 and an PR AUC of 0.379 and the best performing DenseNet-121 model had an ROC AUC of 0.656 and PR AUC of 0.371. According to the PR AUC values, the CVAE model that included kernel regularization and had lower number of latent space dimensions than the CVAE model with the highest ROC AUC, was the best performing model (PR AUC: 0.416, ROC AUC: 0.601).

CONCLUSION: CVAE deep learning models had the highest performance to predict OA incidence using IW-TSE MRIs. Inclusion of age, sex, and BMI in the models improved the performance of the prediction algorithms. In general, the performance of all models was limited showing that the prediction of knee OA incidence is a complex problem. The impact of other MRI sequences, modalities, and data (e.g., genetics) will be investigated in the future.

SPONSOR: None
DICLOSURE STATEMENT: None
CORRESPONDENCE ADDRESS: j.hirvasniemi@erasmusmc.nl.

doi: 10.1016/j.ostima.2023.100112

ESTABLISHING A CONSECUTIVE CLINICAL KNEE OSTEOARTHRITIS IMAGING COHORT USING ARTIFICIAL INTELLIGENCE TOOLS TO ANALYZE KNEE RADIOGRAPHS: A PROOF OF PRINCIPLE

A. Lenskjold [1,2], M.W. Brejnebøl [1,2], J.U. Nybing [1,2], M.H. Rose [3], H. Gudbergsen [4,5], A. Troelsen [6], A. Moller [5], H. Raaschou [2,7], M. Boesen [1,2]

[1] *Dept. of Radiology, Bispebjerg-Frederiksberg Hospital, University of Copenhagen, Copenhagen, Denmark*
[2] *Radiological Artificial Intelligence Testcenter, Copenhagen, Denmark*
[3] *Charlie Tango, Copenhagen, Denmark*
[4] *The Parker Institute, University of Copenhagen, Copenhagen, Denmark*
[5] *Center for General Practice, Dept. of Public Health, University of Copenhagen, Copenhagen, Denmark*
[6] *Dept. of Orthopaedic Surgery, Copenhagen University Hospital Hvidovre & CAG ROAD – Research OsteoArthritis, Denmark*
[7] *Dept. of Radiology, Herlev-Gentofte Hospital, University of Copenhagen, Copenhagen, Denmark*

INTRODUCTION: Traditional knee OA research cohorts are curated to test research hypotheses in controlled environments, but they lack near-clinical prevalence, current trends, and diversity in gene pools from around the world. Recently, artificial intelligence (AI) models have been shown to diagnose and grade the degree of knee OA in agreement with experienced consultants in musculoskeletal radiology.

OBJECTIVE: As a proof of concept, this study aims to create a scalable consecutive clinical knee OA imaging cohort that reflects current trends with limited use of human resources by using various AI tools.

METHODS: We included patients aged 35 to 79 with a weight-bearing knee radiograph from the University of Copenhagen Hospital, Bispebjerg-Frederiksberg Hospital, from January 1, 2016, to December 31, 2021. Four AI tools were applied to the retrospective cohort: 1) CE-marked and FDA-approved knee OA grading tool provided KL grades and minimal joint space width (MJSW) on bilateral frontal radiographs and the presence of patella osteophytes on lateral radiographs, 2) inhouse custom-build convolution neural network (CNN) radiographic view tool supported the OA grading tool confirming the inclusion of correct views, 3) inhouse custom-build CNN knee joint implant tool helped us exclude radiographs with implants, and 4) laterality marker detection tool detected missing or inconsistent markers on bilateral frontal images.

RESULTS: We found 32,707 knee radiographs from 8,641 patients in the PACS and ended up with 25,854 bilateral frontal and lateral radiographs from 8,618 patients and their 9,689 examinations after the cleaning process with the four tools. Most knees (92.5 %) had complete AI-generated OA data (KL grade, MJSW, patella osteophyte results). We used no radiologist reading time, and only 16.0 % of the images were read by humans during quality control processes. It would have taken a radiologist about 800 hours to grade the radiographs if they had spent five minutes per examination.

CONCLUSION: In this study, we showed that a consecutive clinical large-scale knee OA imaging cohort can be created from raw clinical images from the PACS system using a combination of four AI tools and no radiologist readings. This approach will enable us to test previous and new OA hypotheses on broader real-life clinical updated datasets that could help us diversify the findings and prevent data dredging. In addition, our approach can be used to create similar scalable cohorts from other geographic areas. In the future, we plan to add knee radiographs from other hospitals, other modalities, such as CT and MRI, and clinical information from electronic health records.

SPONSOR: An unrestricted Signature Project grant from the Danish Agency for Digital Government sponsored the study and the primary author's salary.
DISCLOSURE STATEMENT: MB and AT are medical advisors for Radiobotics and have assets in the company. AL, MWB, JUN, MHR, HG, AM, and HR have no conflict of interest. The hospital department purchased the knee OA grading AI tool for clinical and research purposes.
CORRESPONDENCE ADDRESS: anders.lenskjold@regionh.dk; anderslenskjold@gmail.com.

doi: 10.1016/j.ostima.2023.100113

IMAGING-BASED CHARACTERIZATION OF 3 DIFFERENT OA ENDOTYPES DERIVED FROM BIOCHEMICAL MARKERS - DATA FROM TWO OBSERVATIONAL COHORTS

J. Bacardit [1], F. Roemer [2], M. Jansen [3], S. Maschek [4], A. Marijnissen [3], S.C. Mastbergen [3], A. Wisser [4], F. Lafeber [3], A. Lalande [5], H. Weinans [3], F. Blanco [6], F. Berenbaum [7], L.A. van de Stadt [8], M. Kloppenburg [8], I.K. Haugen [9], C. Ladel [10], A.C. Bay-Jensen [11], Y. Henrotin [12], A. Struglics [13], A. Mobasheri [14], F. Eckstein [4], W. Wirth [4]

[1] *Newcastle University, Newcastle, United Kingdom*
[2] *Univ. of Erlangen, Erlangen, Germany & Boston University School of Medicine, Boston, MA, USA*
[3] *UMC Utrecht, University of Utrecht, Utrecht, The Netherlands*
[4] *Paracelsus Med. University, Salzburg, Austria & Chondrometrics GmbH, Freilassing, Germany*
[5] *Servier, Suresnes, France*
[6] *INIBIC-Univ.e de A Coruña, A Coruña, Spain*
[7] *Sorbonne University, INSERM Paris, France & AP-HP Saint-Antoine Hospital, Paris, France*
[8] *Leiden University Medical Center, Leiden, The Netherlands*
[9] *Diakonhjemmet Hosp., Oslo, Norway*
[10] *Independent Consultant, Darmstadt, Germany*
[11] *Nordic BioSci., Herlev, Denmark*
[12] *Artialis SA, Liège, Belgium & University of Liège, Liège, Belgium*
[13] *Lund University, Lund, Sweden*
[14] *University of Oulu, Oulu, Finland*

INTRODUCTION: A recent machine-learning study identified 3 different endotype clusters, based on serum and urine biomarker concentration patterns that were consistent between both the APPROACH and the OAI-based FNIH cohort. The clusters were characterized as systemic inflammation (SI), low tissue turnover (LTT), and structural damage of bone and articular cartilage (DAM, Fig. 1).

OBJECTIVE: To evaluate whether the prevalence of joint tissue pathologies (MRI Osteoarthritis Knee Scores (MOAKS)) and femorotibial joint (FTJ) cartilage thickness differ between these clusters, and whether 2-year changes in MOAKS scores and FTJ cartilage thickness differ between these 3 clusters.

METHODS: APPROACH enrolled 297 participants (age: 66.5±7.1y, BMI: 28.1±5.3 kg/m^2, 77.5% women, 55% KLG 2-4) and FNIH 600 OA patients (age: 61.5±8.8y, BMI: 30.7±4.8 kg/m^2, 58.8% women, 87.5% KLG 2-4). Of 295 APPROACH / 600 FNIH participants with biochemical marker levels available, 93/178 were assigned to the LTT cluster, 92/241 to the SI cluster, and 110/181 to the DAM cluster, respectively. Semi-quantitative MOAKS scores were assessed at months 0 and 24 by an experienced radiologist. FTJ cartilage thickness was measured at months 0 and 24 by manual, quality-controlled segmentations. Frequencies were compared using X^2 tests between the clusters, and cartilage thickness measures using t-tests.

RESULTS: In APPROACH, baseline cartilage damage, osteophytes, effusion- and Hoffa-synovitis did not differ between the 3 clusters, while bone marrow lesions (BML) were more severe in the DAM cluster (Fig. 2). Medial meniscus damage was more severe in the LTT than the SI cluster (Fig. 2). In the FNIH cohort, baseline cartilage damage and BMLs were more severe in the DAM and SI clusters than in the LTT cluster (Fig. 2). Moreover, Hoffa-synovitis was more severe in the DAM than in the LTT cluster; no differences were observed for osteophytes or meniscus MOAKS scores (Fig. 2). In APPROACH, FTJ cartilage thickness was lower in the DAM than in the other clusters, while in FNIH, FTJ cartilage thickness was lower in both the DAM and SI than in the LTT cluster (data not shown).

In APPROACH, the DAM cluster showed more 2-year worsening of full thickness cartilage damage, osteophytes, and medial meniscus extrusion than the LTT cluster and more worsening of osteophytes than the SI cluster (data not shown). In FNIH, the DAM cluster displayed more 2-year worsening of cartilage damage extent, lateral meniscus extrusion, and Hoffa-synovitis than the LTT cluster (data not shown). The LTT cluster showed more worsening in BMLs than the DAM cluster, and more worsening in osteophytes than the SI cluster. In both cohorts, change in FTJ cartilage thickness did not differ between clusters (data not shown).

CONCLUSION: Differences in the severity of MR imaging features were more pronounced between clusters in the FNIH than in the APPROACH cohort, potentially because of the greater percentage of knees with radiographic knee OA (KLG2-4). Still, imaging features did not appear to be highly specific for the clusters derived from baseline biochemical markers, most likely because systemic biochemical markers are not only influenced by the selected target knee but also by other joints and tissue changes.

SPONSOR: EU/EFPIA (APPROACH grant n° 115770) and NIH/FNIH.
DICLOSURE STATEMENT: AW, SM, FE, WW: Chondrometrics GmbH; FWR: BICL
ACKNOWLEDGMENT: IMI-APPROACH and OAI participants and investigators
CORRESPONDENCE ADDRESS: wolfgang.wirth@pmu.ac.at.

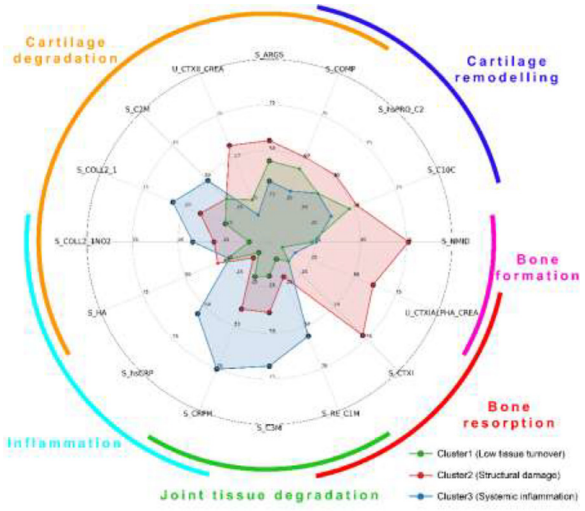

Figure 1: Radar-plot showing the 3 identified endotypes (1: low tissue turnover, 2: structural damage, and 3: systemic inflammation) and the associated serum and urine markers.

doi: 10.1016/j.ostima.2023.100114

EXTERNAL VALIDATION OF AN ARTIFICIAL INTELLIGENCE TOOL FOR RADIOGRAPHIC KNEE OSTEOARTHRITIS CLASSIFICATION: A MULTI-CENTER, RETROSPECTIVE DIAGNOSTIC COHORT STUDY

M.W. Brejnebøl [1,2], A. Lenskjold [1,2], K. Ziegeler [3], H.C. Ruitenbeek [4], J.J. Visser [4], J.U. Nybing [1,2], K.G.A. Hermann [3], E.H.G. Oei [4], M. Boesen [1,2]

[1] *Department of Radiology, Bispebjerg and Frederiksberg Hospital, Copenhagen, Denmark*
[2] *RAIT – Radiological Artificial Intelligence Testcenter, Denmark*
[3] *Department of Radiology, Charité Universitätsmedizin, Berlin, Germany*
[4] *Department of Radiology and Nuclear Medicine, Erasmus Medical Center, Rotterdam, The Netherlands*

INTRODUCTION: In routine clinical practice, radiography of the weight-bearing knee is frequently obtained to support the OA diagnostic process. The reading time of radiographs is short, but the volume of studies is large, resulting in a substantial radiologist workload. Artificial Intelligence (AI) tools for radiographic knee OA severity classification have been commercially available for some time. However, the generalizability of these tools across countries remains limited.

OBJECTIVE: The overall objective of this study was to evaluate a commercially available AI tool for radiographic knee OA classification across a heterogenous clinical dataset. Our specific objectives were:
1-Investigate the overall diagnostic performance of the AI tool for KLG classification.
2-Investigate the sub-group performance for posterior-anterior (PA) vs. anterior-posterior (AP) projection radiographs.

METHODS: This was a multi-center, retrospective diagnostic test accuracy study. We consecutively included seventy-five cases from the production Picture Archiving and Communications System (PACS) of each of the three EU-based study sites, yielding a sample size of n = 225. Inclusion criteria were age >= 20 years, clinical suspicion of knee OA, at least one weight-bearing PA or AP projection knee radiograph and one lateral knee radiograph of the symptomatic knee. Exclusion criteria were knee arthroplasty or other foreign objects near the knee joint, and the study was from an already included patient. The three study sites (Bispebjerg and Frederiksberg Hospital, Copenhagen, Denmark, Erasmus Medical Center, Rotterdam, the Netherlands, and Charité Universitätsmedizin, Berlin, Germany) routinely obtained their frontal knee radiographs differently: one site used PA, one AP, and one full-leg stitched AP where the knee joint was not necessarily centered to the x-ray beam. Only one symptomatic knee was used for each patient. The reference standard was established based on the independent scoring of three professors in musculoskeletal radiology, K-GAH, EHGO, and MB (one from each site). In case of discrepancies, the reference value was the majority vote of the three or by consensus meeting when KLGs differed by two or more. A knee was discarded if two or more scored an image as inadequate for diagnostic use (equivalent to recalling the patient for a new radiograph). MWB performed the AI tool (RBknee^{TM} v2.1) analysis on a local machine. Weighted accuracy for ordinal values (OWA) was used for the ordinal scores, and regular accuracy was used for binary scores.

RESULTS: The study sample had the following characteristics: female sex: 50% (113/225), age: mean (sd) 54.6 years (14.8 years), KLG-0: 49, KLG-1: 60, KLG-2: 46, KLG-3: 39, KLG-4: 15. The AI tool achieved an overall OWA for KLG classification of 88% CI95% [86-90%]. OWAs for KLG classification in the subgroups were: PA-projection 89% CI95% [86-92%], AP-projection 84% CI95% [80-88%], and AP-stitched-projection 89% CI95% [86-92%]. When the KLG was collapsed into the binary presence of knee OA (KLG >= 2), overall accuracy was 86% (180/209) CI95% [81-90%]. For the subgroups: PA-projection 90% CI95% [83-97%], AP-projection 90% CI95% [82-96%], and AP-stitched-projection 78% CI95% [68-88%]. The reference evaluated five studies as inadequate for diagnostic use, and the AI tool produced an error for the target knee in 11/225 (~5%) studies with no overlap between the two sets.

CONCLUSION: We found diagnostic performance of the test AI tool to be at or slightly below previously reported numbers for similar tools, likely due to the more robust cohort design that allows us to generalize to a broad spectrum of daily clinical practices. Still, the AI tool performed similarly to previously reported human readers. The next research steps include evaluating reader performance without and with AI assistance and comparing the findings to the stand-alone AI tools.

SPONSOR: This project has received funding from the European Union's Horizon 2020 research and innovation programme under the grant agreement No 954221.
DISCLOSURE STATEMENT: M. Boesen is a Medical Advisor and shareholder at Radiobotics ApS. Radiobotics ApS was the primary beneficiary of the grant mentioned above. The three departments of radiology were subcontractors. However, the three departments performed all data management, reference scoring, AI analysis, statistical analysis, and manuscript write-up without the involvement of Radiobotics ApS. M.W. Brejnebøl, A. Lenskjold, E. Oei, J.U. Nybing, H.C. Ruitenbeek, K. Ziegeler, J.J. Visser, and K.G. Hermann declare no conflicts of interest in relation to this work.
ACKNOWLEDGMENT: Radiobotics ApS for providing access to their AI tool, RBknee, free of charge.
CORRESPONDENCE ADDRESS:
mathias.willadsen.brejneboel@regionh.dk,
mathiaswbrejne@outlook.com.

doi: 10.1016/j.ostima.2023.100115

COMPUTED TOMOGRAPHY OSTEOARTHRITIS KNEE SCORE (COAKS) CONSTRUCTION, REPRODUCIBILITY AND POTENTIAL FOR STRUCTURAL PHENOTYPING

T.D. Turmezei [1], J.H. Jeon [1], Z. Akkaya [2], N.A. Segal [3]

[1] *Norfolk and Norwich University Hospital, Norwich, UK*
[2] *Department of Radiology and Biomedical Imaging, University of California San Francisco, CA/USA, & Ankara University Faculty of Medicine Department of Radiology, Ankara, Turkey*
[3] *University of Kansas Medical Center, Kansas City, KS, USA*

INTRODUCTION: Computed tomography (CT) has been shown to be more sensitive identifying certain structural features of OA than radiography and MRI. The ability to acquire weight bearing CT (WBCT) at the knee is also an important current advantage over MRI that has created an opportunity to assess the entire weight bearing joint in 3-D. This could have implications for longitudinal monitoring of disease progression and the selection of participants in clinical trials according to structural phenotype.

OBJECTIVES: 1) To introduce the semi-quantitative CT OA Knee Score (COAKS); 2) to report initial interobserver reproducibility; and 3) to demonstrate its potential for structural disease phenotyping.

METHODS: 106 WBCT examinations were sourced from existing research projects at the Department of Rehabilitation Medicine, University of Kansas Medical Center, USA. A 4-point scoring system (0-3) was created for each cardinal radiographic feature of osteoarthritis (J = joint space width; O = osteophytes; C = subchondral cysts; S = subchondral sclerosis) to be assessed at each joint compartment (MTF = medial tibiofemoral; LTF = lateral tibiofemoral; PF = patellofemoral; PTF = proximal tibiofibular). Brief verbal definitions are given for each feature score in table 1. After initial training and grading of all knees by a musculoskeletal radiology clinical fellow (J.J.H.), a reference atlas was created that included a standardised review guide (including display settings and multiplanar reformat orientations), examples of each score for each feature at each compartment, and common pitfalls. Blinded to the imaging data, 10 test knees and 35 study knees were super-selected by their initial scoring to stratify disease features as evenly as possible. No restrictions were placed on the quality of imaging, the presence of ACL reconstruction (an inclusion criteria for one source study), or imaging review platform. T.D.T. trained another consultant musculoskeletal radiologist (Z.A.), who both assessed the 10 test knees, reviewed performance, then repeated the test assessment. Both then scored the 35 study knees without communication during the assessment period. A cloud score sheet was used in Google Sheets (table 2) with the reference atlas in Google Docs, both accessible online or via the respective smart phone / tablet app. The weighted kappa score for interobserver reproducibility was calculated for each structural feature across all compartments. Compartment feature scores were also plotted as heat maps for each knee to provide a visualisation of structural OA phenotype.

RESULTS: The weighted kappa scores (+95% CI) for each feature were: J = 0.87 (0.86-0.89); O = 0.79 (0.76-0.82); C = 0.66 (0.63-0.70); S = 0.84 (0.82-0.86). On average, it took less than 5 minutes to score a single knee. Selected heat maps (figure 1) show how different phenotypes can be ascertained using the COAKS system: RUNA053L is an early MTF phenotype with PF involvement; RUNA045R is a late MTF phenotype with multicompartment disease; RUNA023L is a late LTF phenotype with severe multicompartmental osteophytosis but no other features; RUNA088L is a PF phenotype with small tibiofemoral osteophytes only. A whole joint COAKS score is also possible (out of 48), as is a score by compartment (out of 12) or by feature (out of 12) as desired.

CONCLUSION: COAKS is a feasible semi-quantitative WBCT-based scoring system of knee OA that demonstrates initial substantial to almost perfect inter-observer agreement across radiographic features. The ability of COAKS to score and phenotype the weight bearing knee in 3-D may exceed individual capabilities of MRI and radiography in certain aspects, offering flexibility in phenotyping for patient selection as well as potential sensitivity for longitudinal monitoring of disease severity in clinical trials or cohort studies. It is also possible to use the COAKS in non-weight bearing CT if flagged as such and not used to compare with weight bearing studies.

SPONSOR: None.
DISCLOSURE STATEMENT: NS is a consultant for Integra BioLife, Trice Medical and Pacira Biosciences. TT has been a consultant for Curvebeam AI. ZA is a consultant for Calico Life Sciences LLC.
ACKNOWLEDGEMENT: The authors would like to thank Frank Roemer, Patrick Omoumi, Mohamed Jarraya, James Mackay and Andoni Toms for expert consultation during development of the scoring system.
CORRESPONDENCE ADDRESS: tom@turmezei.com.

Table 1

Score	Joint space width (J)	Osteophytes (O)	Subchondral cysts (C)	Subchondral sclerosis (S)
0	No narrowing	None	None	None
1	<50% narrowing	Small	One cyst at a single location	Possible or suspected
2	>50% narrowing	Medium	Multiple cysts on the same side of the joint	Definite
3	Complete or near complete	Large	Cysts (single or multiple) on both sides of the joint	Severe with bony eburnation, collapse, erosion or deformity

Table 2

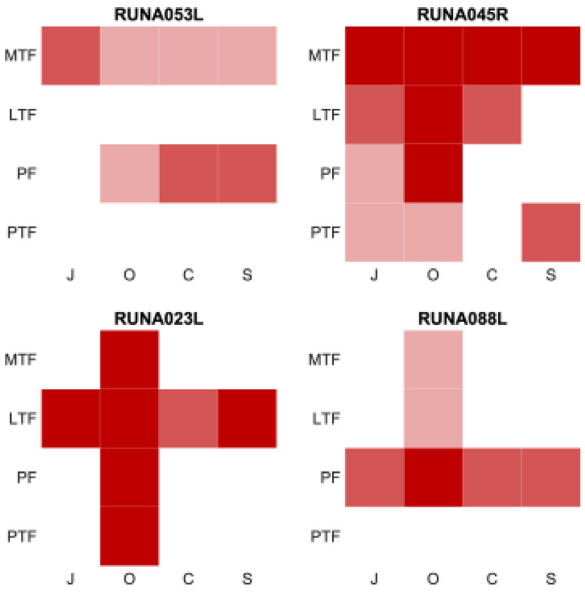

Figure 1

doi: 10.1016/j.ostima.2023.100116

AGREEMENT OF AUTOMATED LAMINAR FEMOROTIBIAL CARTILAGE TRANSVERSE RELAXATION TIME (T2) ANALYSIS WITH MANUAL EXPERT SEGMENTATION

F. Eckstein [1,2], N.M. Brisson [3], S. Maschek [2], A. Wisser [1,2], F. Berenbaum [4], G.N. Duda [3], W. Wirth [1,2]

[1] *Institute of Anatomy & Cell Biology and Ludwig Boltzmann Institute for Arthritis and Rehabilitation, Paracelsus Medical University, Salzburg, Austria*
[2] *Chondrometrics, Freilassing, Germany*
[3] *Julius Wolff Institute, Berlin Institute of Health at Charité - Universitätsmedizin Berlin, Germany*
[4] *Department of Rheumatology, Sorbonne University, INSERM, AP-HP Saint-Antoine Hospital, Paris, France*

INTRODUCTION: Articular cartilage transverse relaxation time (T2) on MRI has been observed to reflect collagen integrity, orientation, and hydration, and to be associated with cartilage histological grading, mechanical properties, and early knee OA status. Previously, we reported high agreement of cartilage segmentations obtained from multi echo spin echo (MESE) MRI, using fully automated deep learning methods, in comparison with manual ones. As these results were based on 3T MRI (of the OAI), we here explored the agreement between fully automated segmentation of MESE cartilage at 1.5T.

OBJECTIVE: To analyze the agreement between automated, U-Net-based segmentation of femorotibial cartilage from MESE by convolutional neural networks vs. manual expert segmentation with quality control of the same images, and to compare laminar femorotibial cartilage T2 between both approaches.

METHODS: We studied 20 ACL-deficient patients with persistent dynamic knee instability (non-copers), 22 without instability (copers), 13 with surgical ACL reconstruction, and 16 healthy controls. Further patient characterizations are described in a parallel abstract at this conference. Sagittal MESE MRIs were acquired at 1.5T (Siemens Avanto; slice thickness/spacing 3/3.5mm, in-plane resolution 0.31mm, TR 1500ms, TE 9.7/19.4/29.1/38.8/48.5/58.2/67.9ms), at baseline (n=71) and 1 year later (n=55). Manual cartilage segmentation was done by experienced readers, with quality control by an expert (Fig. 1). The U-Net was trained using medial and lateral MRIs from the same scanner (training/validation set n=50/9) obtained in volleyball athletes of different age groups, and in patients with posterior cruciate ligament (PCL) surgery, segmented by the above readers. Training of the U-net was performed for both all 7 echos and only the 1st echo. Automated U-Net segmentation was then applied to the current study MRIs, without manual intervention or correction. Yet, automated post-processing was employed to correct obvious segmentation errors. The agreement between manual and automated U-Net-based segmentations was evaluated using the Dice Similarly Coefficient (DSC), and by evaluating systematic differences and correlations in cartilage T2 of the 50% superficial and 50% deep layer.

RESULTS: When all echoes were used for training, the overall DSC was 0.89 for MT/LT, and 0.83 for cMF/cLF. When only the 1st echo was used, DSCs were 0.87/0.88 and 0.81/0.79. Automated analysis overestimated the segmented tissue volume significantly in most regions, with correlations ranging from 0.93-0.96 for all echoes, and from 0.87-0.94 for the 1st echo. Deep layer T2 across the joint was 45.7ms for manual analysis, 45.7ms with all echoes, and 46.1ms with the 1st echo model; superficial layer T2 was 52.1, 53.2 and 54.4ms. There were statistically significant (albeit small) differences of automated vs. manual analysis across most regions for the superficial layer, and for LT and cLF in the deep layer. The correlation of deep layer T2 across the plates ranged from 0.91-0.99 for all echoes model, and from 0.85-0.98 for the 1st echo model, and that of the superficial T2 from 0.86-0.97, and from 0.73-0.81.

CONCLUSION: Fully automated (U-Net-based) laminar analysis of femorotibial cartilage T2 appears feasible at 1.5T, albeit the agreement for T2 at 3T, and that for cartilage thickness was previously reported to be higher. The agreement with manual analysis was greater when training a model with 7 echoes than with the 1st echo only, and it was greater for the deep than for the superficial layer. No significant change in T2 was observed over 1 year; thus, longer intervals may be required for longitudinal validation.

SPONSOR: OVERLOAD - PrevOP (01 EC1408A) and OA-BIO Eurostars (E! 114932). The German project partners received funding from the Bundesministerium für Bildung und Forschung (BMBF).
DISCLOSURE STATEMENT: FE, WW, SM and AW are part time employees of Chondrometrics GmbH; FE, WW, and SM are co-owners of Chondrometrics GmbH. FE has provided consulting services to Merck KGaA, Kolon-Tissuegene, and Novartis. FB is co-owner of 4Moving Biotech. NMB and GND have no conflicts of interest to declare.
ACKNOWLEDGMENT: We thanks the Chondrometrics GmbH readers for image segmentation.
CORRESPONDENCE ADDRESS: eckstein@chondrometrics.de.

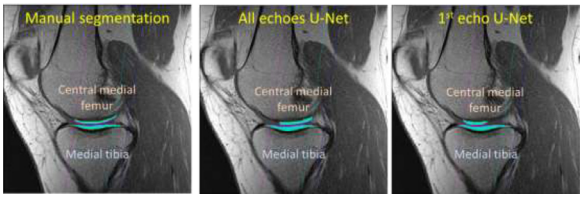

Figure 1: Segmentation of the medial tibial (MT) and weight-bearing (central) medial femoral cartilage (cMF) derived manually with quality control (left), from a U-net CNN model comprising all 7 echoes of the multi echo spin echo (MESE) acquisition (middle), and from one comprising only the 1st echo.

doi: 10.1016/j.ostima.2023.100117

BONE MARROW EDEMA-LIKE IN FEMORAL HEAD OSTEONECROSIS: A SURROGATE OF EARLY COLLAPSE?

J. Berberi [1], B. Vande Berg [2], C. Mourad [3]

[1] *Faculty of Medical Science, Lebanese University, Beirut, Lebanon & Hôpital Henri Mondor, Créteil, France*
[2] *CHC cliniques Mont-Légia, Liège, Belgium*
[3] *Faculty of Medical Science, Lebanese University, Beirut, Lebanon & Swiss Biomotion Lab, Lausanne University, Lausanne, Switzerland*

INTRODUCTION: Osteonecrosis of the femoral head (ONFH) is the leading cause of secondary hip OA in the young population. The occurrence of subchondral fracture is the determining step towards femoral head collapse and OA. Bone marrow edema-like (BME) signal intensity in the femoral head may be an indicator of early collapse in ONFH.

OBJECTIVE: To correlate the presence of BME of the femoral head at MRI with the presence of cortical and subchondral fracture at CT, and with the presence of pain.

METHODS: 76 patients with ONFH (mean age 45.9 years ±9.8 [standard deviation]; 60 male (79%)) underwent radiographs, MRI and CT of the hips with ONFH (n=83) within a short period of time (mean interval, 3.9 days ± 9.08 [standard deviation]). MRI protocol included large FOV coronal T1 and STIR of bilateral hips and small FOV sagittal T1 and FS-IW of the hip in question. Pain was assessed using the Western Ontario and McMaster Universities Arthritis Index (WOMAC). Staging of FHON was performed using MRI and radiographs by a consensus reading between two MSK radiologists according to the 2019 version of the ARCO classification. One radiologist assessed the presence of BME signal intensity of the proximal femur and synovitis/effusion of the hip joint on MRI. One radiologist, blinded to MRI findings and ARCO stage, analyzed CT images to look for the presence of cortical and trabecular fractures. Data was tabulated on Excel sheets and descriptive statistics were performed. Normality of the distribution was assessed using Shapiro-Wilk. Comparison was performed using Student's t-test. Mann-Whitney U-test or Chi-squared test when applicable. A p value of <0.05 was used for statistical significance for the abovementioned tests.

RESULTS: There were 36 (43.4%) hips with BME at MRI (1 ARCO 1; 5 ARCO 2; 20 ARCO 3-A; 6 ARCO 3B and 4 ARCO 4), and 47/83 (56.6%) without BME (20 ARCO 1; 22 ARCO 2; 3 ARCO 3-A; 2 ARCO 3B and 0 ARCO 4). Among hips with BME on MRI, 26 (55.3%) showed fracture at CT (24 cortical and 25 trabecular fractures), while 10 (21.3%) of hips without BME showed fracture on CT (6 cortical and 10 trabecular fractures) (p=0.0015). The WOMAC-pain score was 30.8 ± 22.6 for hips without BME and 39.7 ± 21.4 for hips with BME (p=0.073)

CONCLUSION: in ONFH, the presence of BME on MRI is associated with the presence of fracture on CT, but is not correlated to the severity of pain.

SPONSOR: N/A
ACKNOWLEDGMENT: N/A
CORRESPONDENCE ADDRESS: jessicaberberi@hotmail.com.

doi: 10.1016/j.ostima.2023.100118

EARLY HIP CARTILAGE DEGENERATION IN YOUNG PATIENTS MEETING A CONSENSUS DEFINITION OF FEMOROACETABULAR IMPINGEMENT SYNDROME

H. Zhang [1], J. Cibere [2], C.E. Jones [1], D.R. Wilson [1]

[1] *Center for Aging SMART, University of British Columbia (UBC), Vancouver, BC, Canada*
[2] *Arthritis Research Canada, UBC, Vancouver, BC, Canada*

INTRODUCTION: The role of hip deformities, such as those leading to femoroacetabular impingement (FAI), in hip osteoarthritis is of great interest because of the potential to correct the deformities surgically and protect the joint from degeneration. Evidence linking FAI deformities to cartilage degeneration is conflicting, however. This is partly because of inconsistent definitions of clinical FAI. To address this problem, a recent consensus statement (Warwick consensus) has defined clinical FAI syndrome as a triad of pain, positive physical impingement test, and radiological deformities in the hip joint. It is not clear, however, whether this new clinical definition of FAI is associated with early cartilage degeneration, since the consensus is based on clinical opinion.

RESEARCH QUESTION: Do patients with FAI syndrome (defined by the Warwick consensus) have signs of hip cartilage degeneration?

METHODS: The study was approved by UBC's Clinical Ethics Board (H11-00868 and H11-03332). We recruited participants with FAI syndrome and healthy controls from an MRI and dGEMRIC study (128 participants aged 43.5, 44 males) whose participants were recruited from a population-based study IMPAKT-HIP (Investigations of Mobility, Physical Activity, and Knowledge Translation in Hip Pain) (500 Caucasian Adults aged at 41.7 (20-49), 181 males). Participants were defined as having FAI syndrome if they a) reported hip pain of more than six weeks' duration; b) had a positive standardized impingement test; and c) had a pincer deformity identified in an AP radiograph and/or a cam deformity identified in 3T MRI scan. Healthy hips were defined as those with a) no reported pain; b) a negative standardized impingement test; and c) no pincer or cam deformity on AP radiograph and 3T MRI, respectively. We identified 26 participants (age 44.4±6.0, 9 males) with FAI syndrome hips and 22 (age 44.1±5.5, 5 males) with healthy hips. We assessed the dGEMRIC index in the study hip of each participant using a standard dGEMRIC protocol, in which 0.4ml/kg of 0.5mmol/ml Gd-DTPA^{2-} (0.2mmol/kg, Magnevist Bayer) was given by IV 90min before imaging and 10min weight-bearing exercise was performed right after injection. We segmented the acetabular and femoral cartilage separately and divided both into five regions for comparison. Cartilage layers were projected into 2D maps using spherical coordinates with the normal of the acetabular opening plane/femoral neck axis going through the acetabular center/femoral head center as the zenith axis for acetabular/femoral cartilage (Figure 1). We compared overall hip dGEMRIC scores, femoral and acetabular dGEMRIC scores, and regional dGEMRIC scores between the FAI syndrome hips and the healthy hips using independent-samples T-tests.

RESULTS: The dGEMRIC scores of acetabular cartilage of hips with FAI syndrome are significantly lower than those of healthy hips (p=0.020). The dGEMRIC scores of femoral cartilage and the overall dGEMRIC scores of hips with FAI syndrome are lower, but not significantly, p=0.197 and p=0.104 respectively. Figure 1 shows the comparison results of the regional cartilage dGEMRIC scores.

CONCLUSION: There are signs of cartilage degeneration in hips meeting the new clinical consensus definition of FAI syndrome.

CORRESPONDENCE ADDRESS: david.wilson@ubc.ca.

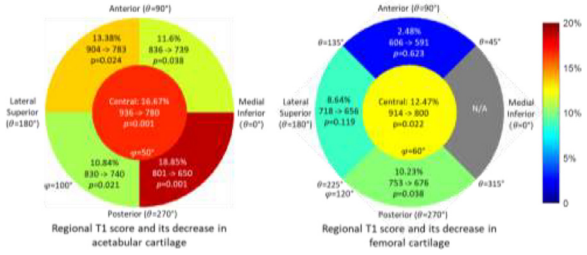

Figure 1 score decreased in all sub-regions of acetabular and femoral cartilage.

doi: 10.1016/j.ostima.2023.100119

SEVERE RESIDUAL LEGG-CALVÉ-PERTHES DISEASE DEFORMITY IS ASSOCIATED WITH REDUCED HIP CLEARANCE AND CARTILAGE HEALTH IN ADOLESCENTS AND YOUNG ADULTS

L.G. Johnson [1], H. Zhang [1], C.E. Jones [1], E.K. Schaeffer [2], K. Mulpuri [2], D.R. Wilson [1]

[1] *University of British Columbia, Vancouver, BC, Canada*
[2] *University of British Columbia, Vancouver, Canada & BC Children's Hospital, Vancouver, BC, Canada*

INTRODUCTION: Legg-Calvé-Perthes disease (LCPD) often results in permanent residual deformity of the femoral head, and many patients experience pain, poor hip function, and early-onset hip osteoarthritis (OA). Our understanding of how LCPD deformity leads to these outcomes is limited. One hypothesis is that an anterior extrusion on the femoral head impinges against the acetabular rim in high flexion postures, but hip clearance in these postures has never been measured in patients with residual LCPD deformity. Additionally, it is not clear how soon cartilage damage occurs in LCPD hips, making it difficult for clinicians to decide the best management approach for patients who do not yet have hip pain.

OBJECTIVE: We answered two research questions:
1-Does increased severity of residual LCPD result in reduced hip clearance in high flexion postures? 2-Is cartilage $T_{1\rho}$ increased in hips with mild and severe LCPD, compared to contralateral hips?

METHODS: We recruited 11 participants (age range: 12-24 years, 2 F/9 M) with stage IV unilateral or bilateral LCPD (13 affected hips, Stulberg I-IV; 9 contralateral) from a tertiary pediatric hospital research database. The affected hip(s) of each participant was scanned in four physiological postures: supine; supine with flexion, adduction and internal rotation (FADIR); seated; and seated FADIR using a 0.5T upright open MRI scanner (MROpen, ASG Superconductors, Genoa, Italy). In each posture, a T_1 GFE sequence (TR=431ms, TE 12ms, 5mm slice thickness, 384×256 matrix) was used to image the femoral head and neck in the α-angle plane, from which hip clearance (β angle) was measured. Both hips of each participant were also scanned in a 3T MRI scanner (Discovery MR750, GE Healthcare, Chicago, IL) using a $T_{1\rho}$ sequence (TR=800ms, TSL [1,15,30,45]ms, 4mm slice thickness, 256×192 matrix). One rater segmented articular cartilage on the femoral and acetabular sides, from which the mean $T_{1\rho}$ relaxation time was calculated. For statistical analysis, affected hips were grouped into 'minor deformity' (Stulberg I/II) and 'major deformity' (Stulberg III/IV) classes. The associations between β angle/$T_{1\rho}$ relaxation time, residual LCPD deformity class, and posture/side of hip (affected vs contralateral) were tested with separate mixed models, with patient as the random variable for both.

RESULTS: A significant reduction in hip clearance in the supine posture was observed between Stulberg I/II and III/IV hips (change in $\beta = -57.0^{\circ}$; 95CI: -84.4°, -29.6°; $p < 0.001$) hips. Non-significant reductions were observed in all other postures due to interaction effects between deformity class and posture. Overall mean $T_{1\rho}$ relaxation time was significantly increased in Stulberg III/IV hips (change in $T_{1\rho} = 3.0$ ms; 95CI: 0.1-5.8; $p = 0.041$) compared to contralateral hips.

CONCLUSION: This study has shown that severe residual LCPD reduces hip clearance compared to mild deformity, and that there are signs of cartilage degeneration in patients with severe deformities during adolescence and young adulthood. The main limitation of this study is the sample size, which is reflective of the difficulty of recruiting patients who have had this rare condition and no longer have regular clinical visits. Despite this, the evidence of early cartilage degeneration supports early surgical intervention to conserve the joint in cases of severe radiographic deformity, even if the patient is asymptomatic during adolescence.

SPONSOR: Canadian Institutes of Health Research, Funding reference #165956
DICLOSURE STATEMENT: L.G. Johnson is supported by Arthritis Society Canada.
ACKNOWLEDGMENT:
CORRESPONDENCE ADDRESS: luke.johnson@hiphealth.ca.

doi: 10.1016/j.ostima.2023.100120

T2 AND T2* RELAXOMETRY OF CARTILAGE AT THE WRIST JOINT: A COMPARATIVE STUDY OF 3T AND 7T MRI

R. Heiss [1], M.A. Weber [2], E. Balbach [1], M. Hinsen [1], F. Geissler [1], A.M. Nagel [1,3], M.E. Ladd [3], A. Arkudas [4], R.E. Horch [4], C. Gall [5], M. Uder [1], F.W. Roemer [1,6]

[1] *Radiology, Universitätsklinikum Erlangen & Friedrich-Alexander Universität Erlangen-Nürnberg, Erlangen, Germany*
[2] *Radiology, University Medical Center Rostock, Rostock, Germany*
[3] *Medical Physics in Radiology, German Cancer Research Center (DKFZ), Heidelberg, Germany*
[4] *Department of Plastic and Hand Surgery and Laboratory for Tissue Engineering and Regenerative Medicine, Universitätsklinikum Erlangen & Friedrich-Alexander Universität Erlangen-Nürnberg, Erlangen, Germany*
[5] *Institute for Medical Informatics, Biometry and Epidemiology, Friedrich-Alexander-Universitat Erlangen-Nürnberg, Erlangen, Germany*
[6] *Chobanian &Avedisian School of Medicine, Boston University, Boston, MA, USA*

INTRODUCTION: MRI of the wrist is one of the most challenging anatomic areas to be examined by MRI due to the small size of tissues including the thin articular cartilage at multiple locations and the triangular fibrocartilage complex (TFCC) with its complex anatomy. Conventional MRI depicts morphologic degenerative changes at the cartilage and at the TFCC usually only at advanced stages of disease. Compositional MRI is able to characterize biochemical tissue properties much earlier than morphologic changes. T2 and T2* relaxometry ("mapping") represent two widely applied techniques, which enable non-invasive quantification of tissues' water content and assessment of collagen content and organization. Both techniques may benefit from higher magnetic field strengths due to a better visualization of small anatomical structures caused by higher contrast-to-noise and signal-to-noise ratios.

OBJECTIVE: To analyze regional variations of T2 and T2* relaxation times in wrist joint cartilage and the TFCC at 3T and at 7T and to compare both field strengths.

METHODS: 25 healthy controls and 25 patients with chronic wrist pain were examined at 3T and 7T MRI on the same day using multi-echo-spin-echo (MESE)or gradient echo (MEGE) T2- and T2*-weighted sequences. 6 different regions of interest (ROI) were evaluated for cartilage and 3 ROIs at the TFCC based on manual segmentation **(Figure 1)**. Paired t-test was used for comparing T2 and T2* values between field strengths and between different ROIs. Spearman's rank correlation was calculated for correlation of T2 and T2* time values between 3T and 7T.

RESULTS: T2 and T2* time values of the cartilage differed significantly between 3T and 7T for all ROIs assessed, with one exception. At the TFCC, no significant differences were observed for T2 values between field strengths. T2* values differed significantly between 3T and 7T for all ROIs of the TFCC. The Spearman's rank correlation between 3T and 7T ranged from 0.03 to 0.62 for T2 and from 0.01 to 0.48 for T2* values **(Table 1)**. T2 and T2* values of cartilage varied between anatomic locations in controls at 3T and at 7T **(Table 2)**.

CONCLUSION: Quantitative results of T2 and T2* mapping at the wrist differ between field strengths and show a poor correlation. Local variations for cartilage T2 and T2* time values are observed in healthy subjects.

SPONSOR: Research grant (2018_01: 7T MRI of the wrist) of the German Roentgen Society (Deutsche Röntgengesellschaft-DRG).
DICLOSURE STATEMENT: FWR: CMO & Shareholder BICL
CORRESPONDENCE ADDRESS: frank.roemer@uk-erlangen.de.

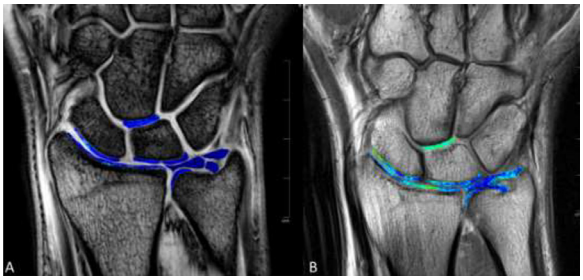

Figure 1. Image analysis. 3T MRI images of the first echo of the T2* (A) and T2 (B) MEGE/MESE sequence of a healthy control with superimposed color-coded maps of T2* and T2 values. Regions of interest (ROI) were placed at the cartilage of the distal radius, the proximal scaphoid, the proximal radial and ulnar lunate, the distal radial ulnar joint and in-between the distal lunate and proximal capitate. Three ROIs were placed at the triangular fibrocartilage complex: at the central disc, and at both the foveal and the apical attachment. The same analysis was also performed at 7T MRI.

Table 1: Comparison of T2 and T2* values at different field strengths for controls and patients with chronic wrist pain at different anatomic locations. P-values and Spearman's rank correlation are given for the comparison between 3T and 7T. DRUJ. distal radioulnar joint; CD. central disc of the TFCC; fA. foveal attachment of the TFCC; aA. apical attachment of the TFCC.

		Controls				Patients			
	Location	3T	7T	p-value	Correlation	3T	7T	p-value	Correlation
T2	Radius	43.8 ± 11.6	48.8 ± 9.8	0.045	0.34	38.2 ± 11.3	49 ± 14.1	0.002	0.45
	Scaphoid	43.9 ± 7.9	56.3 ± 15.6	0.001	0.10	46.5 ± 9.6	53.7 ± 10.2	0.01	0.03
	Lunate (radial)	34.3 ± 7.3	41.9 ± 11	0.03	0.05	34.7 ± 5.5	40.9 ± 9.6	0.01	0.45
	Lunate (ulnar)	34 ± 5.9	42.1 ± 6.4	< 0.001	0.45	35.1 ± 5.6	48.2 ± 9.4	< 0.001	0.58
	DRUJ	32.4 ± 10.5	40.6 ± 15.3	0.04	0.13	39.3 ± 18.2	45 ± 10.9	0.08	0.36
	Capitate/Lunate	44.2 ± 7.2	46.3 ± 13	0.25	0.62	43.4 ± 6.2	51.5 ± 10.2	0.001	0.41
	TFCC CD	23.5 ± 5.9	26.7 ± 10.7	0.48	0.10	24.7 ± 8.5	31.2 ± 13.8	0.12	0.27
	TFCC fA	29.3 ± 8	31.7 ± 16.8	0.38	0.26	33.3 ± 11.2	41.2 ± 26.4	0.06	0.30
	TFCC aA	26.8 ± 6	29 ± 9.8	0.18	0.11	27.3 ± 4.3	32.9 ± 14.9	0.04	0.24
T2*	Radius	14.2±1.6	8.6 + 2.1	< 0.001	0.01	14.4 + 2.5	8.5 + 2.2	< 0.001	0.19
	Scaphoid	17.1 ± 3.2	10.3 + 3.1	< 0.001	0.21	17.6 + 3.4	10.7 + 3.4	< 0.001	0.11
	Lunate (radial)	16.3 ± 4.3	9.4 + 2.6	< 0.001	0.48	16.5 + 3.3	11.1 + 3.4	< 0.001	0.36
	Lunate (ulnar)	17.8 ± 3.1	11.9 + 3.0	< 0.001	0.40	18.8 + 4.4	12.5 + 3.5	< 0.001	0.42
	DRUJ	14.4 ± 2.7	11.4 + 3.4	0.001	0.36	17.9 + 5.0	12.4 + 4.3	< 0.001	0.38
	Capitate/Lunate	19.7 ± 3.3	11.4 + 3.2	< 0.001	0.13	18.2 + 3.3	11.2 + 3.3	< 0.001	0.01
	TFCC CD	10.1 ± 1.2	6.4 + 1.4	< 0.001	0.28	10.9 + 1.5	7.4 + 2.0	< 0.001	0.41
	TFCC fA	11.3 ± 2.0	6.2 + 1.9	< 0.001	0.04	12.7 + 3.0	7.7 + 2.9	< 0.001	0.03
	TFCC aA	10.5 ± 1.5	6.3 + 2.0	< 0.001	0.24	13.2 + 3.0	7.8 + 2.7	< 0.001	0.47

Table 2: Comparison of T2 and T2* values at different anatomic locations at 3T and at 7T. P-values are provided for healthy controls only. DRUJ. distal radioulnar joint; CD. central disc of the TFCC; fA. foveal attachment of the TFCC; aA. apical attachment of the TFCC.

	T2		T2*	
Location	3T	7T	3T	7T
Radius vs. Scaphoid	0.035	0.024	< 0.001	0.045
Radius vs. Lunate (radial)	0.005	0.004	0.03	0.224
Radius vs. Lunate (ulnar)	0.002	0.074	< 0.001	< 0.001
Radius vs. DRUJ	0.102	0.01	0.74	0.001
Radius vs. Capitate/Lunate	0.053	0.665	< 0.001	0.003
Scaphoid vs. Lunate (radial)	< 0.001	< 0.001	0.37	0.29
Scaphoid vs. Lunate (ulnar)	< 0.001	< 0.001	0.36	0.04
Scaphoid vs. DRUJ	0.001	< 0.001	0.003	0.38
Scaphoid vs. Capitate/Lunate	0.329	0.049	<0.001	0.37
Lunate (radial) vs. Lunate (ulnar)	0.933	0.024	0.06	0.004
Lunate (radial) vs. DRUG	0.531	0.629	0.053	0.03
Lunate (radial) vs. Capitate/Lunate	< 0.001	0.002	< 0.001	0.045
Lunate (ulnar) vs DRUJ	0.588	0.138	< 0.001	0.58
Lunate (ulnar) vs. Capitate/Lunate	< 0.001	0.045	0.02	0.40
DRUJ vs. Capitate/Lunate	0.001	0.023	< 0.001	0.81
TFCC CD vs. TFCC fA	< 0.001	0.06	0.001	0.60
TFCC CD vs. TFCC aA	0.018	0.472	0.09	0.84
TFCC fA vs. TFCC aA	0.006	0.092	0.07	0.74

doi: 10.1016/j.ostima.2023.100121

FOUR-DIMENSIONAL COMPUTED TOMOGRAPHY-DERIVED RADIOLUNATE ARTHROKINEMATICS WITH A CASE STUDY IN FOUR-CORNER ARTHRODESIS

T.P. Trentadue [1,2], C. Lopez [1], A.R. Thoreson [1], S. Leng [3], P. Amadio [4], S. Kakar [4], K.D. Zhao [1]

[1] *Assistive and Restorative Technology Laboratory, Mayo Clinic, Rochester, MN, USA*
[2] *Medical Scientist Training Program, Mayo Clinic, Rochester, MN, USA*
[3] *CT Clinical Innovation Center, Mayo Clinic, Rochester, MN, USA*
[4] *Department of Orthopedic Surgery, Mayo Clinic, Rochester, MN, USA*

INTRODUCTION: The radiocarpal joint, which includes articulations between the radius and the proximal carpal row, transmits force through the central column of the wrist. Chronic disruptions to radiocarpal biomechanics are associated with the development of scapholunate advanced collapse (SLAC) pattern OA. While the radiolunate joint is thought to be typically spared in SLAC progression, degenerative changes can present on the proximal lunate. An investigation of radiolunate arthrokinematics may improve understanding of posttraumatic and postsurgical outcomes, including salvage procedures for SLAC wrist such as scaphoid excision with four-corner arthrodesis (SEFCA). Four-dimensional CT, which captures CT volumes over time or motion, has enhanced our ability to quantify arthrokinematics during functional tasks.

OBJECTIVE: We hypothesize that 4DCT-derived radiolunate arthrokinematics during flexion-extension and radioulnar deviation will differ between healthy, uninjured wrists and a wrist three years post-SEFCA.

METHODS: Data were collected from the uninjured wrists of ten participants enrolled in a prospective study of unilateral wrist injury and one participant following SEFCA (n=11, 36% female). The SEFCA arthrodesis was fixed using Kirschner wires prepositioned in the head of the capitate and subsequently advanced into the lunate. Included participants were aged between 18 and 60 years; exclusion criteria included history of injury, surgery, or congenital variant in the contralateral wrist; rheumatologic disease; or connective tissue disease. Static-neutral and dynamic CT data were collected using a dual-source scanner (SOMATOM Flash, Siemens, DE) and commercially-available cardiac sequential scan protocol. 4DCT data were collected over a 1.5-second period as signaled by an ECG simulator. CT volumes were collected at a temporal resolution of 66 ms as participants moved at a cadence of 70 beats per minute (voxel size: 0.234mm × 0.234mm × 0.600mm). Nearest mesh-vertex distances between vertices on the radius and lunate within distance (2.5 mm) and surface-normal angular (60°) thresholds were calculated to define interosseous proximity distributions. Median interosseous proximities at each time point were calculated.

RESULTS: Ten participants were aged mean (SD) 30.3 (6.8) years at the time of imaging; the SEFCA participant was 52 years of age and three years postoperative. Median radiolunate interosseous proximities are presented during flexion-extension and radioulnar deviation (**Fig. 1**).

CONCLUSION: 4DCT has advanced our understanding of wrist arthrokinematics during functional tasks. The current study reveals that radiolunate interosseous proximities in healthy, uninjured wrists remain relatively constant over wrist flexion-extension and radioulnar deviation, with greatest proximities occurring near the extrema of motion. In the SEFCA participant, interosseous proximities were closest in flexion and ulnar deviation; this may be associated with high articular contact pressures in these positions. Interosseous proximities reveal how restricting midcarpal motion in SEFCA impacts adjacent articulations during wrist motion. This study represents a novel use of 4DCT to assess post-arthrodesis outcomes.

SPONSOR: U.S. NIH R01AR071338, T32AR056950, and T32GM065841.
DISCLOSURE STATEMENT: S.K. receives royalties from Arthrex.
ACKNOWLEDGMENT: The authors thank Nikkole Weber, R.T.(R)(CT) for radiation protocol and data collection contributions and Julie Block and Tyson Scrabeck, CCRP, for study coordination.
CORRESPONDENCE ADDRESS: trentadue.taylor@mayo.edu.

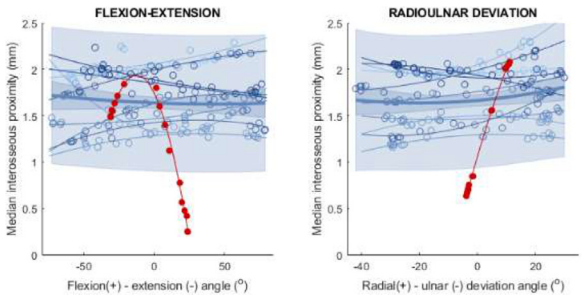

Fig. 1. Median interosseous proximities at the radiolunate joint during wrist flexion-extension and radioulnar deviation. Uninjured wrists are presented in blue, and the SEFCA participant is presented in red (dot = median at timepoint; line = second-order best fit line over time series). The thick blue line (shaded region) represents the best fit line (95% CI) across uninjured wrists.

doi: 10.1016/j.ostima.2023.100122

PREVALENCE OF STRUCTURAL LESIONS AND OSTEOARTHRITIS IN FEMOROTIBIAL JOINTS OF ASYMPTOMATIC PARTICIPANTS FROM THE LAUSANNE KNEE STUDY

C. Mourad [1,2,3], P. Margain [2], S. Zenkhri [1], B.M. Jolles [2], J. Favre [2], P. Omoumi [1,2]

[1] *Department of Radiology, Lausanne University Hospital (CHUV), Lausanne, Switzerland*
[2] *Swiss Biomotion Lab, Lausanne, Switzerland*
[3] *Department of Radiology, Lebanese Hospital Geitaoui, Beirut, Lebanon*

INTRODUCTION: Structural lesions of the cartilage, menisci, and bone are prevalent on knee MRIs in the asymptomatic population. The presence of such lesions may lead to the diagnosis of osteoarthritis (OA) according to imaging criteria. The prevalence of OA at imaging may depend on the definition criteria used (radiographic vs. MRI criteria).

OBJECTIVE: 1) To determine the prevalence of structural lesions of the femorotibial joint in two groups of young and older asymptomatic participants with healthy knees from the Lausanne Knee Study (LKS).
2) To determine the prevalence of OA in that population using radiographic and MRI definitions of OA.

METHODS: Asymptomatic volunteers were prospectively enrolled in this IRB-approved HIPPA-compliant study. Inclusion criteria: age between18-35 or 45-70 years, no knee symptoms in the past 12 months, no history of severe lower limb injury requiring surgery or not, no impairment that might affect gait, BMI≤30.
All participants (n=430, 47.8 years ±16.17 (SD), range 18-70 y, 192 (44.6%) male) underwent a clinical evaluation, including KOOS and WOMAC scores to evaluate pain and knee function, radiographic imaging (weight-bearing Schuss and lateral radiographs of both knees, full spine and lower extremity weight-bearing low dose 3D biplanar radiographs (EOS)), and 3T MRI of a randomly selected knee. MRI protocol included 2D fat-suppressed FSE IW images (sagittal, coronal, and transverse planes), isotropic 3D DESS, high-resolution 3D T1. One musculoskeletal radiologist with 6 years of experience graded radiographs (KL score) and knee MRIs for all structural lesions included in the MOAKS criteria. For this study, only femorotibial compartments will be presented. OA was defined as a KL score≥2 at radiography, or using the criteria proposed by Hunter et al (2011) at MRI.

RESULTS: There were 137 participants in the young (Y) (26.2y±4.7; 65 male (47.4%)) and 293 in the older (O) group (57.9y±7.23; 127 male (43.3%)). Participants had no knee pain or functional impairment (average KOOS 97.6±2.51 vs 97.2±3.78 in Y vs O group (p=0.26); average WOMAC 97.8±5.48 vs 96.7±8.23 in Y vs O group (p=0.16)). Structural lesions were highly prevalent in the femorotibial joints (decreasing order of prevalence): 190 (44.2%) cartilage damage (7 vs 183 in Y vs. O, $p<10^{-5}$), 132 (30.7%) BML (5 vs 127 in Y vs. O, $p<10^{-5}$), 111 (25.8%) meniscal damage (2 vs 109/ in Y vs. O, $p<10^{-5}$), 110 (25.6%) had periarticular cysts (13 vs 97 in Y vs. O, $p<10^{-5}$), 104 (24.2%) participants had osteophytes (3 vs 101/ in Y vs. O, $p<10^{-5}$), 68 (15.8%) Hoffa synovitis (3 vs 65 in Y vs. O, $p<10^{-5}$), 38 (8.8%) synovitis/effusion (3 vs 35 in Y vs. O, $p<10^{-3}$), and 17 (4%) had loose bodies (1 vs 16 in Y vs. O, p=0.019).
76 (17.7%) participants (1 young) had radiographic OA (60 KL2; 16 KL3; 0 KL4), while 24 (5.6%) participants (all from the older group) had femorotibial OA based on MRI criteria, 198 (46%) had normal MRI, and 208 (48.4%) had structural lesions of variable severity that did not fulfill MRI criteria of OA.

CONCLUSION: In a cohort of 430 asymptomatic volunteers with clinically healthy knees, structural lesions were present in up to 54% of femorotibial joints, with their prevalence increasing with age. The prevalence of OA at imaging in healthy knees may be high and depends on the criteria used (prevalence of 5.6% vs. 17.7% when using MRI vs. radiographic criteria).

SPONSOR: This work was supported by the Swiss National Science Foundation, Switzerland (SNSF Grant #CRSII5_177155).
DICLOSURE STATEMENT: Charbel Mourad has received the Swiss Government Excellence scholarship for post-doctoral research for the year 2022-2023.
ACKNOWLEDGMENT: Jean-Baptiste Ledoux, members of Swiss Biomotion Lab.
CORRESPONDENCE ADDRESS: charbel.j.mourad@hotmail.com.

doi: 10.1016/j.ostima.2023.100123

EXTENT OF SUBREGIONAL INVOLVEMENT OF SUBCHONDRAL BML IN INCIDENT KNEE OA IS ASSOCIATED WITH WEIGHT-BEARING KNEE PAIN

C.K. Kwoh [1], F. Roemer [2,3], E. Ashbeck [1], A. Guermazi [2]

[1] *University of Arizona Arthritis Center, Tucson, AZ, USA*
[2] *Chobanian & Avedisian School of Medicine, Boston University, Boston, MA, USA*
[3] *Universitätsklinikum Erlangen & Friedrich-Alexander-Universität Erlangen-Nürnberg, Erlangen, Germany*

INTRODUCTION: Subchondral BMLs have been associated with incident and progressive pain and reported to fluctuate along with concurrent fluctuations in symptoms. While associated with other structural, cellular, and biochemical features of OA that cause pain, BMLs may contribute directly to OA pain via cytokines, NGF, and altered biomechanics in knee OA, though evidence surrounding the role of BMLs and weight-bearing pain, specifically, is limited.

OBJECTIVE: Our objective was to estimate the effect of BML involvement on weight-bearing knee pain following radiographic KOA development, across the whole knee and by bone plate.

METHODS: The OAI is a longitudinal observational study of participants with or at risk of symptomatic KOA. We identified incident cases of radiographic KOA, defined as KLG 2 or 3 on centrally graded x-rays. Participants underwent bilateral posteroanterior fixed-flexion weight-bearing knee radiography at clinic visits annually or biannually through year 10. Non-contrast 3T MRI was also acquired at clinic visits up to year 8. MSK radiologists graded bone marrow lesions (BMLs), effusion-synovitis (ES), Hoffa-synovitis (HS), cartilage and meniscal damage using the MRI Osteoarthritis Knee Score (MOAKS). BML involvement was assessed in 15 subregions: MF (FemCentMed, FemPostMed), MT (TibAntMed, TibCentMed, TibPostMed), LF (FemCentLat, FemPostLat), LT (TibAntLat, TibCentLat, TibPostLat), MPF (FemAntMed, PatellaMed), LPF (FemAntLat, PatellaLat), and SS (TibSubSpCent). The WOMAC questionnaire includes pain assessment during 3 weight-bearing activities: walking on a flat surface, going up/downstairs, and standing, rated on a 5-point scale from none (0), mild (1), moderate (2), severe (3), or extreme (4). The weight-bearing knee pain score was defined as the sum of reported pain scores during these activities (0-12). We fit a proportional odds logistic regression to model weight-bearing knee pain using penalized maximum likelihood estimation; predictors included the number of subregions with BML involvement, other structural damage scores, KLG, age, and BMI at the same clinic visit, as well as sex and race. We similarly fit a model with the number of subregions with BML involvement at the bone-plate level. Models were compared with and without the number of subregions with BML involvement using a likelihood ratio test (LRT). The predicted probability of weight-bearing pain score 4 or greater is reported with nonparametric bootstrap 95% confidence intervals with cluster sampling at the participant-level.

RESULTS: We identified 690 knees contributed by 623 participants with radiographic KOA (i.e., KL2 or KL3 at the time of MRI). The mean participant age was 65 years (SD 9), mean BMI was 29.3 (SD 4.8), 66% reported female sex, and 83% self-identified as white. Predicted probability of weight-bearing pain is reported based on BML involvement, ES, and KLG, from fully adjusted models (Figures 1-2). The number of subregions in the whole knee with BML involvement was associated with weight-bearing pain (LRT p=0.006). The model that included affected subregions in each bone plate implicated BML involvement in the MT (LRT p=0.002).

CONCLUSION: Our findings suggest that the probability of weight-bearing knee pain increases with increasing subregional involvement of BMLs, largely driven by MT BMLs.

DICLOSURE STATEMENT: CKK is a consultant to Tissue Gene, Novartis, Trial Spark, Moebius Therapeutics, Xalud Therapeutics and Express Scripts; FWR is consultant to Grünenthal GmbH and CMO & shareholder of BICL, LLC. AG is shareholder of BICL, LLC and consultant to Pfizer, TissueGene, Novartis, Coval, Medipost, TrialSpark, ICM and AstraZeneca.

CORRESPONDENCE ADDRESS: kwoh@arthritis.arizona.edu.

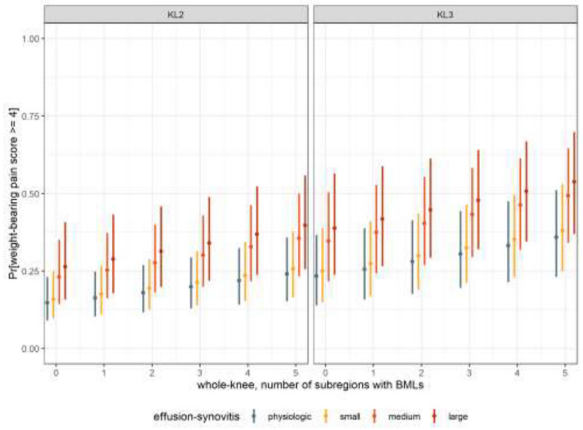

Figure 1. Weight-Bearing Knee Pain and Subregional BML Involvement By Amount of Effusion-Synovitis and Kellgren-Lawrence Grade.

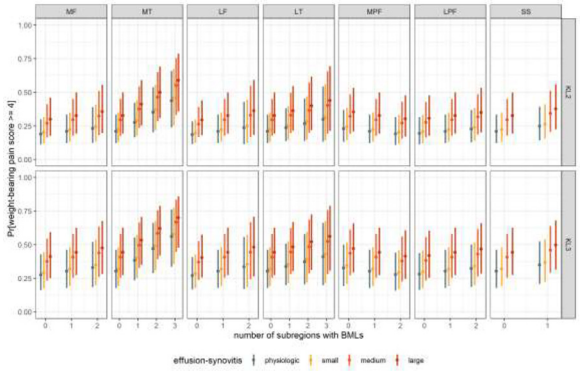

Figure 2. Weight-Bearing Knee Pain and Subregional BML Involvement within Bone Plates by Amount of Effusion-Synovitis and Kellgren-Lawrence Grade. Predicted probabilities based on models that also include age, sex, BMI, race, HS, cartilage damage, meniscal morphology and extrusion. Bars represent 95% confidence intervals.

doi: 10.1016/j.ostima.2023.100124

PATIENTS WITH A NEUROPATHIC-LIKE PAIN PHENOTYPE EXHIBIT MARKEDLY LESS MRI-DETECTED STRUCTURAL JOINT TISSUE DAMAGE COMPARED TO WITHOUT A NEUROPATHIC-LIKE PAIN PHENOTYPE: DATA FROM THE IMI-APPROACH STUDY

M. Jarraya [1], S. Mastbergen [2], J. Collins [3], A. Guermazi [4], N. Eijkelkamp [2], C.K. Kwoh [5], M.A. Bredella [1], R. Edwards [3], F.W. Roemer [6,†], M.P. Jansen [2,†]

[1] *Massachusetts General Hospital, Harvard Medical School, Boston, MA, USA*
[2] *University Medical Center Utrecht, Utrecht University, Utrecht, The Netherlands*
[3] *Brigham & Women's Hospital, Harvard Medical School, Boston, MA, USA*
[4] *VA Boston Healthcare, Boston University School of Medicine, Boston, MA, USA*
[5] *University of Arizona College of Medicine Tucson, Tucson, AZ, USA*
[6] *Friedrich-Alexander-Universität Erlangen-Nürnberg, Erlangen, Germany & Boston University School of Medicine, Boston, MA, USA*

[†]Shared last authorship

INTRODUCTION: A fundamental challenge in treating patients with OA is the discordance between pain and structural abnormalities. OA pain may manifest as different phenotypes, including neuropathic-like pain (NP), but the association of NP phenotype with joint structural abnormalities is unclear.

OBJECTIVE: Compare structural features of knee OA on MRI between patients with NP phenotype and those who do not have a NP phenotype (non-NP).

METHODS: For this cross-sectional study, patients from the IMI-APPROACH clinical cohort were included. The pain-DETECT questionnaire was used to identify patients with a high likelihood of a NP. NP was defined as a score ≥19 and non-NP as a score ≤12 (doi:10.1136/rmdopen-2021-002025). For each patient, an index knee with OA was selected based on ACR clinical criteria as applied in the IMI-APPROACH cohort. All patients with NP were matched in a 1:2 ratio to patients with non-NP. Subjects were matched using KOOS pain scale (as a knee-specific severity score) and SF-36 pain scale (as a general pain severity score). Knee MRIs were obtained for all participants and scored using MOAKS, including cartilage damage (surface area and full-thickness); bone marrow lesions (BML); Hoffa's synovitis and effusion-synovitis; medial meniscal tears, maceration and extrusion; and osteophytes. Frequencies of MRI features were compared between NP and non-NP participants using Fisher's Exact test for categorical variables and Wilcoxon Rank Sum test for continuous variables.

RESULTS: 24 patients fulfilled the criteria of NP and were matched with 48 controls with non-NP. While the baseline age, sex distribution, BMI and pain severity scores were similar for both groups (table 1), patients with NP had a higher proportion of KLG0 and KLG1 (33% each v. 8 and 23% for non-NP respectively). However, patients with non-NP had higher proportion of KLG2 and KLG3 (40% and 27% v. 33% and 0% for those with NP, respectively, p=0.003). Table 2 shows the prevalence of BML, cartilage damage, effusion-synovitis, Hoffa's synovitis, osteophytes, and meniscal tears for patients with NP and non-NP. All these features were more prevalent among those with non-NP reaching statistical significance for most of them, except for Hoffa's synovitis and meniscal extrusion. For instance, those with non-NP had a prevalence of 51% for BML (v. 17% for NP, p= 0.009), 49% of medial meniscus body maceration (v. 9%, p=0.001), and 60% of osteophytes (v. 26%, p=0.011). As for cartilage damage surface area and full thickness (figure 1), the difference between both groups was most striking for the medial tibiofemoral compartment, and comparable for the patellofemoral compartment.

CONCLUSION: In patients matched for similar amounts of knee-specific pain and global pain severity, patients with non-NP show significantly more structural damage on knee MRI than those with non-NP. There is a disconnect between the presence of local tissue damage and pain severity in NP phenotype. Knee OA patients with NP may benefit from personalized treatment that does not target local tissue damage.

SPONSOR: The International Skeletal Society Seed Grant & The David Borsook Project, supported by The Cathedral Fund.

DISCLOSURE STATEMENT: AG has received consultancies fees from Pfizer, Novartis, AstraZeneca, Merck Serono, Regeneron and TissueGene and is shareholder of Boston Imaging Core Lab (BICL), LLC a company providing image assessment services. FWR is shareholder of BICL, LLC and has received consultancies fees from Calibr–California Institute of Biomedical Research and Grünenthal, GmbH. CKK has received consultancy fees from Regeneron, Novartis, Kolon Tissue Gene, Express Scripts, Xalud and has received institutional grants from Lilly, Pfizer, GSK, Cumberland. JC received consultancy fees from BICL.

CORRESPONDENCE ADDRESS: mjarraya@mgh.harvard.edu.

Table 1: Patients characteristics and KL grade for each group (NP and non-NP).

	NP	Non-NP
Baseline Age	64.5 (6.9)	65.7 (7.3)
BMI	30.7 (5.9)	29.1 (6.2)
Female	20 (83%)	38 (79%)
KOOS pain, mean (SD)	50.8 (15.1)	49.8 (13.1)
SF-36 pain, mean (SD)	34.1 (22.8)	39.8 (16.8)

Table 2: Prevalence of BML, Hoffa's synovitis, effusion-synovitis, meniscal tears and extrusion and osteophytes in knee OA patients with NP and non-NP.

	NP	Non-NP	P-value
Moderate BML size (grade 2 or more)	4 (17%)	24 (51%)	0.0092
Any Hoffa's Synovitis (grade 1 or more)	11 (48%)	29 (64%)	0.2049
Any Effusion-Synovitis (grade 1 or more)	7 (30%)	30 (65%)	0.0100
Any Medial Meniscus Body (any tear)	3 (14%)	26 (55%)	0.0014
Medial Meniscus Body (maceration)	2 (9%)	23 (49%)	0.0012
Any Medial Meniscus Posterior Horn (any tear)	6 (26%)	25 (55%)	0.0395
Medial Meniscus Posterior Horn (maceration)	1 (4%)	13 (28%)	0.0253
Medial meniscus extrusion (grade 2 or more)	4 (18%)	18 (38%)	0.1072
Osteophytes maximum anywhere (grade 2 or more)	6 (26%)	28 (60%)	0.0112

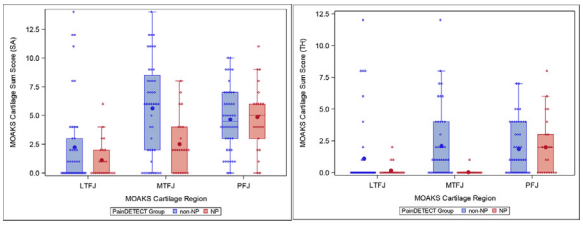

A B

Figure 1: Sum score of MOAKS scores for cartilage damage surface area (A) and full-thickness loss (B) for the medial tibiofemoral joint (MTFJ), lateral tibiofemoral joint (LTFJ), and patellofemoral joint (PFJ).

doi: 10.1016/j.ostima.2023.100125

Osteoarthritis Imaging 3 (2023) 100126

Contents lists available at ScienceDirect

Osteoarthritis Imaging

journal homepage: www.elsevier.com/locate/ostima

17th International Workshop on Osteoarthritis Imaging: Posters

THE RELATIONSHIP BETWEEN KNEE JOINT ALIGNMENT, 3-D JOINT SPACE WIDTH AND SUBCHONDRAL BONE PARAMETERS IN INVIDUALS WITH RADIOGRAPHIC OSTEOARTHRITIS: A MOST INVESTIGATION

B.J. Havard [1], S.E. Ghobrial [2], C.J. Tonkin [3], G.M. Treece [4], A.H. Gee [4], K.E.S. Poole [5], T. Neogi [6], M.C. Nevitt [7], J.A. Lynch [7], N.A. Segal [8], T.D. Turmezei [1]

[1] *Norfolk 8 Norwich University Hospital, Norwich, UK*
[2] *Royal College of Surgeons of Ireland, Ireland*
[3] *Annapolis Community Health Centre, Annapolis Royal, NS, Canada*
[4] *University of Cambridge, UK*
[5] *NIHR Biomedical Research Centre at Cambridge University Hospitals NHS Foundation Trust, UK*
[6] *Boston University School of Medicine, Boston, MA, USA*
[7] *University of California San Francisco, San Francisco, CA, USA*
[8] *University of Kansas Medical Center, Kansas City, KS, USA*

INTRODUCTION: Joint alignment is an important factor in OA affecting how forces pass through the knee. The increasing use of weight bearing computed tomography (WBCT) in OA research has made the weight bearing stance an important consideration in 3-D imaging analysis, but its influence through biomechanics on the joint and subchondral bone is not fully understood.

OBJECTIVE: To investigate the relationship between knee joint alignment and 3-D joint parameters derived from joint space mapping of WBCT imaging in individuals with radiographic OA.

METHODS: WBCT of both knees was acquired at the 144-month visit of the Multicenter Osteoarthritis Study (MOST). Knees with a KLG ≥2 were included in the analysis, taking the side with higher KLG or averaging subsequent results from both sides if equal. Joint space mapping was performed to obtain the 3-D JSW distribution along with femoral (f) and tibial (t) subchondral bone thickness (ST) and trabecular attenuation (TA). Everyone's knee parameter maps were then transferred to a canonical joint surface. Alignment of the knee joint was measured as the angle between the central axis of the distal femur and proximal tibia in a coronal multiplanar reformat slab of the WBCT data: neutral alignment was set as zero with varus signed positive (figure part (a)). Statistical parametric mapping (SPM) was performed using a general linear model to test the dependence of each 3-D parameter distribution on alignment controlling for age, sex, mass, height, and joint space shape modes. SPM results were plotted on the canonical joint surface with unmasked regions representing a significance level of P<0.05.

RESULTS: 136 knees were included in the analysis, 84 of which were females. Mean ± SD age was 66.4 ± 9.8 yrs; mass 85.3 ± 17.8 kg; height 1.69 ± 0.1 m. The distribution of radiographic grading was KL2 = 103; KL3 = 32; KL4 = 1. Mean alignment was 0.38 ± 3.80°. For each degree

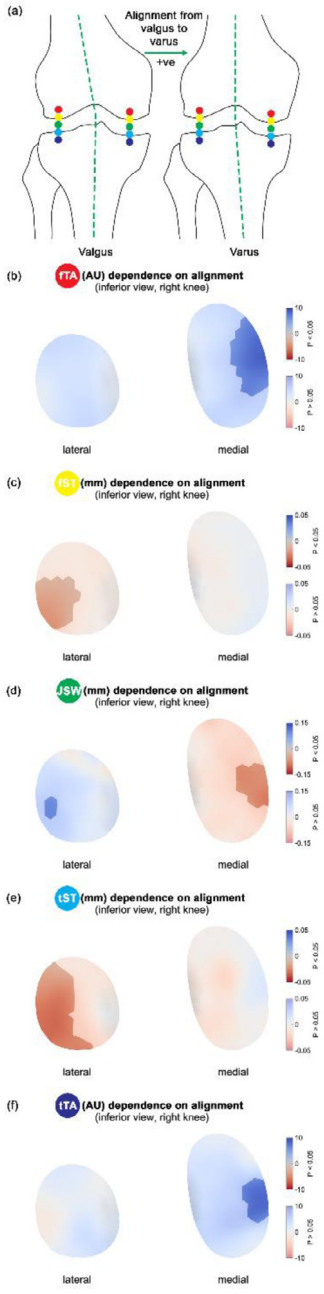

from valgus to varus, JSW was significantly narrower in the medial compartment and wider in the lateral compartment by up to 0.1 mm (figure part (d)). While TA was significantly greater by up to 10 AU in the medial femur (figure part (b)) and medial tibia (figure part (f)), there was up to 0.05 mm significantly thinner ST in the lateral femur (figure part (c)) and lateral tibia (figure part (e)). The opposite effects can be inferred for each degree towards valgus. The same analysis on KLG 0 and 1 knees in the same cohort (mean ± SD alignment 0.66 ± 2.94°) revealed no significant relationships.

CONCLUSION: Subchondral bone plate and trabecular bone appear to behave differently in the medial and lateral compartments when considering knee joint alignment in individuals with OA. Greater subchondral trabecular bone attenuation was seen in the medial compartment with varus alignment, while greater subchondral bone plate thickness was seen in the lateral compartment with valgus alignment. Whether alignment is the cause or effect of OA and any altered biomechanics that may influence bone and joint space behaviour requires further investigation, but this study does establish that the forces associated with alignment appear to have different effects on subchondral bone in different compartments.

SPONSOR: National Institutes of Health, University of Kansas (R01AR071648), University of Iowa (U01AG18832) and University of California-San Francisco (U01AG19069).

DISCLOSURE STATEMENT: NS is a consultant for Integra BioLife, Trice Medical and Pacira Biosciences. TT has been a consultant for Curvebeam AI.

ACKNOWLEDGEMENT: The authors would like to thank participants and staff of the MOST study.

CORRESPONDENCE ADDRESS: tom@turmezei.com

doi: 10.1016/j.ostima.2023.100127

SYSTEMATIC REVIEW OF COMPUTED TOMOGRAPHY PARAMETERS USED FOR THE ASSESSMENT OF SUBCHONDRAL BONE IN OSTEOARTHRITIS

J.E. Schadow [1], D. Maxey [2], T.O. Smith [3], M.A.J. Finnilä [4], S.L. Manske [5], N.A. Segal [6], A.K.O. Wong [7], R.A. Davey [1], T. Turmezei [8], K.S. Stok [1]

[1] *The University of Melbourne, Melbourne, Australia*
[2] *Norfolk and Norwich University Hospitals NHS Foundation Trust, Norwich, UK*
[3] *University of Warwick, Coventry, UK*
[4] *University of Oulu, Oulu, Finland*
[5] *University of Calgary, Calgary, AB, Canada*
[6] *The University of Kansas Medical Center, Kansas City, KS, USA*
[7] *University Health Network, Toronto, ON, Canada*
[8] *University of East Anglia, Norwich, United Kingdom 8 Norfolk and Norwich University Hospitals NHS Foundation Trust, Norwich, UK*

INTRODUCTION: Radiography and MRI are currently regarded as the imaging modalities of choice for OA assessment. However, computed tomography (CT) has several distinct advantages over these modalities, principally the capability of delivering higher resolution 3-D image reconstructions over a wider range of biological scales, in particular with respect to mineralized tissues. This enables greater standardization in analysis of bone structures compared to other imaging modalities. Considering the growing understanding of the importance of bone in OA pathology, we deem it an important juncture to recognize the full scope that CT holds in the imaging assessment of OA.

OBJECTIVE: To systematically review the published parameters for the assessment of subchondral bone in human OA using CT and gain an overview of current practices and standards.

METHODS: Medline, Embase and Cochrane Library databases were search with respective search strategies (search from 2010 to January 2023). Based on pre-determined inclusion and exclusion criteria, search results were screened independently by two reviewers. Eligible studies were conducted in vivo / ex vivo in human adults (>18 years) using CT to assess subchondral bone in any joint with OA. Data was extracted from eligible studies and compiled in a qualitative summary and formal narrative synthesis.

RESULTS: The literature search resulted in 202 included studies. Subchondral bone across nine anatomical locations were assessed using four broad groupings of CT modality: conventional clinical-type CT; quantitative CT for human use; micro-/nano-CT; and cone-beam CT. Six categories were identified for bone parameters measuring features of OA: (i) microstructure, (ii) bone adaptation, (iii) gross morphology (iv) mineralization, (v) joint space, and (vi) mechanical properties.

CONCLUSION: From long-standing roots, CT techniques have been continuing to gain popularity in OA research. We highlight clinically meaningful CT measurements for the assessment of subchondral bone in OA as well as parameters with the potential to perform in this role. We discuss the importance of quantification of parameters to improve their sensitivity and reproducibility. Finally, we emphasize a need for consistency and standardization of measurement protocols to optimize the value of these parameters in future OA research and clinical practice.

SPONSOR: None
DICLOSURE STATEMENT: None
ACKNOWLEDGEMENTS: None
CORRESPONDENCE ADDRESS: kstok@unimelb.edu.au

doi: 10.1016/j.ostima.2023.100128

CALF MUSCLE FAT AND FRAILTY AS SERIAL CULPRITS IN WORSENING KNEE SYMPTOMS AFTER 5 YEARS IN WOMEN: THE 7-YEAR AMBERS COHORT STUDY

A.K.O. Wong [1,2], C. Kennedy [3,4], K. Tam [1,2], S. Liu [1,2], S. Reitsma [3,4], A. Naraghi [1,2], R. Mohankumar [1,2], A. Papaioannou [3,4], J.D. Adachi [3,4]

[1] *University Health Network, Toronto, Canada*
[2] *University of Toronto, Toronto, ON, Canada*
[3] *Hamilton Health Sciences, Hamilton, Canada*
[4] *McMaster University, Hamilton, ON, Canada*

INTRODUCTION: We previously demonstrated that thigh intramuscular fat (IMF) predicts painful and progressive knee OA in the OAI. Another analysis of site-specific associations identified calf IMF as a key correlate of knee pain and function, albeit only within cross-sectional data. More studies are showing the importance of frailty in knee OA progression. While muscle is known to impact frailty, it is unclear whether IMF imparts long-term effects on knee OA through frailty or other pathways.

OBJECTIVE: 1) To evaluate how calf IMF predicts knee symptom progression beyond minimal detectability; and 2) to consider frailty and accelerated frailty as mediators along this pathway.

METHODS: The Appendicular Muscle and Bone Extension Research Study (AMBERS) comprises 312 postmenopausal women 60-85 years old recruited at baseline through primary care in Hamilton, Canada. Participants completed a 1T peripheral MRI (FSE, 10 slices, 0 gap, $0.312 \times 0.312 \times 2.0$mm, TR/TE: 600/23ms, FA=40°) scan of the 66% calf at baseline. At the same site, a 1-slice peripheral QCT scan was prescribed ($0.500 \times 0.500 \times 2.3$mm, 38 kVp energy, 0.3 mA current). Calf IMF was segmented using our fully-automated iterative threshold-seeking algorithm. We explored a second round of IMF segmentation using muscle masks with first round of IMF removed (Fig 1). Muscle was separated from subcutaneous fat and bone using fixed thresholds on pQCT scans after filtration (filter: F03F05F05, inner/outer thresholds: 40 mg/cm^3). Muscle density was computed as mass/volume. Participants were followed annually for 6 years, capturing activities of daily living, quality of life, and comorbidity data to calculate frailty using the cumulative deficits approach (CaMos Frailty Index (CFI)). At year 5 and 6, KOOS, Pain Detect and Gender Role Expectations in Pain (GREP) questionnaires were administered per knee. Use of knee-specific pain medications and corticosteroids was captured. ANALYSES: Group-based trajectory modeling classified CFI trajectory patterns from year 1 to 4, limited to third order polynomials (Fig 2). Change in KOOS from year 5 to 6 was dichotomized based on exceeding minimal detectable change (MDC) per subcategory. To address objective 1, a binary logistic regression analysis measured odds ratios (OR) and 95% confidence intervals. For objective 2, path analysis was applied, exploring CFI at years 1 through 4 or CFI trajectory class as mediators. Total, direct and indirect effects were evaluated. Analyses adjusted for age, BMI, diabetes, corticosteroids, knee pain medications, and presence of neuropathic pain. GREP was used as a weight to mitigate gender bias in self-reporting pain. Knee-level analyses coordinated side of calf scans with side of knee questionnaires.

RESULTS: Among 298 women with complete baseline, year 5&6 data, 112(37.6%) reported knee pain below the significant threshold of 72 by year 6. Individuals with 1-year declines ≥MDCs ranged from 30.3% (symptoms) to 45.6% (quality of life). Mean CFI score increased from 0.173(0.118) at baseline to 0.214(0.131) at year 5. Each SD (4.45%) higher calf IMF was associated with a 1.58(1.06, 2.35)-fold increased odds for KOOS symptom progression ≥MDC, with effect sizes increasing when including round 2 IMF (OR: 1.70(1.13,2.56)). A lower muscle density (SD: -8.21 mg/cm^3) showed a similar effect for KOOS QOL (OR: 2.16(1.50,3.12)). Individually, calf IMF predicted higher/ accelerated CFI (B=0.031, p=0.008, per +SD IMF%; and OR: 1.30(0.97,1.75) for accelerated versus stable CFI); and CFI significantly predicted 1-year KOOS subcategory changes ≥MDCs (ORs: 1.43-2.19 for Year 4 CFI; and 1.70-2.16 for accelerated versus stable CFI). However, the mediated effects of CFI were not significant in path analyses. Total effects of calf IMF on KOOS changes were explained largely by significant direct effects. Effect size and precision was improved after applying GREP as a weight.

CONCLUSION: Although frailty was both a significant outcome of calf muscle adiposity, and predictor of detectable clinical change in KOOS symptoms, there may be more complex mediation pathways at play, obscuring a clear mediation effect for the investigated pathway. Future studies should investigate more proximal mediators before frailty development such as inflammation. Residual low signal fat left unsegmented from an initial review of MR images may contribute to improved distinction across individual knee symptoms despite some of it representing partial voluming.

SPONSOR: Arthritis Society Stars Career Award 21-035, CIHR Project Grant PJT166012,156274.
DISCLOSURE STATEMENT: None.
CORRESPONDENCE ADDRESS: andy.wong@uhn.ca.

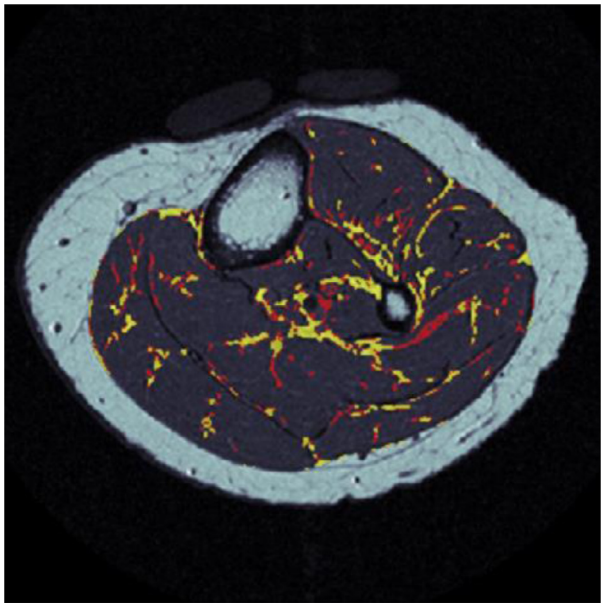

Figure 1. Illustration of first (yellow) versus second (red) round of IMF segmentation by the iterative threshold-seeking algorithm (ITSA). A) Original MR image.

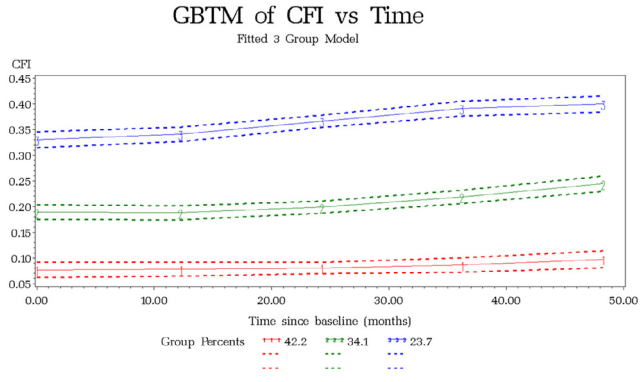

Figure 2. Group-based trajectory modeling (GBTM) of CaMos Frailty Index (CFI) over 4 years – showing accelerated frailty (group 3, blue) versus stability (group 1, red) and moderate increase (group 2, green).

doi: 10.1016/j.ostima.2023.100129

COMPARISON OF FULLY AUTOMATED VS MANUAL IMAGE SEGMENTATION FOR THE ASSESSMENT OF ARTICULAR CARTILAGE T2 RELAXATION TIMES IN KLG0 KNEES WITH AND WITHOUT CARTILAGE DAMAGE - ON BEHALF OF THE OA-BIO CONSORTIUM

A. Wisser [1,2], F.W. Roemer [3,4], F. Berenbaum [5,6], J. Kemnitz [1], A. Guermazi [4,7], N.G. Duda [8], L. Sharma [9], S. Maschek [1,2], F. Eckstein [1,2], W. Wirth [1,2]

[1] *Institute of Anatomy & Cell Biology and Ludwig Boltzmann Institute for Arthritis and Rehabilitation, Paracelsus Med. University, Salzburg, Austria*
[2] *Chondrometrics GmbH, Freilassing, Germany*
[3] *University of Erlangen, Erlangen, Germany*
[4] *Boston University School of Medicine, Boston, MA, USA*
[5] *Dept. of Rheumatology, Sorbonne University, INSERM, AP-HP Saint-Antoine Hospital, Paris, France*
[6] *4Moving Biotech, Lille, France*
[7] *VA Boston Healthcare, Boston, MA, USA*
[8] *Julius Wolff Institute, Berlin Institute of Health at Charité - Universitätsmedizin Berlin, Germany*
[9] *Northwestern University, Chicago, IL, USA*

INTRODUCTION: MRI-detected cartilage damage is associated with elevated cartilage T2 relaxation times on MRI. Further, cartilage damage is more frequently observed in knees at higher risk of developing radiographic knee osteoarthritis (OA). Detection of such early changes by means of MRI may be a useful method to identify participants for future observational or interventional OA studies.

OBJECTIVE: The aim of this study was to compare a U-Net-based, fully automated cartilage segmentation pipeline vs. manual, quality-controlled cartilage segmentations for determining differences in laminar cartilage T2 in Kellgren-Lawrence Grade (KLG) 0 knees with and without MRI Osteoarthritis Knee Score (MOAKS) cartilage damage.

METHODS: The fully automated U-Net-based image analysis pipeline was trained using sagittal multi-echo spin-echo (MESE) MRIs from the Osteoarthritis Initiative (OAI), for which manual quality-controlled segmentations of the respective structures were available. U-Nets for medial (MFTC) and lateral (LFTC) femorotibial cartilage segmentation were trained on all seven echoes of the MESE MRIs of 92 OAI healthy reference cohort (HRC) participants. A third U-Net was trained on bone segmentations of 60 OAI HRC knees. The bone segmentation served to algorithmically determine the weight-bearing femoral region of interest and to select the MRI slices that required cartilage segmentation. MFTC and LFTC U-Nets were then applied to the selected MRI slices of 123 KLG0 knees of the OAI incidence cohort (small sample) with, and 618 KLG0 knees of the same cohort without manual cartilage segmentations available (total of 741 knees = full sample). Automated post-processing was used to identify and correct implausible segmentations. Differences in superficial and deep layer cartilage T2 were compared between knees with vs. without MOAKS cartilage damage in the small sample (both U-Net and manual segmentations) and full sample (U-Net segmentation only). Mean differences were considered statistically significant when the 95% confidence interval did not include 0. MOAKS readings were performed by a very experienced MSK radiologist. Cartilage damage was defined as MOAKS cartilage score >0 in any of the medial or lateral tibial MOAKS subregions, or in the central medial or lateral femoral MOAKS subregions. Effect sizes were expressed using Cohen's D (d).

RESULTS: The full sample comprised knees of 415 women and 326 men (age [mean ±SD]: 60±9 years, BMI: 27±4 kg/m^2). Of these, 408 had no cartilage damage, 115 only medial damage, 149 only lateral damage and 69 had medial and lateral damage. Mean cartilage T2 values for the medial and lateral femorotibial compartments, calculated from the manual and automated segmentations in the small sample, as well as from the automated segmentations in the full sample are shown in Figure 1. In the MFTC, superficial layer T2 was longer in knees with cartilage damage than in those without for manual and automated segmentations of the small sample (d [95% CI] = 0.63 [0.26, 0.63]; d=0.58 [0.22, 0.58]), and also for automated segmentations of the full sample (d = 0.70 [0.53, 0.70]). Deep layer T2 did not differ between knees with vs. without cartilage damage for the automated cartilage segmentation of the large sample and the automated and manual cartilage segmentations of the small sample (d=0.04 to 0.09). Manual cartilage segmentations of the LFTC yielded greater T2 for both the deep (d = 0.48 [0.12, 0.48]) and superficial layers (d = 0.66 [0.29, 0.66]) in knees with vs. without cartilage damage. Results for U-Net segmentations were d=0.59 [0.22, 0.59] (small sample) and d=0.43 [0.27, 0.43] (full sample) for the deep layer and d=0.66 [0.29, 0.66] (small sample) and d=0.59 [0.43, 0.59] (full sample) for the superficial layer, respectively.

CONCLUSION: The fully automated U-Net-based cartilage segmentation pipeline was at least as sensitive to differences in laminar cartilage T2 between KLG 0 knees with vs. without MOAKS cartilage damage as quality-controlled, manual cartilage segmentations. Hence, this approach shows great potential for laminar cartilage T2 analyses and for application to large samples.

SPONSOR: This work was funded as part of the OA-BIO Eurostars-2 project (E! 114932).
DICLOSURE STATEMENT: FE, WW, SM and AW are part-time employees of Chondrometrics GmbH; FE, WW, and SM are co-owners of Chondrometrics GmbH. FE has provided consulting services to Merck KGaA, Kolon-TissueGene, and Novartis. FB is co-owner of 4Moving Biotech. F.W.R. and A.G. are shareholders of BICL, LLC. A.G. is consultant to Pfizer, Kolon TissueGene, Novartis, AstraZeneca, Coval, Medipost and ICM. GND has no conflicts of interest to declare.
CORRESPONDENCE ADDRESS: anna.wisser@pmu.ac.at

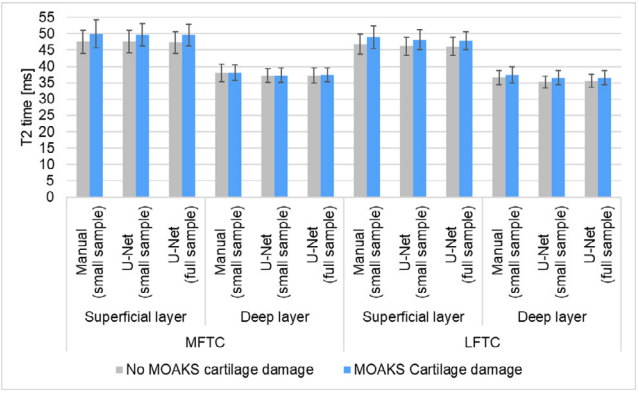

Figure 1. Mean cartilage T2 and standard deviations for the superficial and deep cartilage layer in the medial and lateral femorotibial compartments (MFTC/LFTC) of KLG 0 knees with vs. those without MOAKS cartilage damage. T2 values obtained from the manual and automated segmentations in a smaller sample (n=123), as well as the automated segmentations in a larger sample (n=741).

doi: 10.1016/j.ostima.2023.100130

CARTILAGE TRANSVERSE RELAXATION TIME (T2) AFTER ACL INJURY IN COPERS, NON-COPERS AND ACL-RECONSTRUCTED PATIENTS AND HEALTHY CONTROLS

F. Eckstein [1,2], N.M. Brisson [3], W. Wirth [1,2], S. Maschek [2], A. Wisser [1,2], F. Berenbaum [4], G.N. Duda [3]

[1] *Institute of Anatomy & Cell Biology and Ludwig Boltzmann Institute for Arthritis and Rehabilitation, Paracelsus Medical University, Salzburg, Austria*
[2] *Chondrometrics, Freilassing, Germany*
[3] *Julius Wolff Institute, Berlin Institute of Health at Charité - Universitätsmedizin Berlin, Germany*
[4] *Department of Rheumatology, Sorbonne University, INSERM, AP-HP Saint-Antoine Hospital, Paris, France*

INTRODUCTION: MRI transverse relaxation time (T2) of articular cartilage has been proposed to be a sensitive imaging biomarker for detecting alterations in articular cartilage composition. T2 is thought to reflect collagen integrity, orientation, and hydration, with higher values indicating early cartilage damage, preceding cartilage matrix loss. Further, T2 has been shown to be associated with cartilage histological grading and mechanical properties. However, whether cartilage T2 is sensitive to anterior cruciate ligament (ACL) integrity, dynamic knee stability status, and surgical reconstruction is unclear.

OBJECTIVE: To study whether layer-specific (superficial/deep) cartilage T2 at baseline, or longitudinal change in T2 over 1 year, is associated with ACL injury/repair and dynamic knee stability status. Specifically, we hypothesized that non-surgically treated ACL-deficient patients with persistent dynamic knee instability (non-copers) display higher (change in) cartilage T2 than copers, surgically reconstructed patients, and healthy reference subjects. As it is the location of the main impact during ACL rupture, the posterior lateral tibial subregion (pLT) was selected as primary analytic endpoint, with the lateral tibia (LT) and LFTC/MFTC (lateral/medial femorotibial compartment) being analyzed as well.

METHODS: 20 ACL-deficient patients with persistent dynamic knee instability (non-copers), 22 ACL-deficient patients without that instability (copers), 13 patients with surgical ACL reconstruction (2-183d after MRI), and 16 healthy controls without past knee injury or lower-extremity conditions. Patients were classified as non-copers if meeting at least 2/3 of these criteria: ≥1 episode of giving way in the past 6 months; <85/100 points on the Lysholm Knee Score; limb symmetry index <85% for a single leg jump for distance. Non-copers completed a 3-month intervention comprising lower-limb strength training and neuromuscular re-education; copers received conservative treatment as recommended by their healthcare provider. Surgically treated patients underwent ACL reconstruction by an ipsilateral four-strand semitendinosus tendon autograft. Sagittal multi echo spin echo images (MESE: slice spacing 3.5mm, in-plane resolution 0.31mm) were obtained at baseline and 1 year later. Cartilage segmentation of the MESE was performed manually by experienced readers, with quality control by an expert. Superficial and deep femorotibial cartilage T2 (50% each) were extracted from the segmentations. Statistical analysis was restricted to non-copers versus healthy subjects; all other comparisons were reported as observed.

RESULTS: Baseline pLT superficial (sf) T2 was not significantly greater in non-copers (51.6 ms [95% confidence interval (CI) 49.8, 53.4]) than in healthy knees (51.2 ms [95% CI 49.3, 53.1]; p=0.76 unpaired t-test). pLT sf T2 in copers was 51.0 ms [95% CI 49.5, 52.5], and 51.9 ms [95% CI 50.2, 53.5] in surgically treated patients (Fig. 1). Neither LT, LFTC nor MFTC T2 was suggestive of between-group differences. Deep layer T2 appeared to be slightly elevated (1-2 ms) in non-copers, copers, and surgically treated patients vs. healthy knees in pLT, LFTC and MFTC, but the differences were not statistically significant. 1-year longitudinal change in pLT sf or deep T2 did not appear to differ significantly between non-copers and healthy controls (Fig. 2); this also applied to other cartilage regions/layers/groups.

CONCLUSION: 1.5T MESE T2 failed to detect differences in femorotibial cartilage composition between ACL deficient patients and healthy controls in the current study. Yet, such differences were recently shown using a 3T qDESS sequence in a similar sample size, using the same analysis method.

SPONSOR: OVERLOAD - PrevOP (01 EC1408A) and OA-BIO Eurostars (E! 114932). The German project partners received funding from the Bundesministerium für Bildung und Forschung (BMBF).
DISCLOSURE STATEMENT: FE, WW, SM and AW are part time employees of Chondrometrics GmbH; FE, WW, and SM are co-owners of Chondrometrics GmbH. FE has provided consulting services to Merck KGaA, Kolon-Tissuegene, and Novartis. FB is co-owner of 4Moving Biotech. NMB and GND have no conflicts of interest to declare.
ACKNOWLEDGMENT: We thank the expert readers at Chondrometrics GmbH image segmentation.
CORRESPONDENCE ADDRESS: felix.eckstein@pmu.ac.at

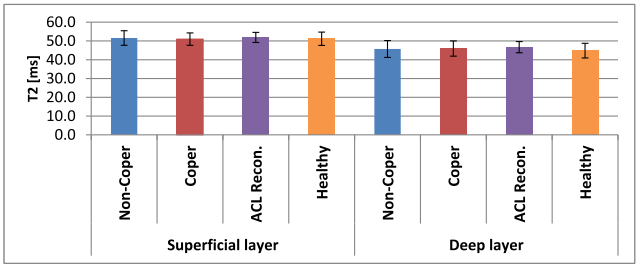

Figure 1. Baseline transverse relaxation time (T2) in the cartilage of the posterior lateral tibia (pLT) in non-copers, copers, patients with anterior cruciate ligament (ACL) reconstruction (surgery), and healthy reference subjects. There were no statistically significant differences between the groups.

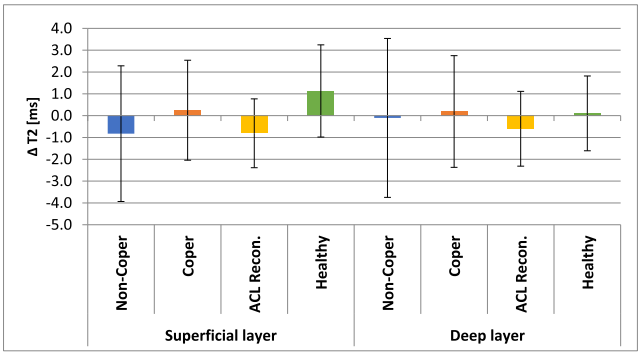

Figure 2. 1-year longitudinal change in the transverse relaxation time (T2) in the cartilage of the pLT in non-copers, copers, patients with ACL reconstruction, and healthy reference subjects. There were no statistically significant differences between the groups.

doi: 10.1016/j.ostima.2023.100131

PREDICTING MECHANICAL LEG ALIGNMENT FROM KNEE X-RAY IMAGES BY UTILIZING DEEP-LEARNING NEURAL NETWORKS

C. Salzlechner [1], C. Lepenik [1], K. Chen [3], C. Stotter [2], T. Klestil [2], R. Ljuhar [1], S. Nehrer [3]

[1] *ImageBiopsy Lab, Vienna, Austria*
[2] *Department for Orthopedics and Traumatology, Landesklinikum Baden-Mödling, Mödling, Austria*
[3] *Department for Health Sciences, Medicine and Research, Danube University Krems, Krems, Austria*

INTRODUCTION: Several studies have linked leg malalignment to early onset and progression of knee OA. Detecting abnormalities in mechanical alignment before radiographic evidence of knee OA is present, might increase the rate of early detection. Hence, conservative joint preserving interventions or even osteotomies could reduce the need or delay full joint replacement. In addition, medical trials often face high dropout rates, consequently, AI based support could improve the recruitment process.

OBJECTIVE: Detecting mechanical leg malalignment: 1) before the malalignment is immediately obvious to the clinician and 2) excluding/including patients recruited for medical trials.

METHODS: This study utilized a dataset of 8,878 digital radiographs ((I) 6,181 AP/PA full-leg x-rays, (II) 2,292 AP/PA knee x-rays with SynaFlexer positioning frame, (III) 405 AP/PA knee x-rays captured without SynaFlexer). The images were obtained from a diverse range of sources, including the OAI study, the University for Continuing Education Krems (AT), and five additional sites in Austria and the US. All knee images in the dataset were accompanied by their corresponding full-leg images, obtained on the same day. To determine the ground-truth hip-knee-ankle angle (HKA), the full-leg images were processed using IB Lab LAMA (ImageBiopsyB Lab, Vienna, Austria), a commercial software that automatically determines clinical measurements from full-leg radiographs. These images were used to train the AI algorithm. The algorithm produced binary outputs for HKA threshold values of 5° (clinically relevant) and 7.5° (clinical trial relevant).

RESULTS: The algorithm reached MAE rates of 0.98° (cropped full-leg), 1.56° (SynaFlexer knee) and 2.10° (non-SynaFlexer knee). Summarizing all image modalities, the overall performance for the 5° threshold was 74-86% Sensitivity and 79-90% Specificity. Following, 7.5° threshold performance reached 81-92% Sensitivity and 85-92% Specificity.

CONCLUSION: While this study primarily focused on absolute HKA threshold values of 5° and 7.5° for varus/valgus classification, this threshold determination process is highly adaptable to accommodate specific use cases, such as the desired angle threshold for classification or the preferred balance between sensitivity and specificity. In addition, overestimated HKA have an elevated angle above the normal range and could proceed towards or above mentioned thresholds.

SPONSOR: Chen K. PhD funding “LowerAustria Society for Scientific Research” (LSC20-020).
DISCLOSURE STATEMENT: Salzlechner C. and Lepenik C. are employees of ImageBiopsy Lab. Ljuhar R. is a shareholder of ImageBiopsy Lab.
ACKNOWLEDGMENT: This manuscript was prepared using an OAI public use data set and does not necessarily reflect the opinions or views of the OAI investigators or the NIH. Lepenik C. thanks Avelar C. for comments on an early version of this article.
CORRESPONDENCE ADDRESS: c.salzlechner@imagebiopsy.com

doi: 10.1016/j.ostima.2023.100132

A DEEP LEARNING APPROACH TO PREDICTING PAIN PROGRESSION IN OSTEOARTHRITIS FROM 3-D KNEE JOINT PARAMETERS: A MOST INVESTIGATION

J.M. Parkin [1], S.E. Ghobrial [2], C.J. Tonkin [3], T. Neogi [4], M.C. Nevitt [5], J.A. Lynch [5], N.A. Segal [6], T.D. Turmezei [1]

[1] *Norfolk 8 Norwich University Hospital, Norwich, UK*
[2] *Royal College of Surgeons of Ireland, Ireland*
[3] *Annapolis Community Health Centre, Annapolis Royal, NS, Canada*
[4] *Boston University School of Medicine, Boston, MA, USA*
[5] *University of California San Francisco, San Francisco, CA, USA*
[6] *University of Kansas Medical Center, Kansas City, KS, USA*

INTRODUCTION: Pain is a defining aspect of OA, but a definitive link between imaging features and pain remains elusive. The ability to establish objective measures of pain and linking these to progression with imaging could help identify important pain phenotypes. 3-D imaging assessment of knee OA has already been proven to be more sensitive and accurate than radiography across various measures, but advantages are yet to translate to assessment and prediction of pain progression. Deep learning models have also been developed from radiographic imaging but have not yet been used with surface-based 3-D imaging data.

OBJECTIVE: To develop a deep learning (DL) model of 3-D knee joint parameters and compare their performance to clinicodemographic and 2-D radiographic models in the prediction of OA pain progression.

METHODS: 391 WBCT studies of both knees acquired at the 144-month visit of the Multicenter Osteoarthritis Study (MOST) were available for study inclusion. Clinicodemographic and radiographic data used from this visit are shown in Table 1. Joint space mapping (JSM) had already been performed to measure 3-D JSW and bone parameters and map them on to a canonical joint surface for each knee. Tibial trabecular attenuation was chosen as a feasibility bone parameter given a known synergy with JSW from a prior study. All data analysis was performed using Python 3.10.11. WBCT data were iteratively reconstructed from point clouds with magnitudes to sparse 3-D arrays using open3d 0.17.0 (Figure 1). Target features were computed using 24-month WOMAC follow-up data consisting of a binary outcome for each Minimally Clinically Important Difference (MCID) increment by 2 or more points at each 8-month interval for each knee (R_MCID and L_MCID). The data was split into a train and test set with a test proportion of 0.3. Multi-class classification using Light Gradient-Boosting Machine 3.3.2 (LightGBM) was performed to model clinicodemographic and 2-D radiographic features to the target feature. Tensorflow 2.12.0 was used to build a convolutional neural network (CNN) to model the sparse 3-D arrays to the target feature with a total of 61,012 parameters. Model performance was assessed using accuracy on the test set.

RESULTS: Mean ± SD age was 63.4 ± 9.5 years, height 169.7 ± 9.5 cm, mass 82.4 ± 17.6 kg, 15m walk time 15.2 ± 1.9 seconds, chair standing time 9.2 ± 2.5 seconds, with 217 females and 385 (98.5%) either white or Caucasian (all other combined). KLG, medial and lateral JSN had a majority class of 0 in both right and left knees. R_MCID had a proportion of 0.69, 0.19, 0.08 and 0.04 and L_MCID a proportion of 0.70, 0.18, 0.08 and 0.04 for 0, 1, 2 and 3 deteriorations over the 24-month follow-up period. Clinicodemographic features had an accuracy of 0.685 and 0.568 with respect to the R_MCID and L_MCID targets, 2-D radiographic features 0.505 and 0.432, 3D-array joint space mapping 0.690 and 0.688, and 3-D array cortical bone mapping of tibial trabecular attenuation 0.738 and 0.675 (Table 2).

CONCLUSION: 3-D quantitative bone and joint parameters in a novel CNN model did improve accuracy in prediction of future pain progression over 2 years in an older adult population with or at risk of developing OA when compared to clinicodemographic and 2-D radiographic features. Further validation is required due to the unbalanced target data, while next-step modelling could also include the raw imaging data. Nonetheless results show that 3-D data extracted from WBCT imaging can be evaluated with DL and appear to be more related to future pain prediction than 2-D radiographic scores and clinicodemographic features. This could be of benefit in selecting participants for clinical trials by pain phenotype, particularly considering analgesic agents such as anti-nerve growth factor molecules that have been of recent interest.

SPONSOR: National Institutes of Health, University of Kansas (R01AR071648), University of Iowa (U01AG18832) and University of California-San Francisco (U01AG19069).
DISCLOSURE STATEMENT: NS is a consultant for Integra BioLife, Trice Medical and Pacira Biosciences. TT has been a consultant for Curvebeam AI and GSK.
ACKNOWLEDGEMENT: The authors would like to thank participants and staff of the MOST study.
CORRESPONDENCE ADDRESS: tom@turmezei.com

Table 1: Dataset feature and outcome descriptions

Feature	Group	Data Type
Age	Clinicodemographic	Continuous
Sex	Clinicodemographic	Binary categorical
Ethnicity	Clinicodemographic	Binary categorical
Height	Clinicodemographic	Continuous
Weight	Clinicodemographic	Continuous
15 meter walk time	Clinicodemographic	Continuous
Chair stand time	Clinicodemographic	Continuous
Kellgren and Lawrence grade	2-D X-ray	Multi-class categorical
Medial joint space narrowing grade	2-D X-ray	Multi-class categorical
Lateral joint space narrowing grade	2-D X-ray	Multi-class categorical
3-D joint space mapping	3-D WBCT	Sparse 3-D array
Cortical bone mapping	3-D WBCT	Sparse 3-D array
MCID in WOMAC over 2 years	Target	Multi-class categorical

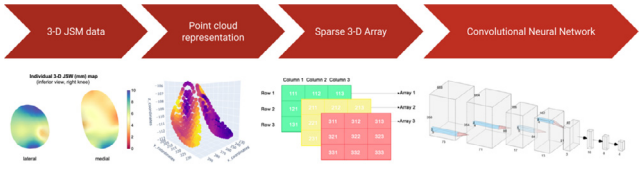

Figure 1: Illustration of the sparse 3-D array generation from point clouds and how they were modelled to the target features.
'Sparse 3-D array' image after from *A computer science portal for geeks* (2023): GeeksforGeeks. Available at: https://www.geeksforgeeks.org/ (Accessed: 03 May 2023).
'Convolutional Neural Network' diagram generated using NN SVG. Available at: https://alexlenail.me/NN-SVG/ (Accessed: 03 May 2023).

Table 2: Model results

Model type	Feature group	Target	Accuracy
LightGBM	Clinicodemographic	Right MCID in WOMAC over 2 years	0.685
LightGBM	2-D X-ray	Right MCID in WOMAC over 2 years	0.505
CNN	3-D joint space mapping	Right MCID in WOMAC over 2 years	0.690
CNN	Cortical bone mapping	Right MCID in WOMAC over 2 years	0.738
LightGBM	Clinicodemographic	Left MCID in WOMAC over 2 years	0.568
LightGBM	2-D X-ray	Left MCID in WOMAC over 2 years	0.432
CNN	3-D joint space mapping	Left MCID in WOMAC over 2 years	0.688
CNN	Cortical bone mapping	Left MCID in WOMAC over 2 years	0.675

doi: 10.1016/j.ostima.2023.100133

MRI-BASED RADIOMICS FOR ASSESSMENT OF THE INFRAPATELLAR FAT PAD'S INFLUENCE ON PATELLOFEMORAL PAIN

I.R. Campos [1,2,3], R.A. van der Heijden [3,4], E.H.G. Oei [3], M. van Middelkoop [5], S. Klein [3], J.S. Cardoso [1,6], J. Hirvasniemi [3]

[1] *Faculdade de Engenharia, Universidade do Porto, Porto, Portugal*
[2] *Instituto de Ciências Biomédicas Abel Salazar, Universidade do Porto, Porto, Portugal*
[3] *Dept. of Radiology 8 Nuclear Medicine, Erasmus MC University Medical Center, Rotterdam, The Netherlands*
[4] *Dept. of Radiology, University of Wisconsin-Madison, Madison, WI, USA*
[5] *Dept. of General Practice, Erasmus MC University Medical Center, Rotterdam, The Netherlands*
[6] *Instituto de Engenharia de Sistemas e Computadores, Tecnologia e Ciência, Porto, Portugal*

INTRODUCTION: The infrapatellar fat pad (IPFP) has been proposed as a source of knee pain in patients suffering from either knee OA or its supposed precursor, patellofemoral pain (PFP). While radiomics has been successfully applied to different MRI data, there is a lack of studies using radiomic features from the IPFP for the assessment of PFP.

OBJECTIVE: The aims of this study were to automatically extract radiomic features from the IPFP and assess the ability of these radiomic features to distinguish between patients with PFP and healthy controls.

METHODS: Sagittal 3D SPGR sequences with and without fat saturation (FS) from the TripleP study (n=64 PFP patients, n=70 controls) were used in the analyses. The IPFP of the 134 knees was automatically segmented using a nnU-Net with a 3D U-Net configuration. The nnU-Net was trained using 30 manually segmented knees and 5-fold cross-validation. Medial and lateral borders of the patella bone were used as anatomical landmarks for the manual IPFP segmentation. Radiomic features related to orientation (n=3), histogram (n=13), shape (n=21), original phase (n=39) and texture (n=376) were extracted (n=452), using the open-source Workflow for Optimal Radiomics Classification toolbox (v. 3.6.0). Elastic Net from the Scikit-learn Python module was used for dimensionality reduction and classification. The hyperparameters were optimized using 5-fold stratified cross-validation with a grid search and 10 repetitions. Three different models were evaluated: 1) basic model consisting of the patients' information (age, sex and BMI), 2) radiomic features model (n=452), and 3) combination of models 1 and 2. The classification performance of the aforementioned models to distinguish between patients with PFP and controls was assessed using the area under the receiver operating characteristic (ROC AUC) and precision-recall curves (PR AUC).

RESULTS: The mean Dice similarity coefficient for the IPFP automatic segmentation was 0.94 (0.02). Visual evaluation showed that up to 15 of the most medial and lateral slices were not correctly segmented. Thus, 15 slices per side were removed from each segmentation mask and the features were extracted from the most central slices of the IPFP. Regarding the results for distinguishing between patients with and without PFP, the basic model resulted in an ROC AUC of 0.67 (SD: 0.08) and an PR AUC of 0.62 (0.14). The radiomic features extracted from the non-FS sequence resulted in an ROC AUC of 0.57 (0.05) and an PR AUC of 0.73 (0.05) for model 2 and in an ROC AUC of 0.57 (0.05) and an PR AUC of 0.71 (0.07) for model 3. The performances of models 2 and 3 were slightly worse when using radiomic features from the FS sequence. However, when using only texture features from the FS sequence in the classification, an ROC AUC of 0.67 (0.05) and an PR AUC of 0.70 (0.10) was obtained.

CONCLUSION: The model with all radiomic features combined was not able to distinguish between patients with and without PFP. However, better performance was obtained when using a subgroup of texture features. The results of this study indicate that texture features extracted automatically from the central part of the IPFP from FS SPGR sequence are promising quantitative imaging biomarkers for the assessment of PFP.

SPONSOR: None
DICLOSURE STATEMENT: None
CORRESPONDENCE ADDRESS: j.hirvasniemi@erasmusmc.nl

doi: 10.1016/j.ostima.2023.100134

DYNAMIC CONTRAST-ENHANCED MRI OF THE SYNOVIUM IN KNEE OSTEOARTHRITIS: SEMI-AUTOMATIC SEGMENTATION OF SYNOVIAL SUBREGIONS AND TEST-RETEST REPEATABILITY

J.M. Mostert [1], T.A. Van Zadelhoff [1], D.H.J. Poot [1], D. Van der Kaaij [1], L. Strong [1], K. Zijlstra [1], E.H.G. Oei [1], R.A. Van der Heijden [1,2]

[1] *Erasmus Medical Center, Rotterdam, The Netherlands*
[2] *University of Wisconsin-Madison, Madison, WI, United States*

INTRODUCTION: Inflammation of the joint lining (synovitis) is often seen in OA, and is strongly associated with both knee pain severity and disease progression. Dynamic contrast-enhanced MRI (DCE-MRI) can be used to visualize the uptake and washout of gadolinium-based contrast, and enables quantification of blood perfusion as a surrogate measure of inflammation. DCE-MRI could therefore be used to characterize the extent of synovitis and serve as a biomarker for response to treatment in clinical trials. However, (semi)-automatic segmentation methods and thorough technical and clinical validation are needed to fully adopt DCE-MRI in this setting.

OBJECTIVE: We aim to evaluate semi-automatic segmentation of synovial subregions and test-retest repeatability of DCE-MRI to measure synovial perfusion in patients with knee OA.

METHODS: Patients with mild-to-moderate knee OA (KLG 1-3) who were allocated to the control group in a prospective randomized controlled trial of genicular artery embolization were included. Patients underwent MRI at 3T (GE Healthcare) at baseline and after 1 month. Image acquisition consisted of native T1 mapping with variable flip angle, followed by a dual-echo SPGR sequence (DISCO; DIfferential Subsampling with Cartesian Ordering), in which the spatial resolution was optimized to allow for visualization of small vessels. After the initial phase, 0.1 ml/kg gadovist was injected and subsequently 34 dynamic phases were acquired, with a temporal resolution of 10.2 seconds.
Segmentation of the synovium comprised an initial rough manual segmentation followed by selection of enhancing voxels using a shuffle transform method. Synovial subregions were created by semi-automatic vessel mapping using MeVisLab and mathematically assigning synovial voxels to the corresponding closest genicular artery. Motion compensation was performed using Elastix (Elastix, version 5.0.1), and native T1 mapping and pharmacokinetic modelling was done using open source software for DCE analysis (MADYM, version 4.21.1). The commonly used combination of the Parker literature arterial input function, and the Extended Toft's model pharmacokinetic model was implemented. Voxelwise perfusion parameters were calculated, after which median Ktrans values were extracted for the whole synovium and separately for each synovial subregion. Agreement was visualized with a Bland-Altman plot, and test-retest repeatability was evaluated using intraclass correlation coefficients (ICC; single rating random sample) and within-subject coefficients of variation (CV).

RESULTS: 30 patients were included, of which two patients were lost to follow-up and one patient was excluded due to errors during image acquisition. For the remaining 27 participants, median Ktrans values ranged from 0.017 to 0.121. ICC of Ktrans for the whole synovium was 0.51, and CV was 0.14. Sensitivity analysis by exclusion of two statistical outliers yielded an ICC of 0.66 and a CV of 0.11. For the individual synovial regions, ICCs ranged between 0.27 and 0.58 while CVs ranged between 0.13 and 0.25.

CONCLUSION: Semi-automatic segmentation of the synovium and synovial subregions through vessel mapping on DCE-MRI in knee OA is feasible. Perfusion parameters determined through pharmacokinetic modeling have moderate repeatability and should be interpreted with caution.

SPONSOR: Stichting Coolsingel, Cook Medical, Erasmus MRace Doelmatigheid
DICLOSURE STATEMENT: E.H.G. Oei has received research support from GE Healthcare. The University of Wisconsin receives research support from Bracco Diagnostics.
CORRESPONDENCE ADDRESS: m.mostert@erasmusmc.nl

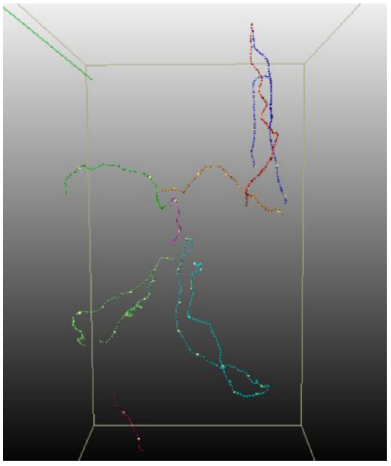

Fig. 1. Example of a semi-automatically segmented vessel structure of the knee using MeVis Lab.

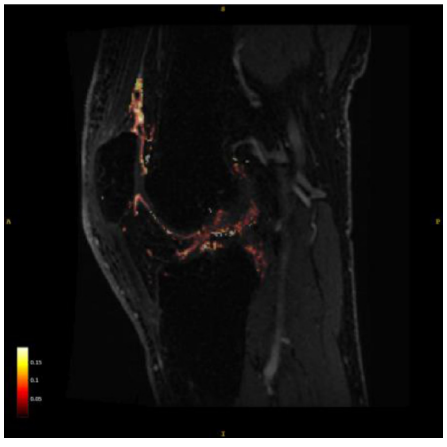

Fig. 2. Example of a DCE-MRI image of a patient with knee osteoarthritis, with the Ktrans map [min-1] of the synovium displayed as overlay.

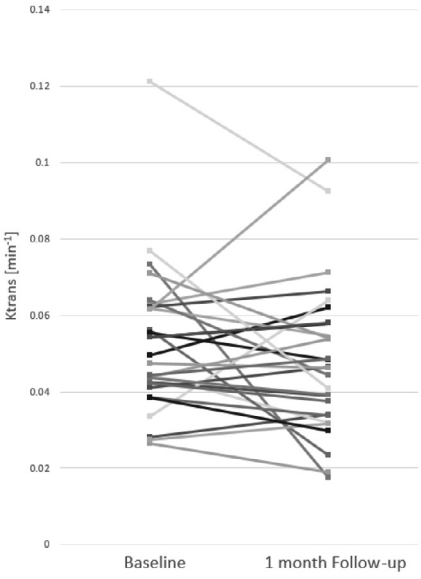

Fig. 3. Change in median Ktrans values for the whole synovium in patients with knee osteoarthritis, measured at baseline and 1 month follow-up

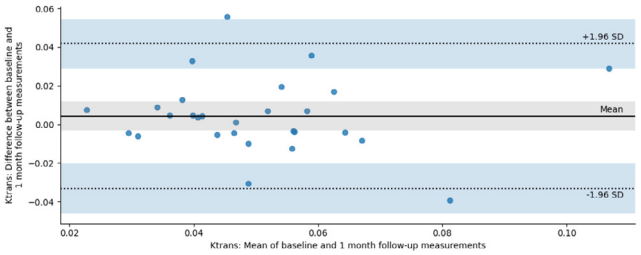

Fig. 4. Bland-Altman plot of Ktrans values [min-1] (baseline and 1 month follow-up) for the whole synovium in patients with knee osteoarthritis.

doi: 10.1016/j.ostima.2023.100135

MENISCAL EXTRUSION IN ASYMPTOMATIC KNEES: THE 3MM CUTOFF MUST BE REVISITED

S. Zenkhri [1], P. Margain [2], J. Favre [1], P. Omoumi [1,2], C. Mourad [1,2,3]

[1] *Lausanne University Hospital CHUV, Lausanne, Switzerland*
[2] *Swiss Biomotion Lab, Lausanne, Switzerland*
[3] *Lebanese Hospital Geitaoui, Beirut, Lebanon*

INTRODUCTION: Meniscal extrusion is frequently encountered in OA, and an arbitrary cutoff value of 3 mm is commonly accepted for a significant extrusion of the body of the medial meniscus (MM). Different methods of measurement have also been described.

OBJECTIVE: We aim to provide the normal range of MM extrusion in different zones in asymptomatic volunteers without radiographic and/or MRI OA and to compare different measurement methods on coronal and sagittal 2D images to those performed on 3D images in radial planes.

METHODS: This is a post-hoc analysis of knee MRIs of 93 participants (39.6±16.0 years; mean ± SD) with asymptomatic, healthy knees (KOOS score 97.42±3.22 and WOMAC score 97.41±7.54) from the Lausanne Knee Study. Inclusion criteria: age between 18-35 or 45-70 years, no knee symptoms in the past 12 months, no history of severe lower limb injury, no impairment that might affect gait, BMI≤30. Imaging protocol included weight-bearing Schuss and lateral radiographs of both knees and 3T MRI of a randomly selected knee. MRI protocol included 2D fat-suppressed FSE IW images (sagittal, coronal, and transverse planes), isotropic 3D DESS, and high-resolution 3D T1. One radiologist measured the maximal extrusion of the MM in the radial plane using 3D FSE T1 images in 4 anatomical subregions: zones II-a (anterior), II-b (anteromedial), III (medial), and IV (posterior). Measurements were also performed on coronal and sagittal 2D images using two different methods: on the image where the maximal extrusion was seen ($method^{Max}$) and on an image selected based on anatomical landmarks ($method^{Landmark}$). Another musculoskeletal radiologist graded knee MRIs for all structural lesions included in the MOAKS criteria. In addition, meniscal extrusion was measured in the sagittal and radial planes to assess interobserver agreement. Measurements on 2D images were compared to those on the radial plane, considered as the reference, using the Bland and Altman method. Sixty-one (65.5%) participants (41.4±16.6 years) who did not have either radiographic OA (KL<2) or MRI-OA (Hunter 2011 criteria) were used to provide the normal range of meniscal extrusion.

RESULTS: Among the 61 participants without radiographic or MRI OA, the mean extrusion of MM was 2.39mm±1.41 (zone II-a), 3mm±0.85 (zone II-b), 2.4mm±0.81 (zone III), and 0.3mm±0.9 (zone IV). The 95^{th} percentile of the reference interval for meniscal extrusion in the radial plane was 4.7mm for zone II-a, 4.4mm (zone II-b), 3.7mm (zone III), and 2mm (zone IV).
By applying a cutoff value of >3mm for significant meniscal extrusion on measurements in the radial plane, 28/61 (46%) would have been categorized as having extrusion in zone II-b and 12/61 (20%) in zone III. In the coronal plane, 13/61 (21%) or 18/61 (30%) would have been categorized as having meniscal extrusion depending on whether measurements were performed using $method^{Landmark}$, or $method^{Max}$ respectively.
In both sagittal and coronal planes, $method^{Max}$ overestimated meniscal extrusion (95%CI for systematic bias=0.5, 1 in the sagittal plan, 0.1, 0.3 in the coronal plane), while there was no systematic bias for $method^{Landmark}$. The width of limits of agreement was similar in both planes and for both methods. Interobserver agreement was moderate for measurements in the radial (ICC=0.67) and sagittal (0.68) plane.

CONCLUSION: This study provided the normal range of meniscal extrusion in asymptomatic knees without radiographic/MRI OA. Applying a 3mm cutoff value for the diagnosis of significant meniscal extrusion would carry a risk to categorize normal menisci as being extruded. Methods of measurement based on anatomical landmarks correlated better with measurements in the radial plane.

SPONSOR: This work was supported by the Swiss National Science Foundation, Switzerland (SNSF Grant #CRSII5_177155).
DICLOSURE STATEMENT: None to declare.
CORRESPONDENCE ADDRESS: Salim.Zenkhri@chuv.ch

doi: 10.1016/j.ostima.2023.100136

A LONGITDUINAL IMAGING PROTOCOL FOR 3D QUANTITATIVE MORPHOMETRIC ANALYSIS OF THE MOUSE KNEE

P. Durongbhan, H. Liu, J.E. Schadow, E. Boersma, K.S. Stok

Department of Biomedical Engineering, The University of Melbourne, Parkville, Australia

INTRODUCTION: Advances in medical imaging allow non-invasive visualisation and quantification of structural changes related to OA progression. Quantitative morphometric analysis (QMA) using micro-computed tomography (microCT) was shown to be sensitive to bone, cartilage, and whole-joint changes in preclinical animal models of knee OA [1]. As elastic links, each distal/proximal component of the joint can move relative to one another - changing the joint pose and affecting whole-joint QMA metrics. Control of joint pose and alignment is vital to maintaining the reproducibility and sensitivity of these measurements.

OBJECTIVE: Develop a novel micro-computed tomography (microCT) imaging protocol that allows reproducible and longitudinal whole-joint QMA measurements of the mouse knee.

METHODS: A mouse positioning device compatible with the *in vivo* microCT animal bed (vivaCT80, Scanco Medical AG, Switzerland) was designed in-house and 3D printed. Seven healthy excess C57Bl/10 male mice (n = 14 knees) were sacrificed and placed in the positioning device, then scanned with microCT at 10.4 μm voxel size. Each mouse was scanned five times, with repositioning between scans. Fully automated joint alignment was done by representing the tibia's rough shape and relative position using lower-order spherical harmonics descriptors (SPHARM), which describe objects of spherical topology as a weighted sum of spherical harmonic basis functions [2]. The joint centre of mass was measured from the aligned images, defined as a vector with length, λ (mm), and orientations, α (°); β (°); and γ (°), connecting the centres of mass of the femur and tibia [1]. Reproducibility was calculated as precision error, expressed in both absolute value (PESD) and coefficients of variation (PE%CV), as well as intraclass correlation coefficient (ICC). The protocol was applied to a longitudinal study using four healthy C57Bl/10 mice (n = 8 knees). Each mouse was scanned *in vivo* weekly for 9 weeks and processed. Joint centre of mass was calculated and its precision expressed as relative standard deviation (RSD).

RESULTS: Exemplar joint centre of mass measurements using the protocol are shown in Figure 1. For repeated measurements, high ICC were obtained for all parameters (ICC λ: 0.832, α: 0.912, β: 0.892, γ: 0.903), indicating excellent reproducibility (ICC > 0.75). Low precision errors (PE(SD) λ: 0.08, α: 4.08, β: 2.87, γ: 4.19; PE(%CV) λ: 2.69%, α: 6.81%, β: 3.03%, γ: 2.79%) were also obtained.

CONCLUSION: The novel protocol, consisting of a positioning device and a SPHARM image processing workflow, enables highly reproducible QMA of the mouse knee. The protocol has been applied to an *in vivo* longitudinal study of an OA mouse model to reveal changes associated with disease progression. Next steps involve validation with histopathological analysis.

SPONSOR: Discovery Projects scheme from the Australian Research Council (DP180101838).
DISCLOSURE STATEMENT: None
CORRESPONDENCE ADDRESS: kstok@unimelb.edu.au

REFERENCES:

[1] Stok, K.S. et al., PLoS One. 11, 2016.
[2] Durongbhan, P. et al., Scientific Reports. 12, 2022.

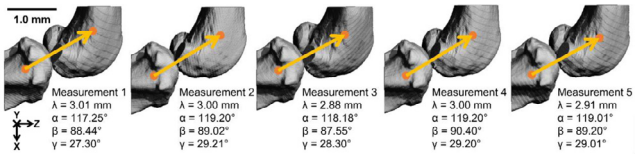

Figure 1. Exemplar repeated measurements using the protocol showing joint centre of mass, with length, λ (mm), and orientation α (°); β (°); and γ (°).

doi: 10.1016/j.ostima.2023.100137

AGE-DEPENDENCE OF SINGLE- AND MULTI-EXPONENTIAL T2 PARAMETERS IN KNEE LIGAMENTS AND TENDONS

H. Lise de Moura [1], R. Kijowski [1], A. Sharafi [2], M.V.W. Zibetti [1], R. Regatte [1]

[1] *Department of Radiology, New York University Grossman School of Medicine, New York, NY, USA*
[2] *Medical College of Wisconsin, Wauwatosa, WI, USA*

INTRODUCTION: There is a limited understanding of differences in the composition and structure of knee tendons (PT) and ligaments (ACL and PCL) of individuals of different ages. These tissues have very short T_2 relaxation times associated with the amount of collagen fibrils and their orientations. A better understanding of the differences associated with age, if any, can help in the early detection of degeneration caused by OA.

OBJECTIVE: To investigate age-related differences in T_2 parameters in the ACL, PCL and PT in the knee joint in healthy volunteers using a T_2-prepared zero echo time (ZTE)-based pointwise encoding time reduction with radial acquisition (T_2-PETRA) sequence.

METHODS: The study group consisted of 16 healthy subjects (8 females, mean age: 29 ± 8yrs, and 8 males, mean age: 35 ± 10yrs) with no known inflammation, trauma, or pain in the knee joint. A ZTE-based 3D-PETRA sequence with MLEV T_2 preparation was used to acquire fat-suppressed 3D T_2-weighted images of the knee joint with echo times (TEs) of 0ms, 0.2ms, 2.6ms, 12.9ms, 12.9ms, and 30ms. The acquisition parameters were as follows: TR/TE=5ms/0.07ms, FOV=200mm × 200mm, flip angle=6°, voxel size=0.78mm × 0.78mm × 0.78mm, receiver bandwidth=399Hz/px, T_1 recovery delay=500ms, number of radial spokes=8000, number of segments=350, number of readouts in each segment=26, and number of Cartesian sample points=1419. Voxel-based relaxometry was done using three exponential models: mono-, bi-, and stretched-exponential. Spearman correlation coefficients were used to determine the association between age and T_2-PETRA parameters. Statistical significance was defined as $p < 0.05$.

RESULTS: In each tissue, moderate-to-strong correlations (0.48-0.59) were found between age and two exponential model parameters: bi-exponential short T_2 and stretching-exponential α. No significant correlations were found for the other parameters.

CONCLUSION: The short T_2 component in the bi-exponential model is associated with the amount of collagen present in the tissues. The positive correlation with age likely indicates an interaction of loosely bound water and collagen. The positive correlation with the stretching parameter α indicates a decrease in the heterogeneity of the water pools. This is in agreement with the short T_2 component correlation, as the short T_2 gets closer to the long T_2, the distribution of relaxation times in the voxels becomes narrower. These results might indicate that degeneration due to age is less severe as it does not affect the ratio between free water in the ligaments and bound water.

SPONSOR: This study was supported by NIH grants, R21-AR075259-01A1, R01-AR076328-01A1, R01-AR076985-01A1, and R01-AR078308-01A1 and was performed under the rubric of the Center of Advanced Imaging Innovation and Research (CAI2R) at NYU Grossman School of Medicine, an NIBIB Biomedical Technology Resource Center (NIH P41-EB017183).
DISCLOSURE STATEMENT: None
CORRESPONDENCE ADDRESS: hector.lisedemoura@nyulangone.org

doi: 10.1016/j.ostima.2023.100138

3-D STATISTICAL SHAPE MODELLING OF THE DISTAL FEMUR IN TROCHLEAR DYSPLASIA

S. Brinch [1], P. Hansen [1], F.H. Linden [1], M Boesen [1], M. Krogsgaard [1], P. Lavard [1], T.D. Turmezei [2]

[1] *Bispebjerg and Frederiksberg Hospital, Copenhagen, Denmark*
[2] *Norfolk and Norwich University Hospital, Norwich, UK*

INTRODUCTION: The shape of the distal femur is characteristic in trochlear dysplasia (TD), which is an important predisposing factor for lateral patellar dislocation and early patellofemoral osteoarthritis. Quantified 3-D evaluation of the distal femur with statistical shape modelling (SSM) could make automated biometric classification of this morphology possible.

OBJECTIVE: To analyse which 3-D shape modes of the distal femur that are significantly related to trochlear dysplastic morphology with patellar instability.

METHODS: 20 healthy volunteers without radiological signs of TD and 20 individuals with Dejour type B or D dysplasia and patellar instability were recruited, both groups aged 18-45 years with no history of arthritis, connective tissue disease, or traumatic knee conditions requiring physical or operative treatment. The TD group were awaiting surgical trochleoplasty after failing conservative treatment. With a 50:50 proportion of left and right knees in the TD group, a random matched 50:50 split of left and right knees were chosen for comparison in the healthy volunteers. Weight bearing computed tomography (WBCT) of the target knee in 20˚of flexion using a Carestream Onsight© scanner, tube settings 90 kV and 6 mA. Reconstructed voxel spacing was isotropic at 0.26mm with an axial field of view and scan range of $23 \times 23 \times 23$ m. The distal femur was semi-automatically segmented and a canonical distal femur registered to each individual femur object, followed by 3-D statistical shape modelling using principal component analysis. Generalised estimating equations (GEE) were used to establish which shape modes were significantly different between the healthy and TD groups. Since sex and the first shape mode (akin to scale) were correlated ($r = 0.68$), sex was removed from the GEE model, which finally included age and the first 6 shape modes.

RESULTS: Mean (± SD) age of all participants was 30.5 ± 5.2 years, with an even split of sexes in both groups. Horn's parallel analysis demonstrated that the first 6 shape modes were beyond noise in the shape model. GEE analysis showed that shape mode 3 (left figure, inferior view right knee) significantly discriminated between healthy and dysplastic knees with an odds ratio of 11.2 (95% CI 1.7-77.4) for each SD of the shape mode ($p<0.001$). This shape mode represents reversal of the normal trochlear groove depth along with suggestion of a supratrochlear spur. No other shape modes were significant (right figure).

CONCLUSION: Individuals with trochlear dysplasia and patellar instability awaiting surgical trochleoplasty can be distinguished from a normal morphology population using 3-D statistical shape modelling. This opens up an opportunity for automated 3-D biometric characterisation of knees in both diagnosing and potentially selecting of specific individuals suitable for trochleoplasty.

SPONSOR: Department of Radiology and Section for Sports Surgery, Bispebjerg and Frederiksberg Hospital, Denmark.
DISCLOSURE STATEMENT: TT has been a consultant for Curvebeam AI.
ACKNOWLEDGEMENT: None.
CORRESPONDENCE ADDRESS: signe.brinch@regionh.dk

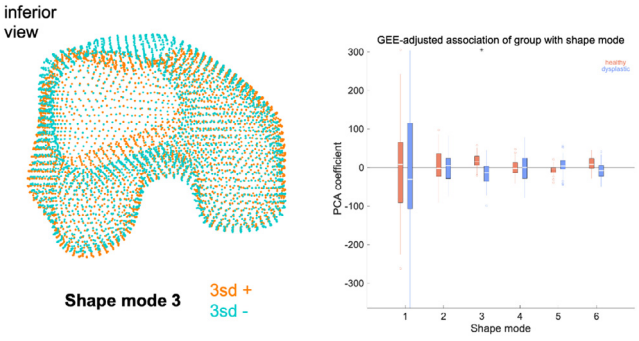

doi: 10.1016/j.ostima.2023.100139

LOW-FIELD MRI OF NON-TRAUMATIC TEMPOROMANDIBULAR DISORDERS: A COMPARATIVE STUDY OF 0.55T AND 1.5T MRI

M. Kopp [1], R. Heiss [1], M. Wiesmueller [1], M. Buchbender [2], M. Kesting [2], A.M. Nagel [1,3], M. May [1], M. Uder [1], F. Roemer [1,4]

[1] *Radiology, Universitätsklinikum Erlangen 8 Friedrich-Alexander Universität Erlangen-Nürnberg, Erlangen, Germany*
[2] *Oral and Maxillofacial Surgery, Universitätsklinikum Erlangen 8 Friedrich-Alexander Universität Erlangen-Nürnberg, Erlangen, Germany*
[3] *Medical Physics in Radiology, German Cancer Research Center (DKFZ), Heidelberg, Germany*
[4] *Chobanian 8Avedisian School of Medicine, Boston University, Boston, MA, USA*

INTRODUCTION: Chronic temporomandibular joint disorders (TMDs) including osteoarthritis are common and cause persistent functional limitations and pain. MRI at 1.5T and 3T is commonly applied for the evaluation of the temporomandibular joint (TMJ). A new generation of modern low-field MRI systems with magnetic field strengths below 1T has shown promising results in different body regions, including musculoskeletal imaging. Low-field MRI has lower signal-to-noise ratio and spatial resolution compared to higher field strengths. No evidence is available regarding the feasibility of modern low-field MRI for assessment of chronic TMDs.

OBJECTIVE: The objective of this prospective study was to evaluate the image quality (IQ) of 0.55T MRI in direct comparison with 1.5T MRI in patients with a variety of TMJ disorders.

METHODS: 17 patients (n = 34 TMJs) with known TMDs were enrolled and both 0.55T and 1.5T MRI were performed on the same day. The protocol included sequences in an open and closed mouth position: a 2 mm coronal proton density-weighted (PDw), a 2 mm sagittal oblique PDw sequence and a 3 mm axial T2-weighted sequence over both TMJ at a closed mouth position. Acquisition time for the 1.5 T MRI was approximately 8 min, for 0.55T it was close to 14 min. Two senior readers independently evaluated the image quality (IQ) focusing on conspicuity of disc morphology (DM), disc dislocation (DD) and osseous joint disease (OJD) for each joint. The IQ and degree of artifacts using a 4-point Likert scale (LS) was assessed for both field strengths. Diagnostic IQ was defined as LS ≥ 3. Non-parametric Wilcoxon test for related samples was used for statistical comparison.

RESULTS: 23 patients (15 female and 8 male) were included (mean age 41±17 years, range: 22–71 years). The median IQ for DM and OJD was inferior for 0.55T compared to 1.5T (DM: 3 (IQR 3 vs. 4 (IQR 4-4); OJD: 3 (IQR 3-4) vs. 4 (IQR 4-4); each $p < 0.001$). For DD the IQ was comparable (4 (IQR 3-4) vs. 4 (IQR 4-4); $p > 0.05$). Sufficient diagnostic IQ (defined as LS ≥ 3) was maintained for DM, DD and OJD in 92% at 0.55T (100% at 1.5%). Minor image artifacts (LS ≥ 3) were more prevalent for 0.55T (29%) compared to 1.5T (12%).

CONCLUSION: Imaging of the TMJ at 0.55T MRI provides lower IQ compared to 1.5T but maintains sufficient diagnostic confidence and seems therefore feasible in clinical routine.

SPONSOR: No funding was received for this study.
DICLOSURE STATEMENT: FWR: CMO 8 Shareholder BICL
ACKNOWLEDGMENT: Imaging Science Institute Erlangen. Sandy Schmidt for technical support during MRI acquisitions.
CORRESPONDENCE ADDRESS: frank.roemer@uk-erlangen.de

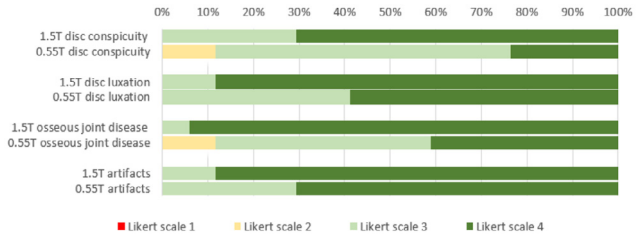

Figure 1. Image quality (IQ) scores on a 4-point Likert scale for 1.5T versus 0.55T MRI. The horizontal bars illustrate the IQ for dis morphology, disc dislocation, osseous joint disease and overall image artifacts. The subjective IQ rating are based on the evaluation of all acquired sequences.

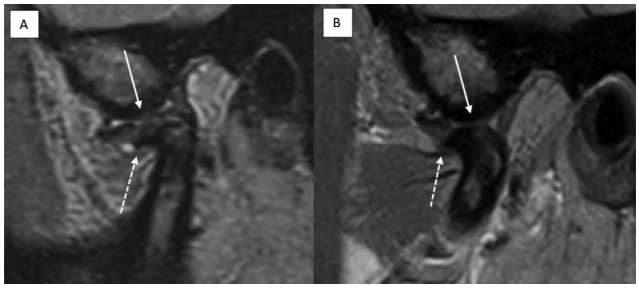

Figure 2. Comparison of image quality (IQ) in an oblique-sagittal proton-density weighted sequences of the same patient at 0.55T (A) and 1.5T (B) with delineation of central disc perforation (white arrow) and degenerative sclerotic changes with osteophytes of the temporomandibular joint (white dotted arrow). On the 4-point Likert scale (LS) the 0.55T IQ was scored with LS =3 and the 1.5T IQ with LS = 4.

doi: 10.1016/j.ostima.2023.100140

PRESENCE AND SEVERITY OF CARTILAGE LESIONS ON WEIGHT-BEARING CT IN COMPARISON WITH MRI

S. Li [1], F. Roemer [2,3], A. Guermazi [2], M.C. Nevitt [4], J.A. Lynch [4], N.A. Segal [1]

[1] *University of Kansas Medical Center, Kansas City, KS, USA*
[2] *Boston University, Boston, MA, USA*
[3] *Universitätsklinikum Erlangen 8 Friedrich-Alexander-Universität Erlangen-Nürnberg, Erlangen, Germany*
[4] *University of California-San Francisco, San Francisco, CA, USA*

INTRODUCTION: Early diagnosis of cartilage pathology holds potential to expedite appropriate management to minimize progression of OA. While regarded as the current standard of care, MRI has been shown to underestimate the extent of cartilage damage in the knee, limiting its sensitivity and specificity when compared to computed tomography arthrography (CTa). If left undetected and untreated, these early features of OA can contribute to worsening structure, pain, and physical function. Since CTa is the gold standard for assessment of cartilage surface morphology and weight bearing can compress cartilage in a functional position, acquisition of weight-bearing CT arthrography (WBCTa) may improve detection of cartilage damage.

OBJECTIVE: Determine the rate of detection and relative severity of cartilage lesions on WBCTa and MRI.

METHODS: In a sample of 65 participants (33 left and 32 right knees), WBCTa images were acquired 1–25 days following MRI collection for evaluation of suspected meniscal or cartilage pathology. Knee cartilage morphology was semi-quantitatively assessed by musculoskeletal radiologists, each with greater than 20 years of experience reading knee MRI (1.5T, TR 3020, TE 36 ms, ET 9, 3 mm thickness, gap 0.8 mm, 17×17 cm FOV, 256×256 matrix) and WBCTa (0.26 mm voxels reconstructed to 2.9 mm thickness, FOV 17.2×15.9 cm, 90–120 kVp, 5.0 mA), using the MRI Osteoarthritis Knee Score (MOAKS). Coding for the scoring system was based on the location of the cartilage lesion, including subregions on the patella, femur, and tibia. Discordance in the presence or absence of cartilage lesions was compared between MRI and WBCTa using McNemar's test and p-values. A p-value <0.05 indicated that the discordance rate for the presence of cartilage lesions statistically differed between the imaging modalities. Severity of the cartilage findings were summarized for WBCTa and MRI using frequencies.

RESULTS: Due to image quality issues on WBCTa, some variables could not be scored for 1-2 knees. Participants were 69.2% women, had a mean±SD age 48.8 years, and BMI of 28.9kg/m^2. When dichotomizing the presence or absence of cartilage lesions (MOAKS-CM>0), WBCTa detected a significantly higher frequency of cartilage lesions than did MRI on the lateral patella, anterior lateral femur, and the anterior medial and central medial tibia (Figure 1). Preliminary data also suggested comparatively higher rates of detection of cartilage lesions on WBCTa than on MRI for the central lateral femur and tibia (Table, left). Cartilage lesion severity was higher on WBCTa for all subregions except for the posterior lateral tibia (Table, right).

CONCLUSION: WBCTa detects a higher rate of cartilage lesions on the lateral patella, anterolateral femur, and the anterior medial and central medial tibia, compared with MRI. Scoring of cartilage lesions on WBCTa also reveals a higher severity of cartilage damage in all knee subregions, other than for the posterior lateral tibia. WBCTa holds promise to provide more clinically useful information regarding knee cartilage morphology than MRI.

SPONSOR: None.
DICLOSURE STATEMENT: NS is a consultant for Trice Medical and Pacira Biosciences. AG is a BICL shareholder and a consultant for Pfizer, Novartis, ICM, Coval, Medipost, TrialSpark and TissueGene. FWR is consultant of Grünenthal and shareholder of BICL.
ACKNOWLEDGMENT: CareStream lent the WBCT scanner used for this study without stipulations regarding its use.

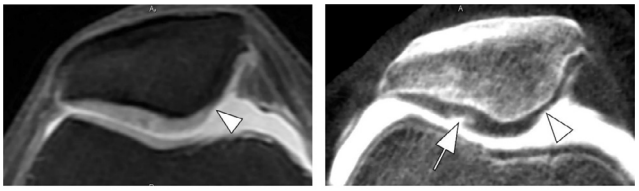

A B

Figure 1. Axial intermediate-weighted fat suppressed MR shows superficial cartilage damage at the medial patella (arrowhead). The lateral patella is morphologically normal. B. Corresponding axial CT arthrography image shows medial patellar cartilage damage in comparable fashion but also depicts a focal superficial cartilage lesion at the lateral patella not seen on MRI (arrow).

	Cartilage Lesion Presence			Cartilage Lesion Severity	
Cartilage Pathology	WBCTa+/ MRI-	MRI+/ WBCT-	McNemar p-value	WBCTa > MRI	MRI > WBCTa
Medial patella‡	10.8%	7.7%	.5637	24.6%	16.9%
Lateral patella	25.4%	1.6%	.0003	31.7%	9.5%
Anterior medial femur	9.2%	6.2%	.5271	13.8%	9.2%
Anterolateral femur	10.9%	1.6%	.0339	15.6%	3.1%
Central medial femur	13.9%	4.6%	.0833	33.8%	10.8%
Posterior medial femur	4.7%	6.3%	.7055	9.4%	6.3%
Anterior medial tibia	23.1%	0.0%	.0001	24.6%	0.0%
Central medial tibia	18.5%	4.6%	.0201	30.8%	6.2%
Posterior medial tibia	9.2%	7.7%	.7630	12.3%	7.7%
Central lateral femur	12.3%	3.1%	.0578	13.8%	7.7%
Posterior lateral femur	3.1%	3.1%	1.0	6.4%	0.0%
Anterior lateral tibia	3.1%	1.6%	.5637	3.1%	1.6%
Central lateral tibia	12.5%	3.1%	.0578	17.2%	4.7%
Posterior lateral tibia	6.3%	12.5%	.2482	6.3%	15.6%

doi: 10.1016/j.ostima.2023.100141

A THREE-DIMENSIONAL STATISTICAL SHAPE MODEL TO DESCRIBE CLINICAL SHAPE VARIATION OF THE PROXIMAL FEMUR IN PATIENTS WITH LEGG-CALVÉ-PERTHES DISEASE DEFORMITY

L.G. Johnson [1,†], J.D. Mozingo [2,†], P.R. Atkins [2], S. Schwab [2], A. Morris [2], S. Elhabian [2], D.R. Wilson [1], H.K.W. Kim [3], A.E. Anderson [2]

[1] *University of British Columbia, Vancouver, BC, Canada*
[2] *University of Utah, Salt Lake City, UT, USA*
[3] *Texas Scottish Rite Hospital, Dallas, TX, USA*

[†]Joint 1st authors

INTRODUCTION: Legg-Calvé-Perthes Disease (LCPD) is a pediatric hip condition that affects approximately 1 in 10,000 children. In LCPD the femoral head is deformed by osteonecrosis, often resulting in a permanent residual hip deformity. Residual LCPD is associated with at least a 20 times greater risk of early-onset OA in affected hips, even in patients with only mild radiographic deformity. Current routine assessment using 2D radiographic imaging does not adequately describe the complex 3D pathomorphology of LCPD. Statistical shape modeling (SSM) provides an objective and compact description of 3D shape variability, which may be used to better describe patient specific LCPD deformity and identify which features lead to early OA.

OBJECTIVES: 1) Construct and evaluate a compact and accurate shape model of LCPDs pathomorphology using open-source SSM software. 2) Examine the relationship between 3D LCPD pathomorphology and corresponding clinical radiographic measurements.

METHODS: MR images (N=13 hips, 11 patients, 3 F/8 M) of affected hips were obtained in a previous study from patients with LCPD (age range: 6-12 years, stage II-IV). Imaging was performed using a GE 1.5T HDxt scanner (Waukesha, WI) with a coronal 3D FSPGR sequence: TR=8.9 ms, TE 2.8ms, flip angle 10°, 1.0mm slice thickness, 288×288 matrix. For this study, MR volumes were resampled isotropically to the smallest voxel dimension (.47 - .63 mm), and two raters manually segmented the proximal femurs. The *ShapeWorks* SSM software (SCI Institute, University of Utah, Salt Lake City, UT) was used to produce an SSM with 512 particles using an incremental optimization routine. Shapes were aligned and scaled with generalized Procrustes analysis. Modes of shape variation were quantified using principal component analysis. The SSM's generalizability to unfamiliar shapes was evaluated with a leave-one-out cross-validation analysis. The relationship between neck-shaft angle, articulo-trochanteric distance and femoral head asphericity with principal component scores was examined with Spearman's rank correlation coefficient (ρ).

RESULTS: The first four shape modes, describing 87.5% of the population variability, were selected to form a compact shape model. With these modes, the generalizability (point-to-point reconstruction error) was <1 mm. Notable associations were observed between mode IV and femoral head asphericity ($\rho = 0.79$), modes II and IV with neck-shaft angle ($\rho = -0.43$, 0.63 respectively), and modes I and II with articulo-trochanteric distance ($\rho = 0.58$, -0.63 respectively).

CONCLUSION: This SSM provides a compact and accurate representation of 3D shape variation in LCPD. Limitations to this model include a small sample size, but nonetheless it generalizes well to unfamiliar LCPD examples. The robust and repeatable methodology will allow the model to be supplemented with additional shapes in future. With this SSM, we aim to evaluate how well clinical metrics based on 2D projections of anatomy can represent the anatomical changes that may lead to OA, and to determine why some patients with little to no radiographic deformity still develop early-onset OA.

SPONSOR: Canadian Institutes of Health Research, Funding reference #165956
DICLOSURE STATEMENT: L.G. Johnson is supported by Arthritis Society Canada.
CORRESPONDENCE ADDRESS: luke.johnson@hiphealth.ca

doi: 10.1016/j.ostima.2023.100142

A MODEL-INVARIANT APPROACH FOR 3D ASSESSMENT OF STRUCTURAL CHANGES IN PRECLINICAL ANIMAL MODELS OF OA

P. Durongbhan, C.E. Davey, K.S. Stok

Department of Biomedical Engineering, The University of Melbourne, Parkville, Australia

INTRODUCTION: Quantitative morphometric analysis (QMA) of joint tissues has been shown to be sensitive to OA in preclinical rabbit and rat models [1,2]. Traditionally performed using workflows based on morphological operations such as dilation and erosion, its sensitivity is dependent on animal scale and voxel size, requiring parametric studies to be performed in every new implementation. We hypothesize that using probabilistic approaches, it is possible to capture OA structural changes while remaining invariant to the animal model and voxel size. In this work, a pilot study developing an empirical and model-invariant approach is conducted to automatically assess osteophyte presence, a hallmark feature of OA.

OBJECTIVE: Develop an empirical probabilistic approach providing an automatic and model-invariant solution to statistically capture morphological changes due to OA by detecting osteophyte activity.

METHODS: Micro-computed tomography scans (SCANCO Medical AG, Switzerland) from previous rabbit and rat studies of OA were used [1,2]. The rabbit dataset (18 μm voxel size) consists of scans from rabbits that underwent ACL transection in the right knee (rabbit OP, $n = 8$), while the left knee was kept as contralateral control (rabbit NO, $n = 8$). The rat dataset (10 μm voxel size) consists of scans from rats that underwent ACL transection and medial meniscectomy in the right knee (rat OP, $n = 11$), while the other was kept as contralateral control (rat NO, $n = 11$). For each image of the joint, the cortical bone of the femur and tibia were segmented, and its 3D thickness was calculated using a sphere-fitting distance transform [3]. A one-voxel-thick outer layer was segmented from the resulting thickness map, and its thickness histogram was empirically estimated by a series of statistical distributions. Parameters describing the best-fit distribution, determined with negative log-likelihood, were analyzed to determine their sensitivity to OA and the presence of osteophytes using paired two-sided t-tests.

RESULTS: Visual inspections revealed clustering of surface voxels with small thickness values around areas with osteophytes (Figure 1a), as compared to those without (Figure 1b). Surface thickness values were optimally fitted to a Gamma distribution using negative log-likelihood for most femur and tibia across both animals. The shape parameter of the fitted Gamma distribution was found to be vary significantly with OA ($p < 0.01$) and in the presence of osteophytes ($p < 0.05$).

CONCLUSION: By combining traditional image processing with empirical distribution fitting, an automated and model-invariant method for structural assessment that is sensitive to OA and the presence of osteophyte can be achieved. Future work will focus on characterizing the underlying biological processes of abnormal bone remodeling to gain insight into the emergence of the fitted Gamma distribution observed in this study.

SPONSOR: Discovery Projects scheme from the Australian Research Council (DP180101838).
DISCLOSURE STATEMENT: None
CORRESPONDENCE ADDRESS: kstok@unimelb.edu.au

REFERENCES:

[1] Stok, K.S. et al., PLoS One 11, 2016.
[2] Besler, B. A. et al., Bone. 146, 2021.
[3] Hildebrand, T. 8 Rüegsegger, P., J. Microsc. 185, 1997.

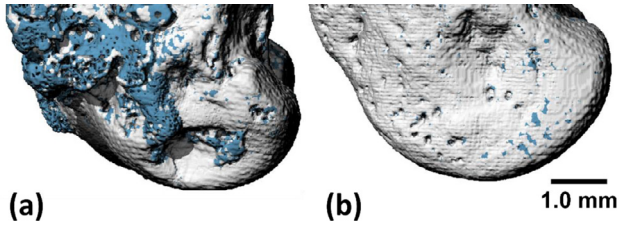

Figure 1. Exemplar cortical surface analysis results obtained using the proposed workflow showing medial femurs of rat (a) NO and (b) OP samples. High-thickness surface voxels are shown in white and low-thickness surface voxels are shown in blue.

doi: 10.1016/j.ostima.2023.100143

BONE CUTS AND IMPLANT PLACEMENTS ACCURACY IN TOTAL KNEE ARTHROPLASTY PERFORMED WITH AN ACTIVE ROBOTIC SYSTEM

K. Cosendey, P. Omoumi, J. Stanovici, B.M. Jolles, J. Favre

Lausanne University Hospital (CHUV), Lausanne, Switzerland

INTRODUCTION: Robotic systems are increasing in popularity for total knee arthroplasty (TKA), particularly for their ability to integrate 3D preoperative planning and computer-assisted robotic cutting devices, potentially minimizing errors associated with bone resections and implant placements. However, there remains a paucity of literature on the accuracy of these novel solutions.

OBJECTIVE: To assess the bone cuts and implant placements accuracy of an active robotic system for TKA.

METHODS: Two experienced orthopedic surgeons performed TKA on ten cadaveric legs using the TSolution One Surgical System (THINK Surgical, CA, USA). Metallic beads were implanted in the legs to allow registering the planning with the actual bone cuts and implant placements. CT scans were used for 3D preoperative planning. Intraoperatively, the surgeons exposed the knee through a medial parapatellar approach, located points on the joint surfaces using a digitizer to register the virtual bones in the planning to the actual bones, supervised the robotic arm cutting the bones, applied bone cement, impacted the implants, and sutured the knee. Postoperative CT scans were acquired to evaluate the procedure. The accuracy was assessed by comparing the position and orientation of planned versus actual cuts and implant placements in the three anatomical planes. The rotation of the tibia in the transverse plane was not assessed, resulting in an assessment of accuracy for 11 degrees of freedom.

RESULTS: The root mean square (RMS) values for all bone cut errors were below 2mm or 2°. The RMS errors for implant placements were below 2mm or 2°, except for femoral and tibial flexion-extension angles (both RMS values 2.9°).

CONCLUSION: This study confirmed the ability of the TSolution One Surgical System to achieve accurate bone cuts and implant placements, with most errors being below 2mm or 2°. The study also suggested that such accurate implant placements require both accurate bone cuts and proper implantation technique. An originality of this study was to measure simultaneously the bone cuts and implant placement accuracy using a particularly robust method combining metallic beads and CT artifact-free implants. Additional studies are needed to determine the optimal implant placements and thus fully release the potential of robotic systems in TKA.

SPONSOR: This research was partially funded by Think Surgical Inc.
DISCLOSURE STATEMENT: None.
CORRESPONDENCE ADDRESS: killian.cosendey@chuv.ch

doi: 10.1016/j.ostima.2023.100144

WHERE ARE WE WITH WEIGHT BEARING COMPUTED TOMOGRAPHY IN OA RESEARCH? A POLL OF ATTENDEES AT THE OARSI 2023 BREAKFAST WORKSHOP

T.D. Turmezei [1], N.A. Segal [2], F.W. Roemer [3], S. Saarakkala [4]

[1] *Norfolk and Norwich University Hospital, Norwich, UK*
[2] *University of Kansas Medical Center, Kansas City, KS, USA*
[3] *Universitätsklinikum Erlangen 8 Friedrich-Alexander Universität Erlangen-Nürnberg, Erlangen, Germany*
[4] *University of Oulu, Finland*

INTRODUCTION: Weight bearing computed tomography (WBCT) has become an increasingly important imaging modality in OA research over the last decade. Several types of imaging device are available with this capability, with the latest having evolved from foot and ankle coverage to complete lower limb and even whole-body imaging in the weight bearing position. This places WBCT at the forefront of new technologies in OA research, with a growing need to understand how it should be applied to impact most effectively on our understanding of OA, its progression, and development of effective therapeutics.

OBJECTIVE: To gain insight at the Osteoarthritis Research Society International (OARSI) 2023 Breakfast Workshop on the users, applications, and future potential of WBCT in OA research.

METHODS: The Breakfast Workshop entitled "Where are we with weight bearing CT in OA research?" took place on 20 March at the OARSI 2023 World Congress in Denver, Colorado, on invitation of the congress program committee. During the discussion-part of the session, attendees were invited to a live on-line poll (Turning Point Solutions) via a QR code. There were five questions curated by the session organisers: Q1. What has been your primary experience with WBCT? Q2. If you have had experience with WBCT, which region of the body has this involved? Q3. In which role do you think WBCT is most justified for use in clinical trials? Q4. What do you think is the most important role for WBCT in OA research? Q5. What is the biggest barrier to WBCT implementation in OA research? A final question asked attendees for their feedback on the poll experience. Only one response could be selected for each question. The poll ran exclusively live at the time of the workshop. Respondents used their smart phone or device to join and answer the questions.

RESULTS: 10 attendees joined the poll but did not answer all questions. Q1. 4/8 (50%) were research users of WBCT, 3/8 (37.5%) non-users, and one user (12.5%) in veterinary practice. Q2. Respondents had most WBCT experience at the knee (5/10, 50%), although a few had experience in multiple body regions (2/10, 20%). Q3. Regarding a justifiable role for WBCT in clinical trials, there was an even split of 5/10 (50%) between replacing radiographs and being used in conjunction with MRI. Q4. The most popular response for the most important role in OA research was measuring JSW (6/10, 60%), but there was also interest in assessing bone shape, meniscal extrusion, and performing WBCT arthrography (1 response each, 10%,). Q5. The majority (6/9, 66.7%) felt that access to technology was the biggest barrier to implementation, but the remainder (3/9, 33.3%) felt that a lack of standardization was the most important issue. Results from Q1-5 are presented along with their choices in the figure. 5/5 (100%) of respondents rated the poll 5/5.

CONCLUSION: Although generalization is not possible with this small study sample, WBCT is considered an important technology with potential for future impact in OA research. Improving access and standardising imaging protocols may increase user engagement to facilitate successful research outcomes. While focus is currently perceived to be on the assessment of JSW, there is an understanding that WBCT can fulfil several roles. Finally, a place for WBCT in OA clinical trials was considered realistic as a replacement for radiographs or for imaging in combination with MRI.

SPONSOR: None.
DICLOSURE STATEMENT: NS is a consultant for Integra BioLife, Trice Medical and Pacira Biosciences. TT has been a consultant for Curvebeam AI and GSK.
ACKNOWLEDGMENT: None.
CORRESPONDENCE ADDRESS: tom@turmezei.com

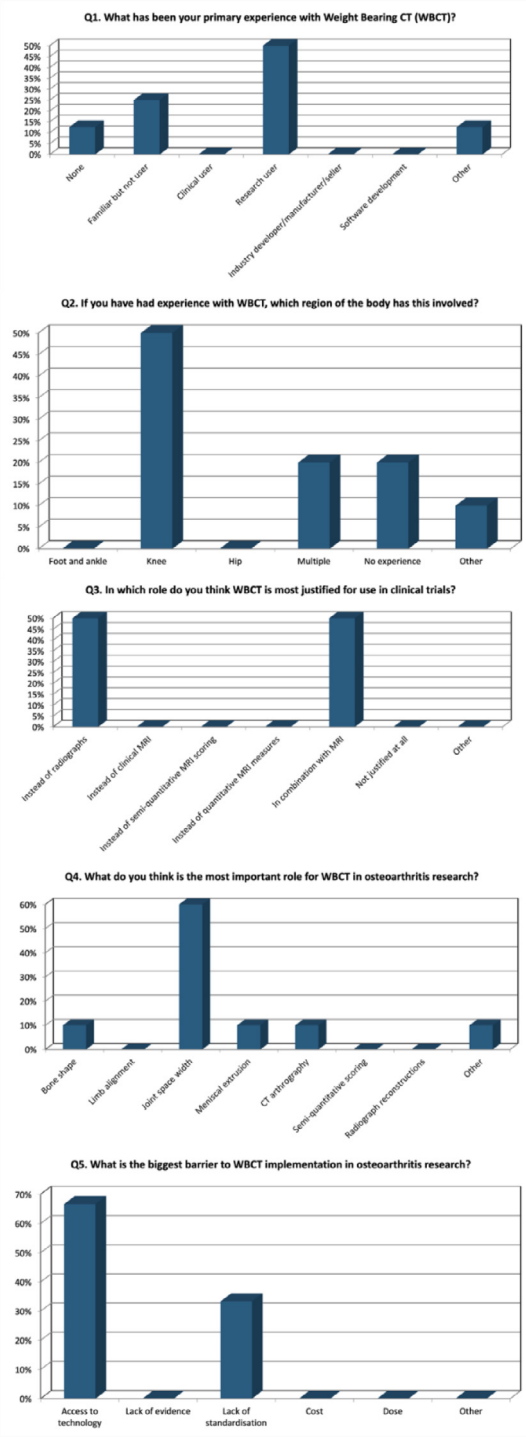

doi: 10.1016/j.ostima.2023.100145

THE ROLE OF MRI IN OSTEOARTHRITIS CLINICAL TRIAL IMAGING: A POLL OF ATTENDEES AT THE OARSI 2023 IMAGING DISCUSSION GROUP SESSION

T.D. Turmezei [1], J. Collins [2], F.W. Roemer [3], F. Eckstein [4], X. Li [5], M.J. Noh [6], C. Scotti [7], F. Cicuttini [8], J.W. Mackay [1], T.M. Link [9]

[1] *Norfolk and Norwich University Hospital, Norwich, UK*
[2] *Brigham and Women's Hospital, Boston, MA, USA*
[3] *Universitätsklinikum Erlangen 8 Friedrich-Alexander Universität Erlangen-Nürnberg, Erlangen, Germany*
[4] *Paracelsus Medical University, Salzburg, Austria 8 Chondrometrics GmbH, Ainring, Germany*
[5] *Department of Biomedical Engineering, Cleveland Clinic, Cleveland, OH, USA*
[6] *Kolon TissueGene Inc., Rockville, MD, USA*
[7] *Novartis, Basel, Switzerland*
[8] *Monash University 8 Rheumatology, Alfred Hospital, Melbourne, Australia*
[9] *University of California, San Francisco, CA, USA*

INTRODUCTION: MRI is now being adopted into roles of patient screening, selection, and outcome assessment in OA clinical trials, yet there are still barriers to universal implementation. Engagement with the OA research community and pharmaceutical industry partners should be a useful reflective exercise that may yield insights to help drive necessary progress in the future.

OBJECTIVE: To gain views from attendees at the Osteoarthritis Research Society International (OARSI) 2023 Congress and Imaging Discussion Group session on the role of MRI in OA clinical trial imaging.

METHODS: The OARSI Imaging Discussion Group session took place on 18 March at the 2023 World Congress in Denver, Colorado, USA, on invitation of the congress committee. All congress attendees were invited to an on-line poll (Turning Point Solutions) via a QR code advertised across the venue and signposted during the session. Questions were curated by speakers and panel members and were available to answer online on the day of the event and during the session: Q1. Are current MRI measures accurate enough to enrich DMOAD clinical trials? Q2. In contrast to X-ray, using abbreviated MRI protocols for screening in DMOAD trials allows for… Q3. When designing a DMOAD clinical trial it is important to only include participants with medial radiographic joint space narrowing. Q4. What is the most promising imaging technology to facilitate future DMOAD development? Q5. How could MRI be best used in OA clinical trials for phenotyping beyond cartilage? Q6. What is your perceived greatest hurdle for a successful DMOAD clinical trial? Only one choice was allowed per question, but free text comment was also permitted. The choices for each question are given in the figure.

RESULTS: Up to 45 individuals responded, 40 present at the session, 5 *in absentia*. Q1. Just over half (21/40, 53%) replied "maybe", suggesting the role of MRI in OA clinical trial enrichment needs clarification. Q2. Most respondents (29/38, 76%) chose the 'all' option, suggesting support for the use of MRI in trial screening across several roles. Q3. There was a spread from "Strongly agree" to "Strongly disagree" suggesting that restricting clinical trials to individuals with medial joint space narrowing was divisive. Q4. Non-contrast MRI relaxometry (11/29, 40%) and MRI inflammation-related measures (8/29, 28%) were most popular. Q5. Synovitis (11/30, 37%) and subchondral bone damage (6/30, 20%) were most popular, but 6/30 (20%) also selected "other". Q6. "Inadequate outcome measures" was most popular (10/29, 35%), but a split between all other options suggested there is still a range of challenges to DMOAD clinical trial success. Results are presented in the figure.

CONCLUSION: The OA imaging research community appears strongly engaged in supporting the use of MRI in OA clinical trials. There are, however, several important areas where clarification and consensus could be enhanced, such as trial enrichment and appropriate OA phenotype selection. Of note, the use of abbreviated MRI protocols in trial screening appeared to be particularly appealing across several roles.

SPONSOR: None.
DICLOSURE STATEMENT: TT has been a consultant for GSK.
ACKNOWLEDGMENT: None.
CORRESPONDENCE ADDRESS: tom@turmezei.com

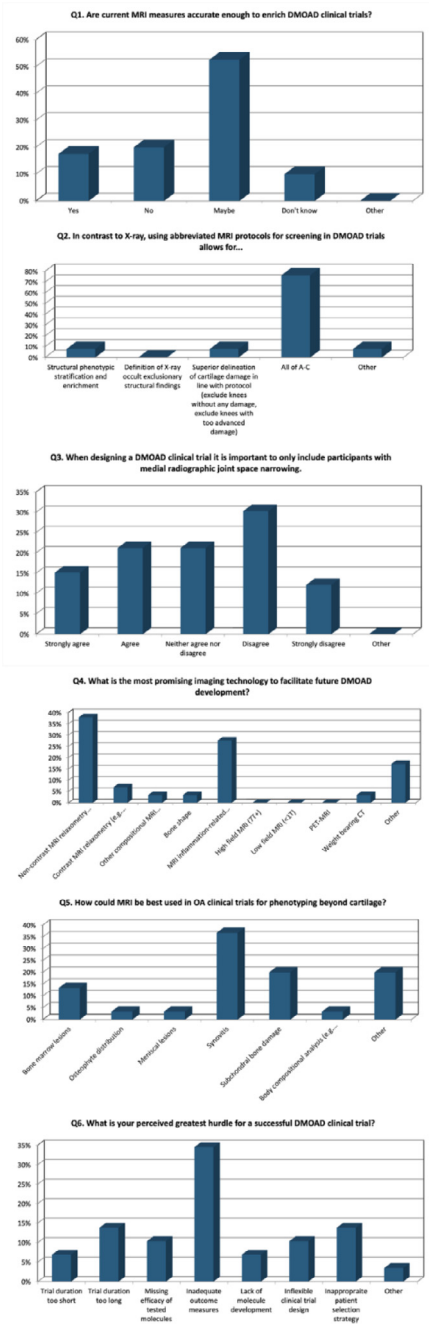

doi: 10.1016/j.ostima.2023.100146